EFFECT OF TEMPERATURE AND VISCOELASTIC CREEP ON THE CLAMP-UP LOAD IN HYBRID COMPOSITE/METAL BOLTED JOINTS

Project Report:

Structural Response of Hybrid Ship Connections Subject To Fatigue Loads

by

Mauricio Fernandez, Graduate Research Assistant,

Vincent Caccese, PhD, P.E, Professor and Principal Investigator

Senthil S. Vel, PhD, Associate Professor and Co-Principal Investigator

Prepared for:

Office of Naval Research

800 N Quincy St.

Arlington, VA 22217-5660

Grant No. N00014-05-1-0735

Dr. Roshdy G.S. Barsoum

Program Manager

University of Maine

Department of Mechanical Engineering

Orono, ME 04469-5711

August 17, 2009

Report No. C-2004-015-RPT-03

EFFECTS OF TEMPERATURE AND VISCOELASTIC CREEP ON THE CLAMP-UP LOAD IN HYBRID COMPOSITE/METAL BOLTED JOINTS

ABSTRACT

Hybrid composite to metal bolted joints are the focus of much research due the inherent advantages that they present. In particular, they are very attractive to designers and engineers alike due to their simplicity and ease of disassembly. However, hybrid connections are particularly susceptible to metal fatigue, stress relaxation primarily due to viscoelastic creep of the composite, thermal effects due to coefficient of thermal expansion mismatch, galvanic corrosion between the dissimilar constituents of the joint and moisture absorption causing differential strain between the metal and composite.

The study presented in this report focuses in an investigation of the effects of temperature and primary creep in hybrid metal to composite bolted connections. The study's relevance stems from the desire to apply this technology to naval applications, where watertight integrity must be maintained. It was then decided to examine this type of connection at the subcomponent level. Therefore, EGlass/vinyl ester plates ½" thick were bolted to aluminum and steel plates of the same thickness with instrumented steel bolts to determine the primary stress relaxation response. Special attention was placed on the effects of temperature change on the stress relaxation that hybrid connections are particularly susceptible from. A model was developed with the sole purpose of integrating the existing coefficient of thermal expansion mismatch between all the joint parts in the scheme of analysis. Experiments were carried out to obtain the CTE of the composite material used in the hybrid connection tests, and a computer program, GASmooth, was specifically written to correct the thermal effects on the stress relaxation data.

The hybrid connection test ran for a period of at least 3 months. Two test phases are distinguishable. The first phase was performed over a period of 25 days (600 hours). Test articles were left to stress relax at room temperature, undisturbed. In the second phase, the test specimens, were temperature cycled 5 times, every 7 days, from room

temperature to 62.5°C ± 1.5°C (144.5°F ± 3°F) in a computer controlled autoclave to observe the effects of larger temperature cycles on the test samples.

The test results presented in this work clearly confirm the dependency of single bolt, hybrid metal to composite connections to temperature changes. They also confirm a moderate dependency on environmental relative humidity fluctuations. Temperature and relative humidity variability have a greater effect in those connections bolting the composite to a metal with a relatively low CTE and Modulus of Elasticity. The analysis tools developed in the effort presented herein corrected the stress relaxation data for temperature shifts. Three different power law expressions were used to analyze the bolt load with respect to time in an attempt to seek alternate and simpler means to fit the data. Second phase test results confirm the importance of post curing the composite material above its service temperature. The first temperature cycle carried with it a dramatic loss of bolt load. Subsequent temperature cycles did not further alter the response of the test articles. Relative humidity changes were seen to affect.

ACKNOWLEDGEMENTS

The authors gratefully acknowledge funding for this project through the Office of Naval Research under grant number N00014-05-1-0735. Dr. Roshdy Barsoum of ONR is the cognizant program officer. His support and encouragement is greatly appreciated. The authors would also like to thank the assistance of the project team at the University of Maine including undergraduate students Jacob Folz, Brendan Owen, and graduate students Keith Berube and Radek Glaser. Also acknowledged is the assistance of Dr. Jose Daniel Diniz Melo, chair of the Department of Engineering Materials, Universidade Federal do Rio Grande do Norte, Brazil, for assisting in the DMA segment of this project.

TABLE OF CONTENTS

Page

EFFECTS OF TEMPERATURE AND VISCOELASTIC CREEP ON THE CLAMP-UP LOAD IN HYBRID COMPOSITE/METAL BOLTED JOINTS

1. INTRODUCTION

Exploring joining concepts for naval applications and developing experimental and analytical methods to assess their reliability under sea loads have been the focus of much research. Adhesive bonding and mechanical fasteners, such as rivets and bolts, have been the center of much analysis done on joint design. Bolted connections, in particular, have attracted the attention of engineers due to their relative simplicity and their undeniable benefit when it comes to ease of disassembly. Hybrid, metal-to-composite bolted connections, the focus of this effort, combine two dissimilar materials. The advantages of such a design are evident as synergistic material combinations can be introduced in the construction of a naval structure, in an attempt at reducing its system weight, increasing functionality and enabling easier access for maintenance. On the other hand, the hybrid nature of this type of connection makes them more complex to analyze for metal fatigue, stress relaxation due to the viscoelastic creep of the composite, thermal effects due to the coefficient of thermal expansion mismatch, galvanic corrosion between the dissimilar constituents of the joint and moisture absorption causing differential strain between the metal and the composite. Stress relaxation and creep in bolted hybrid composite-to-metal connections is the subject of this investigation because these types of joints tend to lose initial preload which can subsequently compromise the connection integrity. This is especially true since bolting typically stresses the composite in the through the thickness direction, where the behavior of the composite material is dominated by the viscoelastic nature of the matrix material. The potential result of this stress drop in the connection, if excessive, would be the loss of watertight integrity, with its catastrophic consequences. It is desired to develop a connection design methodology that includes the stress relaxation over time in the fastening bolts after the initial load has been applied.

Research previously carried out at UMaine by Pelletier et al. [2005] on the topic of creep in hybrid bolted connections loaded in through the thickness compression showed a strong temperature dependence. Small variations in environmental temperature were sufficient to cause evident shifts in bolt load. It is therefore vital to better understand the effects of these temperature swings in the performance of these hybrid connections. The purpose of this effort is to analyze the isolated effects of temperature and primary creep on the load change in bolted composite to metal connections stressed in the thickness direction. A deeper knowledge in the behavior of these types of connections will allow for more reliable designs.

1.1. Objectives

This work focuses on quantifying the stress relaxation of transversely compressed bolted composite to metal connections. Experiments on bolted hybrid connections at the sub-component level revealed a strong temperature effect on the bolt load state. No quantification of this effect has been made available yet. The purpose of the effort presented here is to analyze and quantify the effects of temperature variations on the stress relaxation. Research and work is proposed in the following areas:

1. Experimental study of the effects of temperature,
2. Experimental acquisition of the Coefficient of Thermal Expansion of the EGlass/vinyl ester composite material tested,
3. Development of a model to characterize the thermal effects in hybrid connections.

1.2. Literature Review

Today's structures require joints to transfer loads from member to member. Hybrid composite-to-metal connections offer many advantages, the main one being the reduction in total structural weight. But these types of joints also present a greater challenge than those found joining homogeneous, isotropic materials due to the property differences in the materials.

Composite materials, which are anisotropic in nature, do not easily accommodate stress concentrations. Also, they present intrinsic weak directions not generally found in

isotropic materials. Other disadvantages of using composite materials in a hybrid connection are the potential onset of galvanic corrosion and the initiation of ply delaminations. In a bolted hybrid connection, the viscoelastic nature of the matrix material dominates the through the thickness behavior of the composite, causing it to creep. This, in turn, can lead to stress relaxation of the bolts fastening the connection, resulting, for example, in a total loss of watertight integrity. The literature review that follows is centered in research on stress relaxation in bolted hybrid connections, with an emphasis placed on analyses focused in the through the thickness direction.

Maintaining adequate bolt clamp-up load can significantly affect the strength of the connection. One example is shown by Sun et al. [2002] who demonstrated the importance of clamp-up force on bolt strength through finite element analysis and experimental validation. The strength of double lap shear pin joints made of T800H/3900-2 graphite epoxy was highly dependent on clamp-up stress. They also showed that increasing the clamping area resulted in stronger joints.

1.2.1. General Creep Response

Findley et al. [1976] defined creep as the slow and continuous deformation of a material under constant stress. It is generally described in terms of its three stages, which are shown in Figure 1.1. The first stage is called primary creep. Here, creep occurs at a decreasing rate from a rapid start. The second, called secondary creep stage, proceeds at a nearly constant rate. The third and last stage, the tertiary stage, occurs at an increasing rate and terminates in fracture.

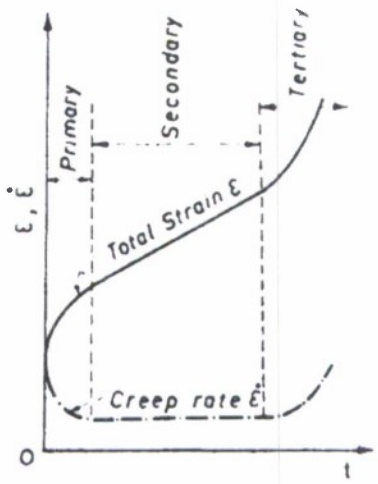

Figure 1.1 – Three Stages of Creep [Findley et al., 1976]

Composite materials exhibit a strong tendency to creep. This is due to the viscoelastic nature of the matrix material. Temperature changes, even mild ones, have also shown a strong effect on the creep behavior of composite materials. Relative humidity variations are also known to affect the creep response, although to a much lesser degree. Previous work done in those areas is presented in Section 1.2.3.

Kim and Sun [2002] demonstrated that under stress a reinforced polymer exhibits a time dependent and nonlinear behavior in all but the fiber direction. Under constant strain, stress is shown to relax and the amount of stress relaxation depends upon the constituent properties and relaxation time. They proposed a method to numerically model the relaxation and recovery behavior of AS4/PEEK composite by employing a one parameter plastic potential function.

1.2.2. Creep-Induced Stress Relaxation in Bolted Connections

Steel and aluminum have been the structural materials of choice since the Industrial Revolution when it is desirable to use metals. Hence, stress relaxation in bolted connections joining metallic structures has extensively been researched in the literature. On the other hand, composite materials for structural applications have only recently attracted the attention of engineers. Therefore, considerable less work has been done to develop methods of detecting the loss of bolt load in composite and/or hybrid

composite to metal connections due to creep in the thickness direction. This is especially true when one considers that there are numerous types of composite material systems, each having a different viscoelastic creep response.

As it was mentioned above, the viscoelastic property of the matrix material is the largest contributing factor to creep in composite materials. This is especially true in the through the thickness direction, that is, perpendicular to the fibers. The reason resides in the fact that the majority of the manufactured composite laminates are not reinforced in the thickness direction, and this result in stress relaxation in the mechanical fasteners joining parts made of this type of material. Reinforcing in the direction perpendicular to the fibers would significantly reduce creep effects.

When bolts are used as fasteners and these experience stress relaxation, they will undergo a loss of preload. The extent of this loss should be quantified to allow for reliable and dependable joint designs and to better estimate the performance of these connections over their lifetime. Shivakumar and Crews [1982] presented their work on bolt clamp-up relaxation in simple T300/5208 graphite/epoxy connections. They concluded that clamp-up force undergoes significant relaxation even at room temperature dry conditions. Relaxation of 30 percent was predicted for exposure duration of 20 years. Increased rates of relaxation were shown at elevated temperature and moisture content. They performed viscoelastic finite element analysis with some experimental verification. This work included the effects of temperature and humidity and they developed the expression relating the nondimensional clamp-up load loss versus time as follows:

$$\frac{P_t}{P_0} = \frac{1}{1 + \frac{F_1}{\alpha_{TH}{}^n} \cdot t^n} \tag{1.1}$$

where P_t is the load at time t, P_0 is the initial clamp-up load, F_1 is a material dependent constant, n is the viscoelastic power law constant for the material and α_{TH} is a hygrothermal shift factor which accounts for variations in temperature and humidity. When no hygrothermal shift is considered, Equation (1.1) can be reduced to the following:

$$\frac{P_t}{P_0} = \frac{1}{1 + F_1 \cdot t^n} \tag{1.2}$$

A demonstration of the sensitivity of Equation (1.1) to the parameters F_1, n and α_{TH} is given in Figures 1.2 – 1.4. In Figure 1.2, n and F_1 were held at 0.2 and 0.02, respectively and α_{TH} was varied from 0.001 to 1.0. Decreasing the value of α_{TH} has the effect of shifting the P_t/P_0 curve downward proportionally to the decrease of α_{TH}. Figure 1.3 shows the influence of F_1 on P_t/P_0 by holding α_{TH} at 1.0 and n at 0.2 while varying F_1 from 0.01 to 1.0. Decreasing F_1 shifts the P_t/P_0 curve upward, unproportionally to F_1. The final plot in this series, Figure 1.4, fixes F_1 and α_{TH} at 0.02 and 1.0, respectively while varying n from 0.05 to 0.5. Decreasing n also shifts the P_t/P_0 curve upward, unproportionally as well to n.

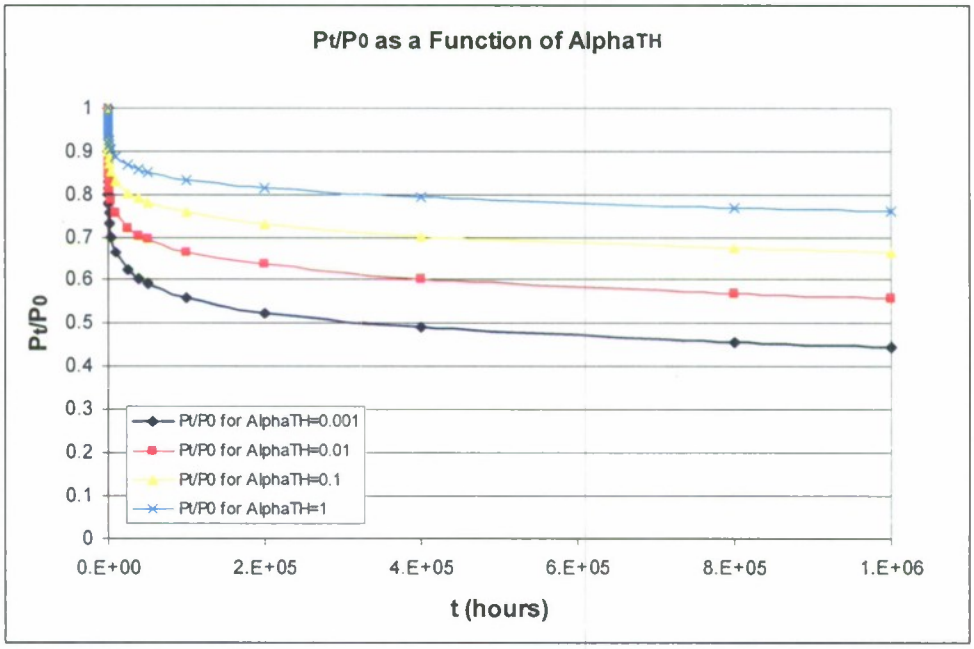

Figure 1.2 – P_t/P_0 as a Function of α_{TH}, for n = 0.2 and F_1 = 0.02

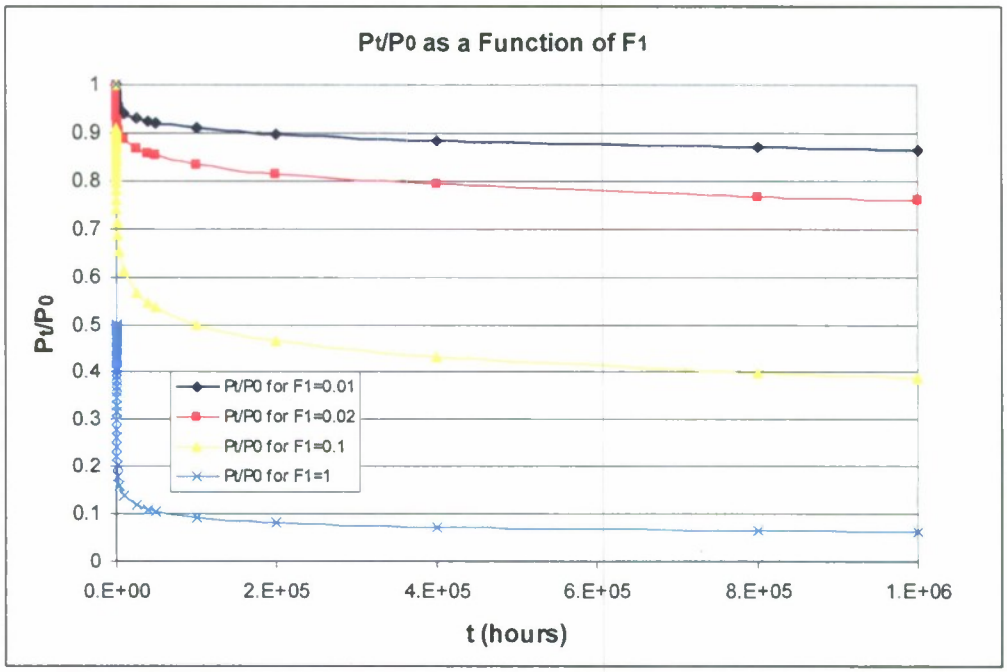

Figure 1.3 – P_t/P_0 as a Function of F_1, for $\alpha_{TH} = 1$ and n = 0.2

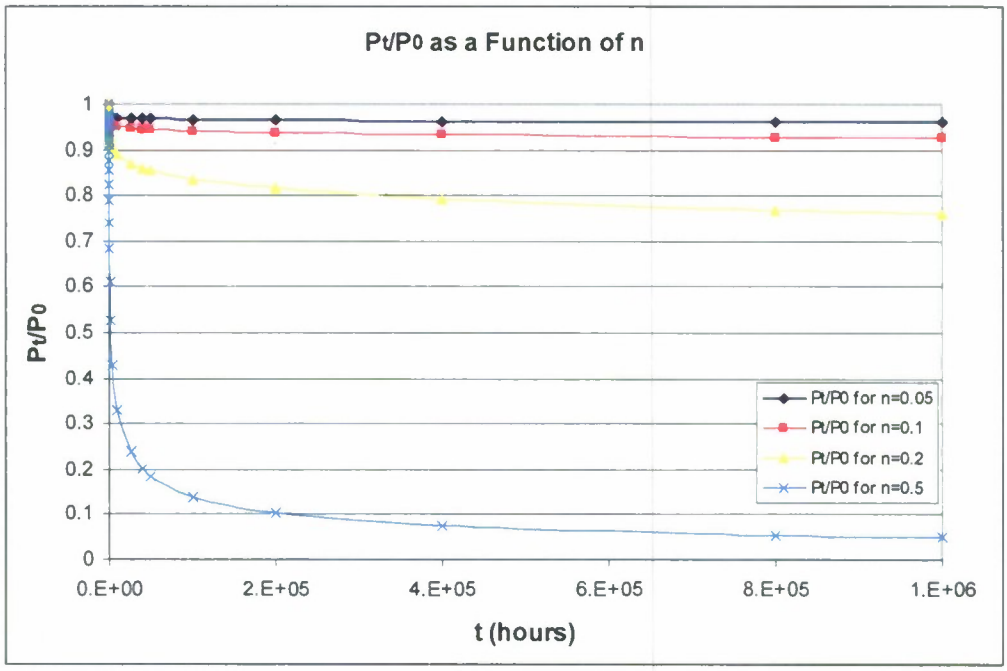

Figure 1.4 – P_t/P_0 as a Function of n, for $\alpha_{TH} = 1$ and $F_1 = 0.02$

A pioneering work on EGlass/vinyl ester composite bolted connections was presented by Weerth and Ortloff [1986]. Their test set up consisted of an EGlass/vinyl ester cylindrical coupon sandwiched between 2 washers held together by a bolt, as shown in Figure 1.5.

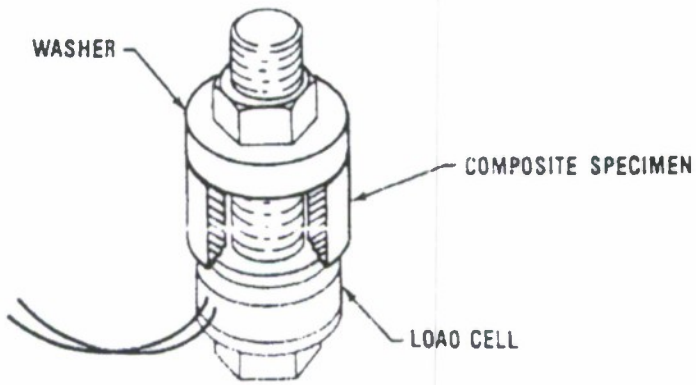

Figure 1.5 – Bolted Composite Connection used by Weerth and Ortloff [1986]

The load history was read through the use of washer load cells and a computerized data acquisition system. A 0.625 inch diameter bolt was used in conjunction with a composite having a bearing area of 0.462 square-inches. Specimens were preloaded at an ambient temperature of 70°F which was increased to 120°F during the relaxation phase. Tests were run for periods of 1 day, 1month, 1 year, 5 years and 10 years. The loss of preload was found to be 15, 28, 36, 41 and 43 %, respectively. The load loss data was found to fit the power law form, and the preload loss was predicted using the following power law equation:

$$P_t = P_0 \cdot t^{\left(1.482 \cdot 10^{-11} \cdot P_0^{2.244} - 0.0497\right)} \tag{1.3}$$

where P_t is the load in pounds in the connection at any time, P_0 is the initial preload and t is the time in hours. A graphical representation of Weerth and Ortloff's power law equation is shown in Figure 1.6. It is noted that this study did not quantify the increase in bolt load clamp-up force due to the increase in temperature at the start of the test. This can be predicted using their test geometry and estimations of the material properties.

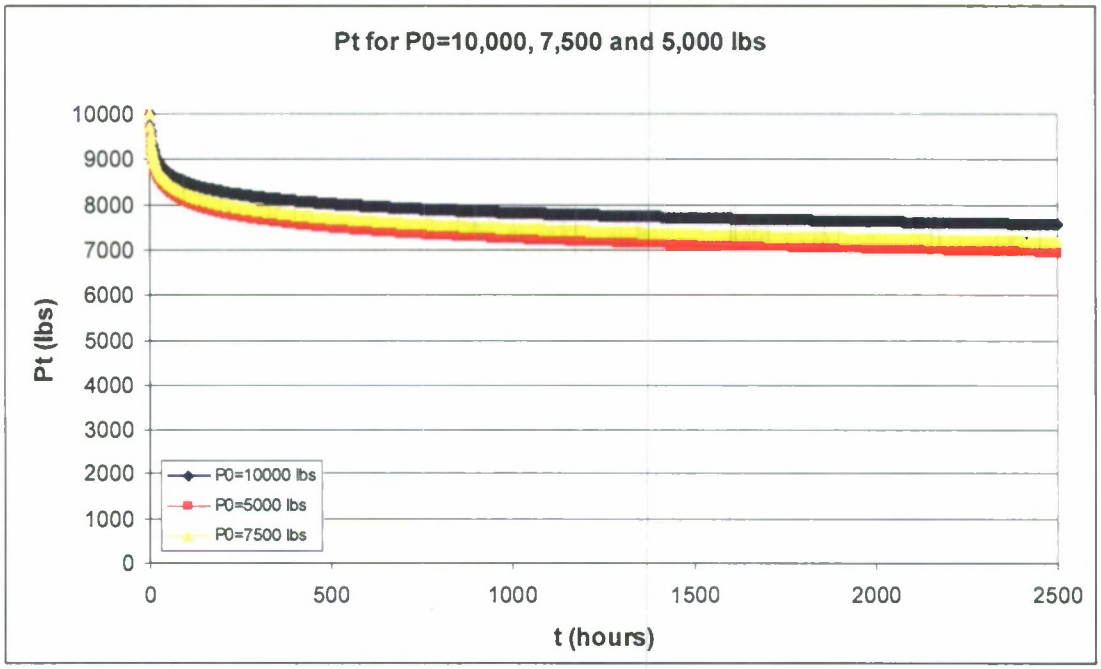

Figure 1.6 – Representation of Weerth and Ortloff's Power Law Equation

Fox [1994] presented a study on bolted EGlass/vinyl ester joints using 5/8" diameter load sensing bolts with a tapered head adapter to quantify the effect of countersunk head bolts on the connection response. Single-lap shear joints were chosen to conduct this investigation. The ½" thick, quasi-isotropic composite plate was bolted to a 3/8" thick steel plate with washers below the plate. He performed relaxation and lap shear tests. Relaxation tests were carried out for approximately 120 hours. The reduced data was found to fit Equation (1.1). Temperature and humidity were not varied during the tests, thus introducing the constant k, defined by the expression:

$$k = \frac{F_1}{\alpha_{TH}^{\ n}} \tag{1.4}$$

and substituted in Equation (1.1) to simplify it. This is the same as setting $\alpha_{TH}^{\ n}$ equal to 1 in Equation (1.1). For highly torqued tapered head bolts this resulted in constants k=0.0861 and n=0.2519. They also found that if the initial clamping force is low, the load loss can decay to near zero in a very short period of time. Data on bearing strength tests suggested that there may be a moderate increase in strength with clamp-up load.

Adding stitching in the through the thickness of a composite can be used to improve the creep resistance in bolted connections. Pang and Wang [1999] studied the effects of through the thickness stitching on the creep resistance of a carbon/glass fiber/epoxy composite material. The composite was made up of 5 layers of bi-directional carbon fiber cloth sandwiched between two layers of bi-directional EGlass cloth. The matrix was an epoxy resin known as EPOCAST 50-A/946. Three types of threads were tested to determine whether thread strength had any effect. The thread used in the tests was a cotton yarn (Tex = 300), a carbon yarn (Tex = 200), and a thick carbon yarn (Tex = 800). In addition, two stitch densities were considered. Spacing the stitching rows at 5 mm pitch produced high density stitching. Low density stitching was achieved using a row pitch of 10 mm. The composite was fabricated using a standard wet lay-up. Pang and Wang [1999] found that stitching in the loading direction was very effective in reducing the creep rate. Out of the three fibers, the 800 Tex carbon was the most efficient in reducing the creep response, followed by the 200 Tex carbon, and the 300 Tex cotton. Also found was that the density of the stitching affects the creep rate, with the smaller stitch pitch more effective at reducing the creep response.

Caccese et al. [2004] presented a paper focusing on experimentally quantifying real time changes in bolt load of composite/metal connections. A proof-of-concept model was created consisting of a fiber reinforced composite panel bolted to a steel frame. A piezoelectric actuator bonded to the center of the composite panel was used to provide controlled vibration input, as shown in Figure 1.7. The response of the panel was measured using either shear accelerometers or dynamic strain sensors located at the four corners of the composite panel.

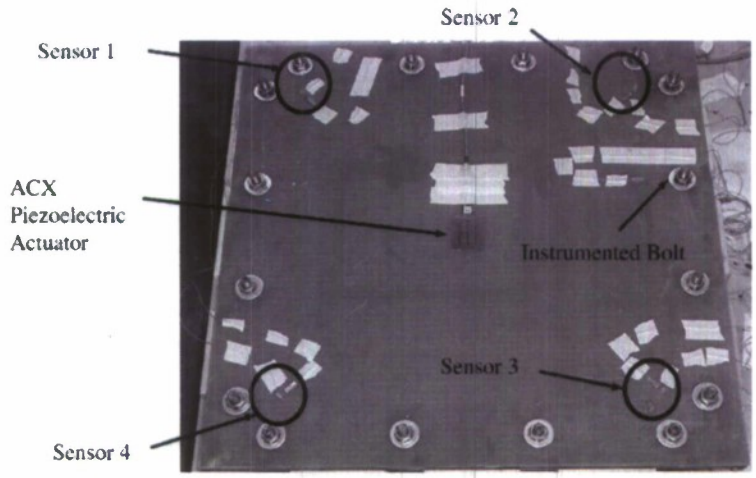

Figure 1.7 – Test panel showing sensors and actuators. Caccese et al. [2004]

Three measuring methods were presented: (1) evaluation of changes in fundamental modal properties; (2) evaluation of transfer functions with the structure subjected to a high frequency input; and (3) evaluation of transmittance functions with the structure subjected to a high frequency input. The technique using fundamental mode properties was only able to detect changes in bolt load when all of the 16 bolts in the panel were loose. The use of transfer functions was effective to a higher degree, but they finally concluded that the technique using transmittance functions to evaluate changes in bolt tensioning level showed the most promise as it was able to reliably detect small changes in bolt load.

Kabche et al. [2005] investigated the structural response of a hybrid composite to metal bolted joint panel assembly, under uniform pressure loading. The overall objective was to implement a watertight, hybrid joint concept. To reduce stress levels on the joints due to the applied bolt torque, a continuous doubler plate was used. Hence, the total bolt load was distributed over a larger area in an attempt at reducing stress relaxation effects (Weerth and Ortloff, 1986). The hybrid joint was used to connect composite panels to steel I-beam members. These panels were loaded to a peak pressure of 248kPa, well above the design pressure of 82.74kPa, and watertight integrity of the joint was maintained, with no visible damage at the connection interface.

Ireman (1998) investigated the non-uniform stress distributions through the thickness of bolted composite lap joints in the vicinity of a bolt hole using a three

dimensional finite element technique. An experimental program was conducted to measure deformations, strains, and bolt load on test specimens for validation of the numerical model developed. In the experiments, a number of parameters such as laminate lay-up, laminate thickness, bolt diameter, bolt type, clamping force and lateral support were varied. The laminates in the joints were manufactured from the Ciba-Geigy unidirectional prepreg system HTA/6376. The stacking sequences of the laminates were a quasi-isotropic $[(\pm 45/0/90)_4]_{S32}$, and $[(\pm 45/0/90)_8]_{S64}$ and a zero-dominated $[(\pm 45/90/0_2/90/0_2)_2]_{S32}$. Two types of bolts were used: counter sunk and protruding head. Tests results showed that the stress distribution in the through the thickness direction of the laminate was non-uniform, with a concentration at the shear plane. It was determined that this non-uniform stress distribution was caused by the bending and tilting of the bolt, which always occurs when a single-lap joint is loaded. Also found was that in the joint using countersunk bolts, nearly all the bearing load was carried by the cylindrical part of the hole, while in the joint with protruding head bolts, the bearing load was distributed over the entire thickness of the laminate. The effects of increased bolt diameter on the contact stress distribution for a joint with protruding head bolts showed that this contact stress was more evenly distributed over the thickness of the laminate compared with the case where a bolt with a smaller diameter was used.

Ireman (1998) also investigated the effect of increased laminate thickness for a joint with a countersunk bolt. He observed that the entire bearing load was again carried by the cylindrical part of the hole, but that the shape of the contact stress distribution was different compared with the case where a thinner laminate was used. The contact area was smaller and the stress concentration and gradient close to the shear plane were considerably higher.

The author concluded that torque-tightening reduces the strain level compared with finger-tightening. Higher strain levels were generally observed in the specimens with countersunk bolts compared with specimens with protruding head bolts. Furthermore, the friction coefficient was very uncertain since it was assumed on the basis of friction coefficient measurements at fracture surfaces. He finally stated that friction coefficient measurements for material combinations used in composite bolted joints were therefore an important subject for future research.

1.2.3 Temperature, Humidity and Environmental Effects on Creep

Katouzian and Bruller (1995) investigated the effect of temperature on the creep behavior of neat and carbon fiber reinforced PEEK and epoxy resins. Two composite materials were used in their study: an epoxy resin matrix reinforced with T800 carbon fibers and a semi-crystalline PEEK matrix reinforced with IM6 carbon fibers. The fiber volume fraction for each of the composites was found to be approximately 60%. Also tested were the neat resin matrices of each composite. Creep experiments were performed in creep fixtures utilizing lever arm action with force amplifications of 10:1 and 25:1. Dead weights acting at the ends of the lever arms generated the tensile force needed for the experiments. The high temperature tests were performed in thermostatically controlled chambers. The creep specimens used were 150 mm x 10 mm x 1mm (5.9 in. x 0.394 in. x 0.039 in.). Fiberglass end tabs were used on all specimens and all creep tests took 10 hours to complete. The neat PEEK matrix was tested at 23°C (73.4°F), 60°C (140°F), 80°C (176°F), and 100°C (212°F), while the reinforced material was tested at 23°C (73.4°F), 80°C (176°F), 100°C (212°F), and 120°C (248°F). The neat and reinforced epoxy materials were tested at 23°C (73.4°F), 80°C (176°F), 120°C (248°F), and 140°C (284°F). Room temperature tests (23°C (73.4°F)) were conducted at five stress levels ranging between 10% and 70% of the ultimate tensile strength. Load levels were reduced as the test temperature was increased. The test specimens were allowed to cure at the test temperature to ensure even heat distribution throughout the specimens. The authors of this study used the nonlinear viscoelastic constitutive equations proposed by Schapery, widely used in modeling the time-dependent response of both neat resins and composites in the absence of significant damage growth, to model the results of the creep experiments, with a maximum error of 3%. For both the neat and the reinforced epoxy they discovered that the linear viscoelastic limit shifted to lower values with increasing temperature. It was also found that the instantaneous creep response was far less sensitive to temperature that the transient response. The instantaneous creep response showed slight increases with increasing temperature, and it was found to be linear up to stress levels of 20MPa (2,900 psi). The transient creep

response showed a nonlinear dependence on temperature. It also showed very little influence from temperatures between 23°C (73.4°F) and 80°C (176°F), but increases to 140°C (284°F) showed significant effects. A comparison between the PEEK and the epoxy resins revealed a greater influence of temperature on the creep response of the PEEK resin than that of the epoxy resin. The results of the PEEK resin showed that the linear viscoelastic limit shifted to lower values with increasing temperature. This was not evident in the reinforced PEEK resin where the linear limit was approximately 25MPa (3,625 psi) for all tests. The authors concluded that the instantaneous response is linear and temperature-independent over the stress levels used in practical applications and that the influence of temperature on the time-dependent response of the materials was found to be nonlinear.

Cain et al. (2006) investigated the post-cure effects on EGlass/vinyl ester fiber reinforced polymer composites manufactured using the vacuum-assisted resin transfer molding (VARTM) method. A total of eight panels were fabricated using 24 oz. plane weave EGlass (55% warp, 45% weft) and a brominated vinyl ester resin (38% styrene). Of these, four were 35 in. x 35 in. (0.89 m x 0.89 m) pseudo-quasi-isotropic panels, fabricated with a ten-layer $[0/+45/90/-45/0]_S$ lay-up. These panels were used in both ultimate tensile strength tests and tensile fatigue tests. The four remaining panels measured 22 in. x 22 in. (0.56 m x 0.56 m), and were fabricated with an eight-layer $[\pm 45]_{2S}$ lay-up. These panels were used to investigate shear properties of the material under quasi-static tension to characterize shear (resin dominated) properties. The DMA temperature sweeps and DMA creep tests were performed on small samples taken from these panels. A list of panel designations is given in Table 1.1.

To directly and quantitatively assess the degree of cure, the Fourier transform infrared spectroscopy technique (FTIR) was used to track the C=C styrene and methacrylate double-bond conversion during the process of vinyl ester network formation from the free radical curing process. Following the post-cure, specimens were machined and stored overnight at room temperature, and on the following day, testing began (designated as day 1 testing). Testing was repeated on days 10, 30, 100, and 300. The authors concluded that the mechanical properties of ambient cured VARTM EGlass/vinyl ester resin composites are significantly affected by the degree of cure and conversion of

resin constituents. Given low degrees of cure (e.g., no post-cure) following fabrication, the laminates changed significantly over 300 days in terms of degree of conversion as well as viscoelastic properties, static resin dominated mechanical properties and fatigue performance of fiber dominated laminates. FTIR testing showed that the degree of conversion in the non post-cured resin approached that of the post-cured resin after storage at room temperature for 300 days. Creep results showed that post-curing greatly reduced the creep behavior of the matrix, and that the non post-cured samples showed decreasing creep response with time at room temperature, suggesting an increase in crosslink density with either time or post-cure, but little or no change in the material after post-curing. Among the three non ambient post-cure conditions, successively higher post-cure temperatures resulted in moderate decreases in creep response. The authors also found that a post-cure of at least 82 °C for 2 hours was sufficient to bring about stability in the state of cure and the resulting mechanical properties.

Table 1.1 - Post –Cure Conditions for Each Panel (Cain et al., 2006)

Panels	Lay-up	Post-cure Conditions
PQ01-NPC	$[0/+45/90/-45/0]_S$	No post-cure
PQ02-71	$[0/+45/90/-45/0]_S$	71°C (160°F) for 4 hours
PQ03-82	$[0/+45/90/-45/0]_S$	82°C (180°F) for 4 hours
PQ04-93	$[0/+45/90/-45/0]_S$	93°C (200°F) for 4 hours
4501-NPC	$[\pm45]_{2S}$	No post-cure
4502-71	$[\pm45]_{2S}$	71°C (160°F) for 4 hours
4503-82	$[\pm45]_{2S}$	82°C (180°F) for 4 hours
4504-93	$[\pm45]_{2S}$	93°C (200°F) for 4 hours

Hygrothermal effects, the change in properties due to moisture absorption and temperature change, also alter the behavior of a composite structure. Chen and Kung [2002] developed and analytical method to evaluate the clamp-up torque hygrothermal sensitivity of a composite bolted joint. A double-lap T300/5205 composite joint with a

steel bolt, a lay up of $[\pm 45/0_2]_{2S}$, and a thickness of 6.7 mm was used for the numerical approach. It was then compared to experimental results from IM7/8552 specimens. The connection consisted of a plate of composite bolted through the center, and the analysis focused in the through the thickness direction. Washers of different thicknesses were used on either side to sandwich the composite and provide a relatively uniform loading condition. In order to simplify the model, a few assumptions were made: (1) linear theory was applied to the bolt axial 1-D case; (2) the washers exerted a uniform stress to the laminate; (3) the stress in each ply of the composite was considered uniform in the through the thickness direction; (4) stress relaxation/creep was ignored and (5) temperature and humidity effects acted independently from each other. Both numerical and experimental results showed that the clamp-up torque on the bolted connection was extremely sensitive to changes in temperature and humidity. They also discovered that, after the bolt size, the washer to bolt diameter ratio was the most important geometrical factor when designing a composite joint and that long-term effects, such as stress relaxation and creep, should be investigated to provide further design guidelines integrating the hygrothermal sensitivity of bolted composite connections.

Bathgate et al. [1997] studied the influence of temperature on the viscoelastic creep response of stitched and unstitched composites. The specimen was fabricated placing five layers of bi-directional carbon fiber cloth between two layers of bi-directional EGlass cloth. The matrix was the epoxy resin EPOCAST 50-A/946. A modified lock stitch pattern was used. To assess whether a low stiffness thread would achieve the same effect in terms of suppressing creep strain, both cotton threads (cotton yarn Tex = 300) and carbon threads (carbon yarns Tex = 200 and Tex = 800) were used. Tensile creep tests were conducted at temperatures of 35, 55 and 70°C, and rupture testing was conducted at 80°C. At each temperature, 30, 50 and 70MPa stress levels were applied, respectively, to specimens which were: unstitched, cotton stitched (pitch = 5 mm), carbon stitched (pitch = 5 mm) and thick carbon stitched (pitch = 10 mm). The temperature variation was kept constant with ±1.5°C. The authors arrived at the following conclusions: (1) creep strain increased with temperature and stress; (2) stitching in the loading direction significantly improved the creep deformation and the creep rupture resistance, and (3) the denser the stitch pitch, the lower the creep response.

Benkhedda et al. [2008] presented a method to evaluate the effect of temperature and relative humidity on the transient hygrothermal transverse stresses (through the thickness) distribution during the moisture desorption phase. In this way, such stresses can be calculated without the computation of the moisture concentration, through laminated plates. The method took into account the variation of the modulus of elasticity due to humidity, which according to the authors is likely to cause stress relaxation. A graphite/epoxy (T300/5208) laminated plate with a stacking sequence given by $[+20,-20]_{2S}$ was exposed to different environmental conditions for a duration of 422.2 hours. Plots of the transverse residual stresses distribution within the thickness of the plate at 20, 40, 60 and 80°C and for relative humidity levels of 0, 33, 66 and 100% revealed that these stresses were significantly reduced as the temperature increased. The residual transverse stress was found to be almost constant within the thickness of the plate at high temperature and for all humidity levels.

1.3. Methods of Measuring Creep and Stress Relaxation

The ASTM standards contain methods of measuring both creep and stress relaxation. Testing can be performed in tension, compression, bending, and torsion, depending on which load case is closest to actual application. Of particular note are ASTM F1276-99 [1999], ASTM D2990-01 [2001], and ASTM E 328-02 [2002].

ASTM F1276-99 describes a method to test the creep relaxation of laminated composite gasket material. A compressive stress is applied to the material between two platens. The stress is applied using a nut and bolt. The relaxation is measured using a dial indicator. The dial indicator is set to zero when no load is applied to the bolt. The bolt is then tightened to the desired stress level and a reading is taken (D_0). The dial indicator is then removed, and the specimen fixture is then placed in an oven for 22 hours at 100 ± 2 °C. The fixture is then cooled to room temperature, and the dial indicator is reattached and zeroed. The nut is loosened and a reading is taken with the dial (D_f). The percent relaxation is then calculated by:

$$Relaxation, \% = [(D_0 - D_f) / D_0] \times 100 \quad (1.5)$$

ASTM D 2990-01 gives methods for testing tensile, compressive, and flexural creep and creep-rupture of plastics. The method consists of applying the desired load, and then measuring the extension or compression of the specimen at specific time intervals of 1, 2, 12, and 30 minutes, 1, 2, 5, 20, 50, 100, 200, 500, 700, and 1000 hours. Temperature and relative humidity is also recorded during testing to monitor environmental factors. Strain is reported for tension or compression tests by dividing the extension or compression, at given times, by the initial gage length. Maximum strain at the midspan is calculated for flexural tests.

ASTM E328-02 provides methods of testing stress relaxation in materials under tension, compression, bending, and torsion loads. The testing requires the specimens to be subjected to an increasing load until the desired initial strain is attained. Once the initial strain is reached, the specimen is constrained, and the initial stress can be calculated from the initial load. Load readings are continuously taken for the duration of the test. Plots are then made of the stress over time.

Strain gages may be used to measure the strain in the specimen over time during experimentation, but they present problems when working with plastics. The major concerns are local heating due to the current in the gage, and the difficulty in aligning the axis of the gage so that different components of the strain are completely separated. Strain gages are also a concern in long-term testing due to creep of the adhesive used to bond the gage to the specimen. For these reasons, using an extensometer is usually the best way to measure the strain during creep tests.

1.4. Previous Work on Stress Relaxation Performed at UMaine

Pelletier et al. (2005) experimentally investigated the primary stress relaxation response in hybrid metal to composite bolted connections. The composite used was a Vacuum Assisted Resin Transfer Molding manufactured EGlass/vinyl ester. The metal part was made of aluminum 6061-T6. One group of tests was performed utilizing a compression block fixture to quantify the stress relaxation of the composite material subjected to a relatively uniform stress state in the through the thickness direction. The compression block test article was a square of 2 in. x 2 in. with a constant thickness of ½

inch. It was cut from a 2 ft. x 4 ft. panel of EGlass/vinyl ester with a quasi-isotropic lay-up given by the stacking sequence expression of $([(\pm 45)_f,(0/90)_f]_4)_S$. These tests were run at ambient conditions and took 90 days to complete. The other testing consisted of a composite plate bolted to an aluminum plate of identical geometry using a single instrumented steel bolt passing through the center of both plates. The main objectives were to study the effects of stress concentrations and bolt re-torquing on stress relaxation. Three different composite thicknesses were tested. The lay-up for the ½ in., ¾ in., and 1 in. thick panels were $([(\pm 45)_f,(0/90)_f]_4)_S$, $([(\pm 45)_f,(0/90)_f]_6)_S$, and $([(\pm 45)_f,(0/90)_f]_8)_S$, respectively. The length and width of the composite articles was chosen to be 10 times their thickness. These tests were also run at ambient conditions for 90 days.

The bolt load with respect to time, for the hybrid connection, was analyzed in the form of a simple power law expression given by Equation 1.6 as follows:

$$P_t = \beta \cdot P_1 \cdot t^{-\alpha} \tag{1.6}$$

In this expression, P_t is the load at time t, P_1 is the initial preload in pounds, t is the time in days and α and β are constants that depend on constituent materials, geometry and test conditions. Constants α and β were determined using a least square power law fit of the relaxation data with the time offset by 0.007 days (10 minutes) to account for the fact that Equation (1.6) can not be resolved with time equal to zero. The constant β was found to be dependent primarily on the pressure distribution in the connection, whereas α was found to be dependent on factors such as initial preload level, specimen thickness, material properties, temperature and humidity.

The authors of this study concluded that reloading the bolted connections allowed them to retain more of the initial preload. They observed, however, that reloading made the connections particularly susceptible to temperature fluctuations. The rate of stress relaxation increased for those test articles that were reloaded while having a milder but nonetheless present effect on those that were not, for temperature increments of only 5 to 10°F.

It becomes essential to better understand the affect of temperature on the stress relaxation condition, due to the fact that these temperature variations were found to have a significant effect on the results of the hybrid metal to composite bolted connections.

Furthermore the influence of temperature was not accounted for at the time of data reduction and analysis and computation of constants in Equation 1.6 above did not integrate the crucial thermal expansion properties of the materials in the hybrid joint tested. Creep causes a decrease in bolt load that can easily be quantified over time for constant temperature conditions. In the absence of creep, a change in temperature will cause a change in bolt load due to the different thermal expansion coefficients of the parts in the hybrid joint. In reality, these two mechanisms influence their behavior simultaneously. It is then necessary to formulate a model that takes into consideration the material properties, including the thermal expansion coefficients, of all the parts in the hybrid composite to metal bolted connection, to better answer the question of how do temperature and creep affect the hybrid joint and its stress relaxation response. One of the purposes of the effort here presented is aimed at answering this question.

2. THERMAL EXPANSION COEFFICIENT TESTS

This chapter describes the plan that was followed to obtain the coefficient of thermal expansion (CTE) of the composite material used in the hybrid metal to composite bolted connection test articles. Finding this material property proved to be imperative in order to effectively study the effects of temperature change in this type of hybrid joints. A series of experiments were performed at the Department of Materials Engineering of the Universidade Federal do Rio Grande do Norte, in Natal, Brazil. Two different test beds were used: a DMA and a TMA. The test coupons used in these experiments were cut from the same EGlass/vinyl ester composite panel used to fabricate the hybrid connection test specimens. This panel was manufactured at the University of Maine Crosby Laboratory, using the VARTM (Vacuum assisted Resin Transfer Molding) process. The results of these tests are presented in this section, and they are also compared to those obtained by a commercially available composite software tool, CompositePro. The second section presents the model used to factor in the effects of temperature change in the behavior of this type of hybrid joints. It also describes the computer program, GASmooth, that was created at the Mechanical Engineering Department of the University of Maine to reduce and temperature correct the bolt load data generated by tests run on single bolt, hybrid aluminum to EGlass/vinyl ester connections utilizing the above-mentioned model.

2.1. Measurement of the EGlass/vinyl ester CTE

The successful analysis of the effects of temperature on bolt load in the hybrid joints tested in this study called for the determination of the coefficient of thermal expansion (CTE) of the EGlass/vinyl ester composite material used in these bolted connections. The objective is to develop a model which will enable the prediction of the stress state of the hybrid connection system in a simple and efficient manner. Information on the CTE of numerous materials is readily available in the literature for the metallic materials making up the connection, namely aluminum and steel, but a reliable value for the composite part was lacking. Therefore, a series of tests were designed and

conducted with the goal of obtaining the CTE of the composite material actually used in these connections. All CTE test specimens were cut at the University of Maine from the same composite panel used to put the hybrid joints together and tested at Universidade Federal do Rio Grande do Norte, Natal, Brazil.

This section includes a detailed description of the tests conducted to find the CTE of the EGlass/vinyl ester composite material. The operational procedures and the results of these tests are also discussed.

2.1.1 Test Methodology

All CTE tests were performed under the supervision of Dr. Jose Daniel Diniz Melo. Figure 2.1 shows the 8mm cubic CTE specimens used in these experiments. They were machined to meet the ASTM E 831-05 standard and they were cut from a ½"-thick EGlass/vinyl ester panel fabricated at the University of Maine Crosby Laboratory. This composite panel was the same one used to assemble the hybrid Aluminum to EGlass/vinyl ester connection specimens utilized during the stress relaxation studies. They had a quasi-isotropic lay-up given the stacking sequence $([(\pm 45)_f,(0/90)_f]_4)_S$.

Figure 2.1 - CTE Specimens

The experimental program presented includes a series of tests run on a Dynamic Mechanical Analyzer, DMA, and a sub-series run on a Thermo Mechanical Analyzer, TMA. These tests followed the general recommendations set forth by the test standard ASTM E 831-05.

The test matrix shown in Table 2.1 summarizes the CTE tests run on a DMA instrument. These tests were performed to obtain the CTE of the composite material below its glass transition temperature, T_g. The DMA had the Gas Cooling Accessory option, or GCA, connected to it to extend its lower operating range to -150°C. This feature allowed starting the tests well below room temperature. Seven specimens, numbered 1 to 7, were tested, all in the through-the-thickness direction. The first six were tested "as received". The 7th was post cured to a temperature of 180°C for 1 hour before the actual CTE test, to analyze the effects of post curing the resin on both the CTE and the T_g of the composite material. The conditions which these samples were tested under are also presented in Table 2.1.

Table 2.2 summarizes the test sub-series run on a TMA platform. These tests were carried out to observe the effect of obtaining the CTE of the composite material above its T_g, and started at room temperature. Ten samples were tested and a constant heating rate of 5°C/min was applied over the temperature range of 25°C to 120°C. As in the DMA tests, a load force of 0.1N was applied to the sensing probe. Synthetic air atmosphere was used during the measurements with a flow rate of 50 ml/min. The temperature range at which the CTE was determined was 80°C to 115°C. Specimens numbered 1a to 1d (a total of four pieces) were tested in the through-the-thickness direction (direction 1). Six more samples, numbered 2a to 2c and 3a to 3c (three of each), were tested in the two in-plane directions (directions 2 and 3).

Table 2.1 – DMA Test Matrix

Specimen #	Module	Baseline Calibration	Equilibrium Temperature	Isothermal Interval @ Eq. Temp	Heat Rate	Static Force Applied to Clamp
1 -Through the Thickness	DMA Controlled Force	Quartz -20°C to 120°C	-20°C	15 min	5°C/min to 120°C	0.1N
2 - Through the Thickness	DMA Controlled Force	Quartz -20°C to 120°C	-20°C	15 min	5°C/min to 120°C	0.1N
3- Through the Thickness	DMA Controlled Force	Quartz -20°C to 120°C	-20°C	15 min	5°C/min to 120°C	0.1N
4 - Through the Thickness	DMA Controlled Force	Quartz -30°C to 120°C	-30°C	15 min	5°C/min to 120°C	0.1N
5- Through the Thickness	DMA Controlled Force	Quartz -30°C to 120°C	-30°C	15 min	5°C/min to 120°C	0.1N
6- Through the Thickness	DMA Controlled Force	Quartz -30°C to 120°C	-30°C	15 min	5°C/min to 120°C	0.1N
7 Post Cured @ 180°C for 1 hour Through the Thickness	DMA Controlled Force	Quartz -30°C to 180°C	-30°C	15 min	5°C/min to 180°C	0.1N

Table 2.2 – TMA Test Matrix

Specimen #	Test Direction	Temperature Range	Heating Rate	# of Tests	Applied Load Force
1a	Through the Thickness	25°C to 120°C	5°C/min	1	0.1N
1b	Through the Thickness	25°C to 120°C	5°C/min	1	0.1N
1c	Through the Thickness	25°C to 120°C	5°C/min	1	0.1N
1d	Through the Thickness	25°C to 120°C	5°C/min	1	0.1N
2a	In-Plane 2	25°C to 120°C	5°C/min	1	0.1N
2b	In-Plane 2	25°C to 120°C	5°C/min	1	0.1N
2c	In-Plane 2	25°C to 120°C	5°C/min	1	0.1N
3a	In-Plane 3	25°C to 120°C	5°C/min	1	0.1N
3b	In-Plane 3	25°C to 120°C	5°C/min	1	0.1N
3c	In-Plane 3	25°C to 120°C	5°C/min	1	0.1N

2.1.2. DMA Tests and Procedures

DMA experiments were processed and test procedures followed the general guidelines established by the ASTM E 831-05 Standard. The instrument used was a DMA Q800 from TA Instruments. A photograph of it is shown in Figure 2.2.

Figure 2.2 - DMA Q800 (TA Instruments, New Castle, DE USA)

The Q800 is based on a combined motor and transducer design. It uses advanced, non-contact magnetic linear drive motors to control stress and it measures strain with a highly sensitive linear optical encoder. Optical encoders provide exceptional resolution compared to typical LVDT technology. The Q800 also features a unique air bearing design for low friction, low mass, high stiffness clamps which can be individually calibrated for data accuracy, and an automated furnace which can be combined with the Gas Cooling Accessory to provide for efficient and precise temperature control over a very broad temperature range. Figure 2.3 depicts the various parts of the Q800 DMA.

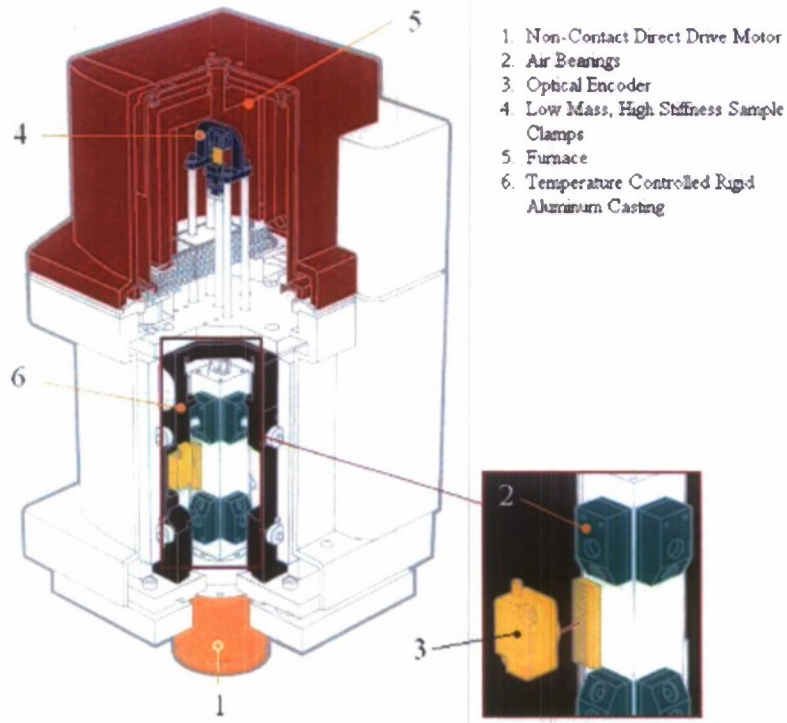

Figure 2.3 - TA Instruments Q800 DMA Schematic Diagram

The instrument is operated through a computer which also stores the output data from the experimental runs.

Although the Q800 DMA was not specifically designed to measure CTE data due to its low mass, high stiffness stainless steel clamps instead of the low thermal expansion quartz or alumina clamps common in TMAs, it can be adapted to do so by previously performing a baseline correction to compensate for all the uncertainties coming from the clamp fixture. Calibration and baseline correction procedures are explained next and in Section 2.1.2.1. Figure 2.4 shows a photograph of the penetration clamp kit used during the CTE runs. One of the seven composite coupons tested can also be seen in the photograph.

Figure 2.4 - Penetration Clamp Fixture

2.1.2.1. Q800 DMA Calibration

The manufacturer recommends that the instrument be calibrated at least once a month, mainly to validate its electronics and its force transducer. This monthly calibration is accomplished through the use of the Thermal Advantage Instrument control software. The ordinary calibration of the DMA is for position. The purpose of this routine is to calibrate the absolute position of the drive shaft (and slide) as read by the optical encoder. It also factors in the clamp mass and stiffness. The position calibration is usually done when the instrument is moved or turned off. The instrument stores the clamp position in memory until the next calibration. An error is generated if the stored

position is lost. For the penetration clamp fixture, the steps to calibrate the DMA for position are:

1. Perform a "clamp check". First press the "Drive" key. This will release the clamp, making it float (recall the air bearing). Manually position the clamp in the middle of its range of travel and release it. The clamp should maintain its position or slowly drift up or down. If the clamp mass has already been calibrated and it rapidly sinks or rises, then the clamp position requires calibration. Then go to step 2 below.
2. Calibrate the clamp position. First select Calibrate/Position from the menu. Then the fixed and moveable parts of the penetration clamp fixture are removed. Next, press the Furnace button to close the furnace. Click on the Calibrate button and the rest is automatically done for the user.

The Q800 DMA also allows for temperature calibration. It is typically done for experiments in which precise transition temperatures are essential or if, for example, a high rate of temperature increase is used and it is necessary to consider the temperature lag. The Q800 measures the temperature using two CHROMEL/ALUMEL thermocouples. The sample and reference thermocouples sense the temperature of the sample and heater and relay the readings to the instrument. When desired, the temperature calibration is performed using materials of known melting points, like Indium and Zinc. The procedure is very simple: the theoretical and measured melting temperatures of these reference materials are filled in a table, and the equipment is automatically calibrated using this data.

2.1.2.2. DMA Testing Procedure

Testing can be started once the Q800 DMA has been properly calibrated and the Gas Cooling Accessory (GCA) connected to both an inlet port in the Q800 and to a COM port in the computer that manages both the DMA and the GCA. The GCA is basically a liquid nitrogen tank that is used to test samples at sub ambient temperatures. By controlling the injection and heating of N_2 in the furnace, temperatures can reach as low as -150°C and as high as 600°C in a regulated manner. Figure 2.5 shows the Q800 DMA's GCA.

Figure 2.5 - Q800 DMA Gas Cooling Accessory (GCA)

2.1.2.3. The Control Specimen

An 8mm tall cylindrical Copper coupon was used as the control specimen. It was used to make sure that the instrument was properly calibrated and in good operating order.

2.1.2.4 The Quartz Specimen

A Quartz piece was utilized to obtain the baseline curves. Figure 2.6 shows a photograph of the Quartz sample mounted on the DMA's clamps, ready for testing. The reason Quartz is the material usually chosen to obtain these baselines is because of its very low CTE compared to that of Stainless Steel, which is the material the clamps are made of. These baselines were automatically subtracted by the DMA software from their corresponding composite specimen output curves to compensate for all the uncertainties originating from the clamp fixture. In total, three curves were generated:

1. Quartz -20-120 baseline, spanning from -20°C to 120°C.
2. Quartz -30-120 baseline, spanning from -30°C to 120°C.
3. Quartz -30-180 baseline, spanning from -30°C to 180°C.

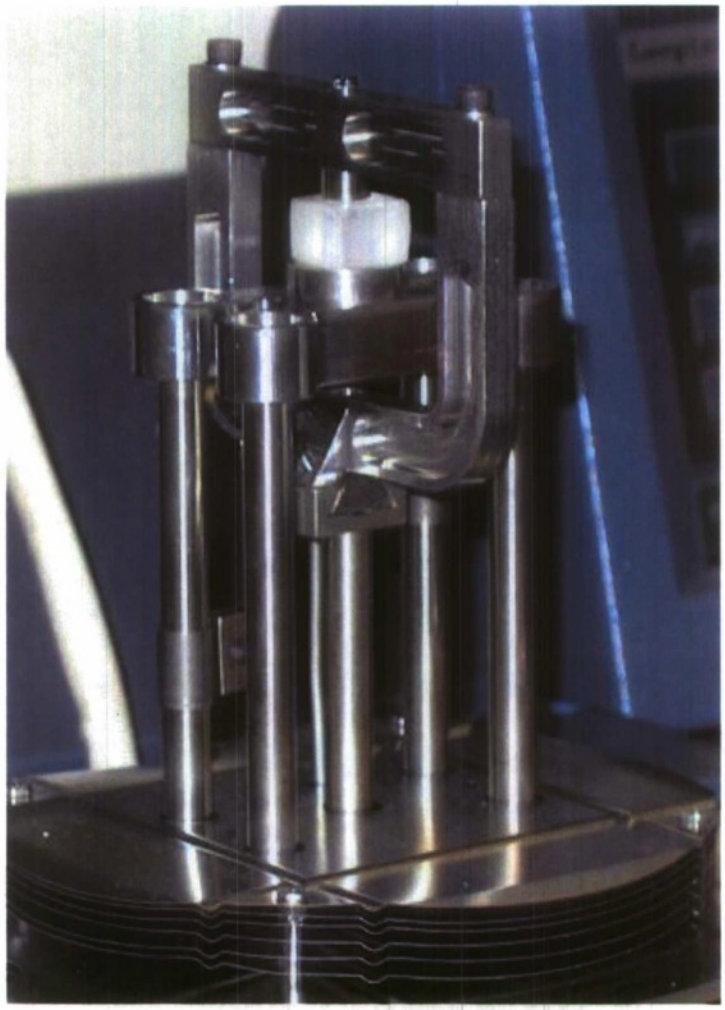

Figure 2.6 - Quartz Sample

Seven different composite specimens were tested in the DMA. Samples 1, 2 and 3 used the Quartz -20-120 baseline. Samples 4, 5 and 6 used the Quartz -30-120 baseline. Finally, sample 7, which underwent a one-hour post curing process at 180°C, used the Quartz -30-180 baseline. In all, twelve experiments were conducted in the Q800 DMA, including those for the Quartz and the Copper coupons. A summary of all the DMA runs is shown in Table 2.3 for easy reference, and the results of these are presented in the next section.

Table 2.3 - Q800 DMA Test Runs

Specimen #	Module	Baseline Calibration	Equilibrium Temperature	Isothermal Interval @ Eq. Temp	Heat Rate	Static Force Applied to Clamp
1 Through the Thickness	DMA Controlled Force	Quartz -20°C to 120°C	-20°C	15 min	5°C/min to 120°C	0.1N
2 Through the Thickness	DMA Controlled Force	Quartz -20°C to 120°C	-20°C	15 min	5°C/min to 120°C	0.1N
3 Through the Thickness	DMA Controlled Force	Quartz -20°C to 120°C	-20°C	15 min	5°C/min to 120°C	0.1N
4 Through the Thickness	DMA Controlled Force	Quartz -30°C to 120°C	-30°C	15 min	5°C/min to 120°C	0.1N
5 Through the Thickness	DMA Controlled Force	Quartz -30°C to 120°C	-30°C	15 min	5°C/min to 120°C	0.1N
6 Through the Thickness	DMA Controlled Force	Quartz -30°C to 120°C	-30°C	15 min	5°C/min to 120°C	0.1N
7 Post Cured @ 180°C for 1 hour Through the Thickness	DMA Controlled Force	Quartz -30°C to 180°C	-30°C	15 min	5°C/min to 180°C	0.1N
Quartz -20-120	DMA Controlled Force	Baseline	-20°C	15 min	5°C/min to 120°C	0.1N
Quartz -30-120	DMA Controlled Force	Baseline	-30°C	15 min	5°C/min to 120°C	0.1N
Quartz -30-180	DMA Controlled Force	Baseline	-30°C	15 min	5°C/min to 180°C	0.1N
Copper	DMA Controlled Force	Quartz -20°C to 120°C	-20°C	15 min	5°C/min to 120°C	0.1N
Copper	DMA Controlled Force	Quartz -30°C to 120°C	-30°C	15 min	5°C/min to 120°C	0.1N

2.1.2.5. DMA Results and Discussion

The results of the CTE tests run on the Q800 DMA platform are presented in this section. All the composite samples, except for one, were tested "as received", meaning no preconditioning was done prior to the run. The exception was specimen 7, which endured a post curing process by bringing its temperature to 180°C for one hour. Table 2.4 summarizes all the results obtained for these seven specimens. For all these samples, the CTE was found by tracing the slope to the Strain vs. Temperature curve, between 0°C and 50°C, before the visible change in slope that indicates the presence of a T_g. This T_g was measured at the intersection point of the tangents to either slope, before and after the kink.

Table 2.4 - CTE and T_g Experimental Results

Specimen #	Test Temperature Range, °C	Calculated CTE	CTE Measuring Range, °C	Calculated T_g, °C
1 Through the Thickness	-20 to 120	$46.43 \cdot 10^{-6}$/°C	0 to 50	78.70
2 Through the Thickness	-20 to 120	$45.68 \cdot 10^{-6}$/°C	0 to 50	77.92
3 Through the Thickness	-20 to 120	$41.41 \cdot 10^{-6}$/°C	0 to 50	78.50
4 Through the Thickness	-30 to 120	$47.11 \cdot 10^{-6}$/°C	0 to 50	78.92
5 Through the Thickness	-30 to 120	$49.26 \cdot 10^{-6}$/°C	0 to 50	77.75
6 Through the Thickness	-30 to 120	$44.64 \cdot 10^{-6}$/°C	0 to 50	78.18
7 Post Cured @ 180°C for 1 hour Through the Thickness	-30 to 180	$46.38 \cdot 10^{-6}$/°C	0 to 50	110.02

The results of the two control runs are shown in Table 2.5 for reference and to prove the validity of the testing procedure. The CTE numbers obtained for the Copper control sample are compared with those reported by the ASTM E 831-05 standard. Notice that the results are in very good agreement.

Table 2.5 - Copper Control Test results

Specimen	Test Temperature Range, °C	Calculated CTE	ASTM E 831-05 Reported Test Results	ASTM E 831-05 Literature Results @50°C	CTE Measuring Range, °C
Copper Control	-20 to 120	$16.68 \cdot 10^{-6}$/°C	$17.8 \pm 0.9 \cdot 10^{-6}$/°C	$16.91 \cdot 10^{-6}$/°C	25 to 75
Copper Control	-30 to 120	$15.84 \cdot 10^{-6}$/°C	$17.8 \pm 0.9 \cdot 10^{-6}$/°C	$16.91 \cdot 10^{-6}$/°C	25 to 75

Figure 2.7 shows the actual DMA output chart for specimen 1. This figure also shows how the CTE and T_g were obtained. The graph shows a relatively uniform CTE from about 0°C to 70°C.

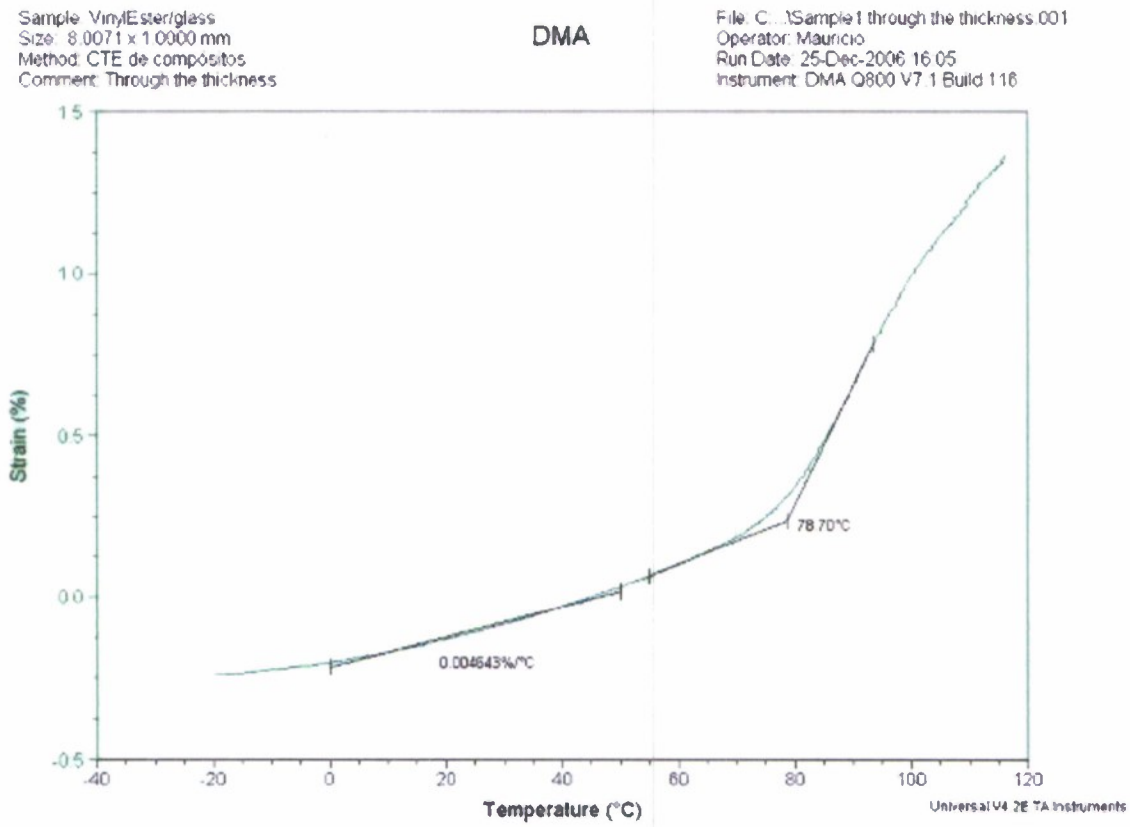

Figure 2.7 - Composite Specimen 1 DMA Output Chart

Figure 2.8 shows the strain-temperature curves for specimens 1, 2 and 3, superimposed for comparison between each other. The same is presented in Figure 2.9 for specimens 4, 5 and 6. Notice that in both cases, the curves do not perfectly superimpose one on top of the other due to small structural variations between samples.

A very small difference in resin volume fraction can give very different CTE and T_g results. This is because the continuous resin matrix phase has a larger influence on the transverse CTE of the composite than the fiber inclusions. In general, the higher the resin volume fraction is, the higher the CTE value obtained. On the other hand, lower CTE values result for a higher fiber volume fraction. It is necessary to keep in mind that these 8mm cubic specimens (see Figure 2.1 above) were cut from a relatively large panel, and sample variation will be unavoidable, no matter how consistent the manufacturing and the machining process are.

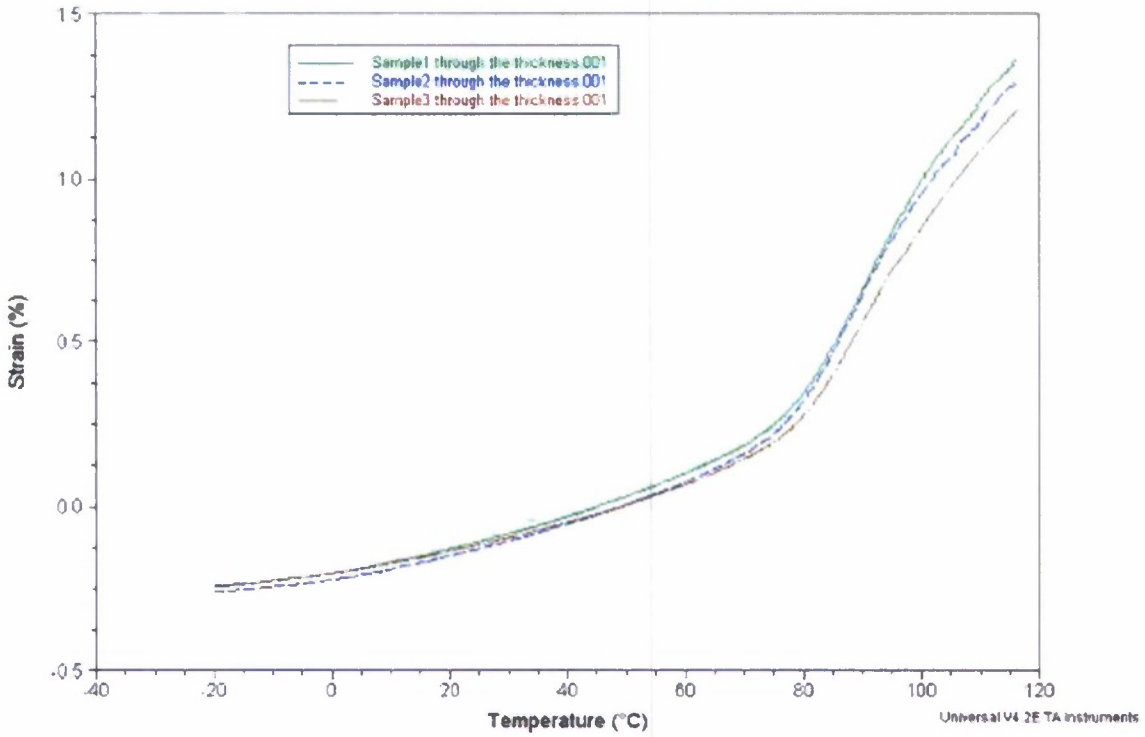

Figure 2.8 - Overlay of Samples 1, 2 and 3

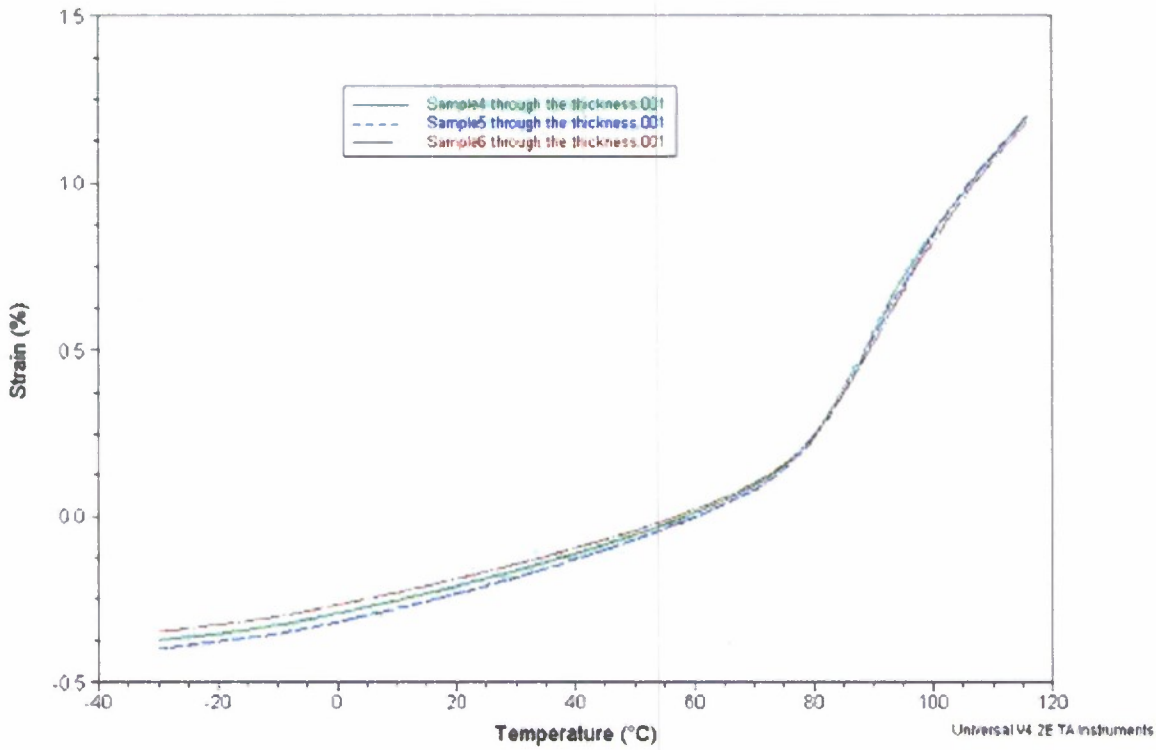

Figure 2.9 - Overlay of Samples 4, 5 and 6

Lastly, Figure 2.10 depicts the output curve and analysis of Specimen 7. This last sample underwent a post curing process in which its temperature was increased to 180°C and maintained at that level for one hour. After cooling, it was tested to learn how this post curing process had affected its thermal properties. Notice that post curing the specimen does not seem to change the CTE obtained before the T_g. It does, however, change its T_g by about 32°C.

The graphical results for test coupons 2, 3, 4, 5 and 6 are presented in Appendix A. The quartz baseline calibration plots and the two copper control runs are also shown in this Appendix.

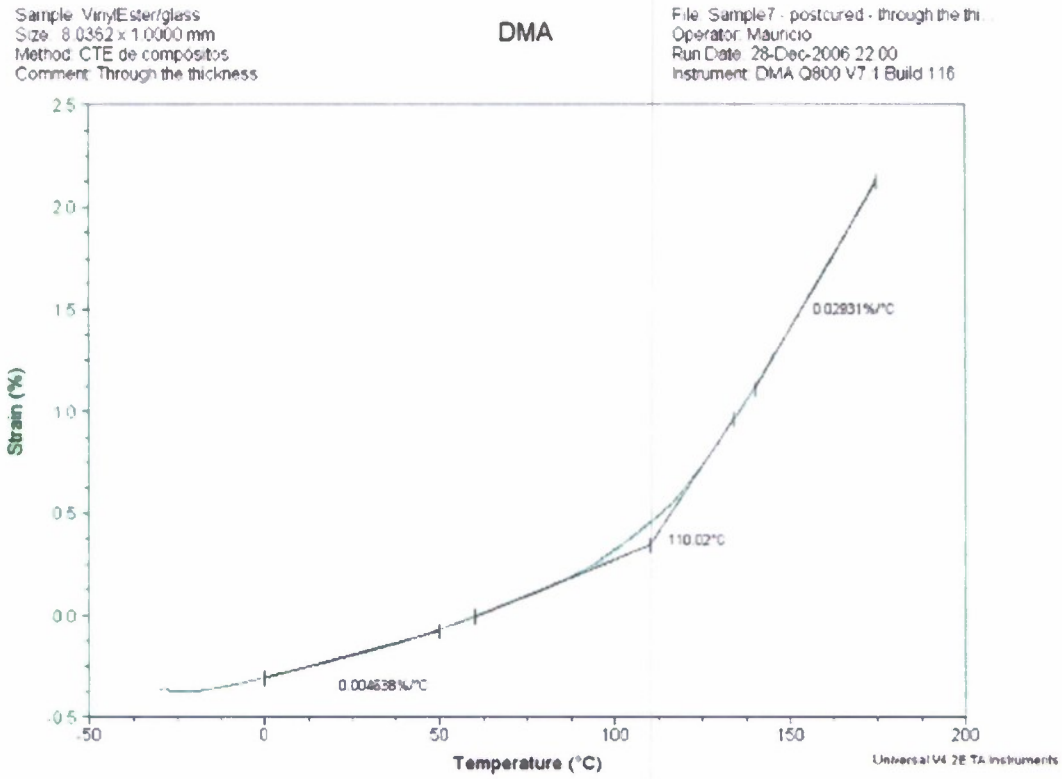

Figure 2.10 - Specimen 7 CTE and T_g Analysis

In summary, the T_g and the CTE can be obtained with reasonable repeatability by starting the tests at sub ambient temperature. The average CTE value for the EGlass/vinyl ester composite material was found to be 45.75×10^{-6}/°C (25.42×10^{-6}/°F). The average T_g was found to be 78.33 °C (173 °F). Notice that the post cured sample was not included in the above averages as it was preconditioned prior to testing. Post curing resulted in virtually no change in the CTE with a measured value of 46.4×10^{-6}/°C and raised the T_g to 110°C.

2.1.3. TMA Tests and Procedures

A sub-series of tests were performed on a Thermo Mechanical Analyzer to examine the consequences of obtaining the CTE above the T_g of the composite material. The procedure followed the general recommendations set forth by the ASTM E 831-05 Standard Test Method for Linear Thermal Expansion of Solid Materials by Thermomechanical Analysis. The instrument used to run these experiments was a Shimadzu TMA-50 Thermo Mechanical Analyzer like the one shown in Figure 2.11.

The TMA-50 is a versatile dilatometer with three measurement modes: expansion, penetration and elongation. The performance of these tests is done through the use of a magnetic force coil which applies a positive or negative load to the sample. A linear variable displacement transformer (LVDT), measures the expansion or contraction of the sample. A simple schematic figure of a typical TMA instrument is shown in Figure 2.12. Since this instrument measures the change in dimension of a sample over a given temperature range, it must be calibrated for both temperature and displacement signals.

Figure 2.11 - Shimadzu TMA 50

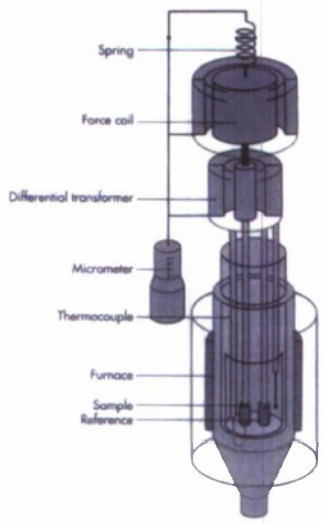

Figure 2.12 - TMA Diagram

2.1.3.1. Temperature Calibration

The temperature is calibrated using about 2 mg of pure metal melt point standards like Indium or Tin, which are available from the National Institute of Standards and Technology (NIST). This material is sandwiched between two flat platens. The upper "platen", carrying a force load transferred by the TMA expansion probe, tries to flatten the sandwiched material which resists this action due to its natural crystalline structure. As the temperature increases, the material melts and begins to flow. It is then displaced by the compressive action from the upper platen, which causes it to move downwards towards the base platen. This displacement is then detected by the LVDT. A typical calibration setup is shown in Figure 2.13. This illustration shows the pure metal melt point standards, silver, aluminum and tin in this case, separated by aluminum discs. The actual calibration procedure goes as follows: with the TMA's furnace in the up position and the sample probe resting on the sample platform with –1 g of force, the signal is zeroed out. Then the furnace is lowered and the sample probe raised from the sample platform. The sample cell is now mounted directly beneath the probe. The probe is next lowered and centered on the cell lid. After that, the furnace is closed and the signal is allowed to settle out. The run parameters are entered and the calibration is then started. Table 2.6 exhibits these calibration parameters.

Table 2.6 - Typical Temperature Calibration Parameters

Heating Rate	10°C/min
Hold Temperature	25°C above onset temp.
Hold Time	0 min
PID's	10, 10, 10
ATM	N2 @ 50ml/min
Sampling Interval	1 sec
Sample Load	-1g

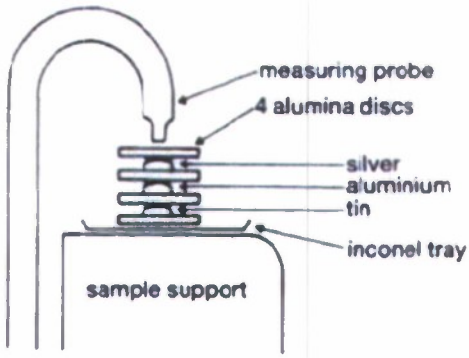

Figure 2.13 - TMA Typical Temperature Calibration Setup

The output data can be analyzed as soon as the run terminates. The point at which the probe begins to fall is called the onset point. This point is determined by extrapolating two lines tangent to either slope and finding their intersect on the temperature scale. Two onset temperatures are needed, T1 and T2. The information can be entered into the TMA-50 calibration function (FUNC 7) once these are obtained.

2.1.3.2. Displacement Calibration

Calibrating the displacement signal is relatively easy. A solid sample of known dimensions, as determined by a set of micrometers, is used. This micrometer should be properly calibrated and able to read in millimeters to three decimal places. The sample should not be any longer than 2.500 mm and the measuring surfaces should be flat, smooth and parallel. Also, the displacement signal calibration should be carried out at room temperature following the procedure outlined in Table 2.7.

The specimens tested in the TMA-50 were cubes of 8 mm cut from the same ½"-thick EGlass/vinyl ester composite panel utilized to fabricate the hybrid aluminum to composite bolted connections (see Figure 2.1). These CTE samples were machined to meet the ASTM E 831-05 standard, which states that specimens shall be between 2 and 10 mm in length and shall have flat and parallel ends to within ±25 μm. Much care was exercised to assure these pieces did not undergo any physical change during manufacturing. The goal was to avoid any changes in the structure of these samples which would therefore mask their real material properties. To accomplish such an

objective, a great deal of caution was applied to avoid excessive heat buildup during cutting and polishing of the cube's surfaces. Cooling solution was also not used to avoid the fluid from seeping into the material.

Table 2.7 - TMA Typical Displacement Signal Calibration Procedure

1. Measure the sample length using the micrometers
2. Access the calibration function FUNC 7
3. Select SIG GAIN (TMA)
4. Set SIG GAIN = 1 and press ENT
5. With the furnace in the down position and the sample probe resting on the sample platform (-1g of force), zero out the TMA signal
6. Raise the sample probe, mount the sample directly beneath the probe and then lower the probe onto the sample
7. Allow to signal to settle out
8. Record the TMA signal on the LCD screen
9. Return to FUNC 7 and enter the value into SG1 measured
10. Once this value is entered in the calibration, the measured TMA signal value on the main screen will reflect the actual sample length

2.1.3.3. TMA Testing Procedure

The Shimadzu TMA-50 is a well suited instrument for measurements of expansion coefficients and transition temperatures on relatively small samples, in a conveniently short time. The CTE test is started by placing the specimen prepared at the University of Maine Crosby Laboratory on a support within the furnace. Resting upon it is a probe to sense changes in length, which are measured by a sensitive position transducer, normally an LVDT. A load force of 10 grams was applied to the sensing probe. The probe and support are made from quartz glass (vitreous silica), which has a low, reproducible, and accurately known coefficient of thermal expansion, and also has a low thermal conductivity, which helps to isolate the LVDT from the changing temperatures in the furnace. A thermocouple near the sample indicates its temperature. There was provision for establishing a flowing gas atmosphere through the instrument, to

prevent oxidation for example, and also to assist in heat transfer to the sample. Therefore, nitrogen gas was used during the measurements at the flow rate of 50ml/min. A constant heating rate of 5°C/min was applied over the temperature range of 25°C to 120°C. All tests were run at room temperature. The temperature interval at which the CTE was obtained was 80°C to 115°C.

As it was mention above, a total of 10 specimens were tested following the test matrix summarized in Table 2.2. This testing methodology is laid out by the ASTM E 831-05 Standard. The first four, tagged 1a to 1d, were tested in the through-the-thickness direction (or direction 1). Then two sets of three samples, numbered 2a to 2c and 3a to 3c, were tested in the two in-plane directions (or directions 2 and 3, respectively). The results are presented in the next section.

2.1.3.4. TMA Results and Discussion

The results of the series of tests run in a TMA platform are presented in this section. All the samples were tested "as received", meaning no preconditioning was done prior to the test run. As it was mentioned above, four specimens, tagged 1a to 1d, were tested in the through-the-thickness direction. Figure 2.14 shows the results for the specimen 1a.

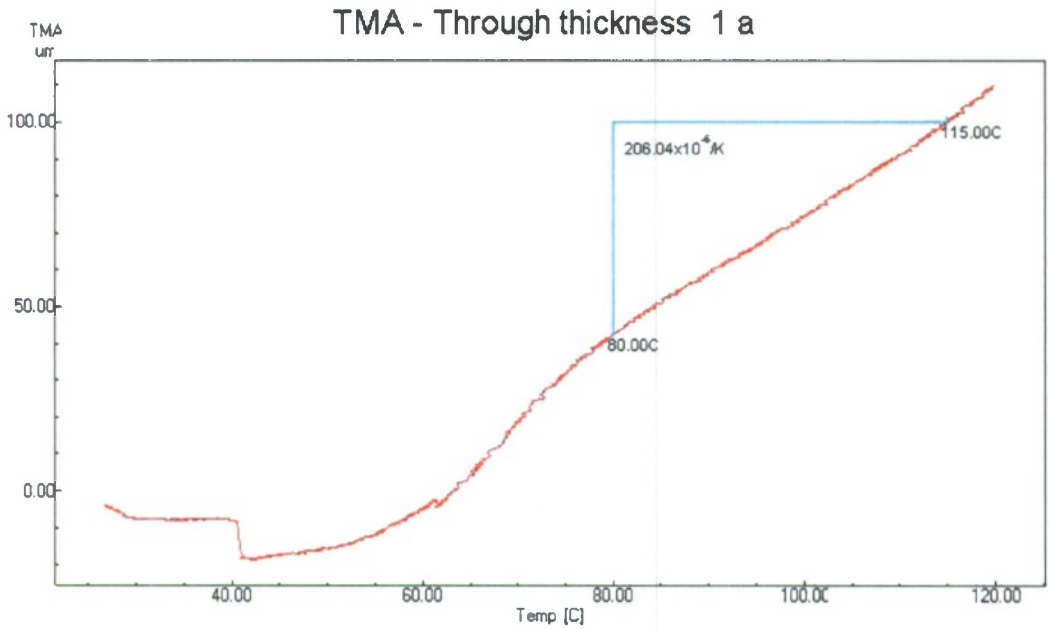

Figure 2.14 - Specimen 1a strain-temperature plot and CTE

Notice that this figure includes the CTE for this specimen as calculated by the slope of the strain-temperature curve, from 80°C to 115°C. The CTE values for the specimens 1a to 1d are summarized in Table 2.8. They are presented in °K, which can also be in °C as the changes in temperature are a 1:1 ratio.

Table 2.8 - Through the Thickness CTE Results

Sample #	Test Direction	CTE Above T_g
1a	Through-the-Thickness	$206.04 \cdot 10^{-6}$ /°K
1b	Through-the-Thickness	$222.64 \cdot 10^{-6}$ /°K
1c	Through-the-Thickness	$203.67 \cdot 10^{-6}$ /°K
1d	Through-the-Thickness	$206.57 \cdot 10^{-6}$ /°K

These measured CTE values came out excessively large, although they were repeatable and consistent. To verify the tests were carried out properly, two samples of known CTEs (Copper and Lead) were taken and processed following the same protocol. It was then confirmed that the instrument was calibrated and that the procedure was correct as the measured figure for the Copper and Lead samples perfectly matched those reported in the literature. Thus, as far as it can be said, the results above reported were correct.

Further analysis of the through the thickness results revealed that the CTE was obtained above the T_g for each specimen. A change in curvature is evident in all four plots, and it happens at around 75°C. That inflection point usually suggests the presence of a T_g, and it coincides with the T_g obtained with the DMA tests. It is then concluded that the TMA-reported CTEs were obtained above the T_g of each specimen.

It was earlier mentioned that a total of six samples were also tested in the two in plane directions (or directions 2 and 3, respectively), using the same TMA instrument and following the same testing procedure as with the through the thickness specimens. The pieces tested were named 2a to 2c and 3a to 3c. The results are presented in Appendix B. Table 2.9 summarizes the results obtained for these test articles. In the two in-plane

directions the results are not conclusive at all. These are expected results because of the significant influence of the fibers in the in-plane directions and also because of the distribution within the sample, difference in volume fractions between samples, miss orientation, etc. Thus, it is concluded that the measured in-plane CTEs measured by TMA testing are not meaningful and that the DMA test results should be used in future analyses.

Table 2.9 - In-Plane CTE Results

Sample #	Test Direction	CTE
2a	In-Plane 2	$-0.50 \cdot 10^{-6}$ /°K
2b	In-Plane 2	$1.57 \cdot 10^{-6}$ /°K
2c	In-Plane 2	$-3.82 \cdot 10^{-6}$ /°K
3a	In-Plane 3	$-9.04 \cdot 10^{-6}$ /°K
3b	In-Plane 3	$2.25 \cdot 10^{-6}$ /°K
3c	In-Plane 3	$14.54 \cdot 10^{-6}$ /°K

2.1.4. CompositePro Results

The CTE results obtained by the DMA tests were compared to those produced by CompositePro, a software tool developed by Peak Composite Innovations, a small company based in Littleton, Colorado. This Windows™ based application promises to be not just another computer program, but a practical design and analysis tool as it uses composite industry accepted methods and algorithms for its calculations. Figure 2.15 shows the actual report printed out by the application upon completion of an investigation performed on a 51% fiber volume fraction, ½"-thick EGlass/vinyl ester composite laminate. The second section of this report shows the typical material properties entered for both the fiber and the matrix components. It is assumed that the CTE of the EGlass fibers and the vinyl ester matrix are 3.0 $x10^{-6}$/°F and 360 $x10^{-6}$/°F, respectively. The third section shows the calculated micromechanics properties for the fundamental lamina. The last section of the report presents the 3D laminate properties. The CTE, CTEz, has been

isolated for identification purposes. Notice the obtained through-the-thickness CTE value, CTEz, of 3.031×10^{-5} in/in/°F (or 30.31×10^{-6} /°F = 54.56×10^{-6} /°C), which has been isolated to the right of the figure for identification purposes. DMA tests averaged to 25.42×10^{-6} /°F (45.75×10^{-6} /°C). Furthermore, in the case of a very small cube such as tested in the DMA apparatus, it may be more appropriate to neglect the thickness changes caused by the Poisson's effect and assume that $\sigma_x = \sigma_y = \tau_{xy} = 0$. In that case the CompositePro show the resulting CTE as CTE33=25×10^{-6} /°F, which is very close to the test results.

CompositePro Report

Title: 1/2" EGlass/vinyl ester Laminate 51%FV

Date: January-21-2008

Time: 8:00 PM

Fiber/matrix Properties

Fiber = EGlass Matrix = Vinyl ester

E1f (psi) = 1.050E+07 E1m (psi) = 4.600E+05

E2f (psi) = 1.050E+07 E2m (psi) = 4.600E+05

G12f (psi) = 4.400E+06 G12m (psi) = 1.699E+05

G23f (psi) = 4.400E+06 NU12m = 3.800E-01

NU12f = 2.000E-01 CTE1m (in/in/F) = 3.610E-05

NU23f = 2.000E-01 CTE2m (in/in/F) = 3.610E-05

CTE1f (in/in/F) = 3.000E-06 CME1m (in/in/%m) = 0.000E+00

CTE2f (in/in/F) = 3.000E-06 CME2m (in/in/%m) = 0.000E+00

CME1f (in/in/%m) = 0.000E+00 Km (Btu/hr/ft/F) = 8.000E-02

CME2f (in/in/%m) = 0.000E+00 +S1m (psi) = 1.050E+04

K1f (Btu/hr/ft/F) = 7.420E-01 -S1m (psi) = -1.600E+04

K2f (Btu/hr/ft/F) = 7.420E-01 S12m (psi) = 2.270E+04

+S1f (psi) = 2.700E+05 DENm (lb/in3) = 3.683E-02

-S1f (psi) = -1.600E+05

DENf (lb/in3) = 9.400E-02

End Area (in2) = 6.710E-04

Micromechanics Lamina Properties

Fiber is: EGlass

Matrix is: Vinyl ester

Extentional Properties:

E1(psi) = 5.580E+06 E2(psi) = 1.450E+06 E3(psi) = 1.450E+06

G12(psi) = 4.738E+05 G13(psi) = 4.738E+05 G23(psi) = 3.333E+05

NU12 = 2.882E-01 NU13 = 2.882E-01 NU23 = 4.377E-01

Thermal Expansion Coefficients (Units = in/in/F)

CTE1 = 4.337E-06 CTE2 = 2.500E-05 CTE3 = 2.500E-05

Moisture Expansion Coefficients (Units = in/in/%)

CME1 = 0.000E+00 CME2 = 0.000E+00 CME3 = 0.000E+00

Physical Properties (K Units = Btu/hr/ft/F):

K1 = 4.176E-01 K2 = 1.803E-01 K3 = 1.803E-01

Density (lb/in3)= 6.599E-02

Ultimate Strains:

+e1 = 2.468E-02 +e2 = 5.826E-03 +e12 = 1.258E-02

-e1 = -1.462E-02 -e2 = -8.878E-03 -e12 = -1.258E-02

Lamina Properties

Property EGVE51%

E11 (psi) 5.580E+06

E22 (psi) 1.450E+06

E33 (psi) 1.450E+06

G12 (psi) 4.738E+05

G13 (psi) 4.738E+05

G23 (psi) 3.333E+05

NU12 2.882E-01

NU13 2.882E-01

NU23 4.377E-01

CTE11 (in/in/F) 4.337E-06

CTE22 (in/in/F) 2.500E-05

CTE33 (in/in/F) 2.500E-05

CME11 (in/in/%m) 0.000E+00

CME22 (in/in/%m) 0.000E+00

CME33 (in/in/%m) 0.000E+00

+eps11 (in/in) 2.468E-02

+eps22 (in/in) 5.826E-03

+gam12 (in/in) 1.258E-02

-eps11 (in/in) -1.462E-02

-eps22 (in/in) -8.878E-03

-gam12 (in/in) -1.258E-02

K1 (Btu/hr/ft/F) 4.176E-01

K2 (Btu/hr/ft/F) 1.803E-01

K3 (Btu/hr/ft/F) 1.803E-01

DEN (lb/in3) 6.599E-02

Layup

Ply # Lamina Type Thickness(in.) Angle(deg.)

1 EGVE51% 1.563E-02 45.0

2 EGVE51% 1.563E-02 -45.0

3 EGVE51% 1.563E-02 0.0

4 EGVE51% 1.563E-02 90.0

5 EGVE51% 1.563E-02 45.0

6 EGVE51% 1.563E-02 -45.0

7 EGVE51% 1.563E-02 0.0

8 EGVE51% 1.563E-02 90.0

9 EGVE51% 1.563E-02 45.0

10 EGVE51% 1.563E-02 -45.0

11 EGVE51% 1.563E-02 0.0

12 EGVE51% 1.563E-02 90.0

13 EGVE51% 1.563E-02 45.0

14 EGVE51% 1.563E-02 -45.0

15 EGVE51% 1.563E-02 0.0

16 EGVE51% 1.563E-02 90.0

17 EGVE51% 1.563E-02 90.0

18 EGVE51% 1.563E-02 0.0

19 EGVE51% 1.563E-02 -45.0

20 EGVE51% 1.563E-02 45.0

21 EGVE51% 1.563E-02 90.0

22 EGVE51% 1.563E-02 0.0

23 EGVE51% 1.563E-02 -45.0

24 EGVE51% 1.563E-02 45.0

25 EGVE51% 1.563E-02 90.0

26 EGVE51% 1.563E-02 0.0

27 EGVE51% 1.563E-02 -45.0

28 EGVE51% 1.563E-02 45.0

29 EGVE51% 1.563E-02 90.0

30 EGVE51% 1.563E-02 0.0

31 EGVE51% 1.563E-02 -45.0

32 EGVE51% 1.563E-02 45.0

2D Laminate Properties

Extentional Properties:

Ex(psi) = 2.721E+06 Ey(psi) = 2.721E+06 Gxy(psi) = 1.028E+06

NUxy = 3.231E-01 NUyx = 3.231E-01

Flexural Properties:

Exb(psi) = 2.606E+06 Eyb(psi) = 2.457E+06

Thermal Expansion Coefficients (CTE Units = in/in/F, CTEk Units = 1/in/F)

CTEx = 9.244E-06 CTEy = 9.244E-06 CTExy = 2.120E-15

CTExk = -2.193E-20 CTEyk = 4.980E-21 CTExyk = -4.128E-20

Moisture Expansion Coefficients (CME Units = in/in/%, CMEk Units = 1/in/%)

CMEx = 0.000E+00 CMEy = 0.000E+00 CMExy = 0.000E+00

CMExk = 0.000E+00 CMEyk = 0.000E+00 CMExyk = 0.000E+00

Physical Properties:

Density (lb/in3)= 6.599E-02 Thickness (in)= 5.002E-01

3D Laminate Properties

Extentional Properties:

Ex(psi) = 2.722E+06 Ey(psi) = 2.722E+06 Ez(psi) = 1.600E+06

Gxy(psi) = 1.029E+06 Gxz(psi) = 4.035E+05 Gyz(psi) = 4.035E+05

NUxy = 3.229E-01 NUyx = 3.229E-01

NUxz = 3.023E-01 NUzx = 1.777E-01

NUyz = 3.023E-01 NUzy = 1.777E-01

Thermal Expansion Coefficients (CTE Units = in/in/F)

CTEx = 9.244E-06 CTEy = 9.244E-06

CTEz = 3.031E-05

CTExy = 2.119E-15 CTEyz = 0.000E+00 CTEzx = 0.000E+00

Moisture Expansion Coefficients (CME Units = in/in/%m)

CMEx = 0.000E+00 CMEy = 0.000E+00 CMEz = 0.000E+00

CMExy = 0.000E+00 CMEyz = 0.000E+00 CMEzx = 0.000E+00

Thermal Conductivity (K Units = Btu/hr/ft/F)

Kx = 2.990E-01 Ky = 2.990E-01 Kz = 1.803E-01

Kxy = -1.217E-11

Physical Properties:

Density (lb/in3)= 6.599E-02 Thickness (in)= 5.002E-01

Figure 2.15 – CompositePro Results for a ½'-thick Quasi-Isotropic EGlass/vinyl ester Laminate

2.2. Temperature Effects in Hybrid Metal-to-Composite Bolted Connections

An instantaneous change in temperature in a homogeneous, isotropic material tends to produce a change in its dimensions. Usually, if the temperature of such material increases and the material is free to expand in all directions, it will do so. On the other hand, if the material temperature decreases, it will contract in all directions. The strains that develop due to a change in temperature are called thermal strains. Thermal strains are considered positive if the material expands, and negative if the material contracts. Thermal strains are defined by the equation:

$$\varepsilon_t = \frac{\delta_t}{L} = \alpha \cdot (\Delta T) \tag{2.1}$$

where δ_t represents the elongation (or contraction) due to the temperature change ΔT, L is the length of the part and α is the coefficient of thermal expansion, a material property.

The analysis of hybrid bolted connections exposed to variable temperature conditions is a little more challenging than that of joints which mate parts made by the same type of material. The reason is the mismatch in the coefficients of thermal expansion of the materials that constitute the connection. It is then necessary to develop a technique that allows for the analysis of hybrid joint bolt load data which has been affected by temperature fluctuations during the experimental runs. Hence, the primary objective of this section is to propose a model that closely predicts the change in bolt load factoring in the isolated effects of temperature.

2.2.1. Hybrid Thermal Model

To illustrate the effect of temperature on a hybrid connection, let's consider two dissimilar materials, Material 1 to Material 2 used in a bolted connection as depicted in Figure 2.16. The assumption is that the connection is held at a temperature T, and that at this temperature the joint is at its baseline stress level. Also, negligible creep effects are assumed in the development of this model. All the variables used in the development of this model are presented below:

t_1 – Material 1 thickness

t_2 – Material 2 thickness

D_b – Bolt diameter

D_I – Influence Zone diameter

E_b – Modulus of Elasticity of bolt material

E_1 – Modulus of Elasticity of Material 1

E_2 – Modulus of Elasticity of Material 2

K_1 – Stiffness of Material 1

K_2 – Stiffness of Material 2

K_b - Stiffness of bolt

α_b – Coefficient of Thermal Expansion of bolt material

α_1 - Coefficient of Thermal Expansion of Material 1

α_2 - Coefficient of Thermal Expansion of Material 2

δ_{t1} – Thermal elongation or unconfined growth of Material 1

δ_{t2} – Thermal elongation or unconfined growth of Material 2

δ_{tb} – Thermal elongation or unconfined growth of bolt

Δ_b – Net length change of bolt

$\Delta_{1,2}$ – Net length change of both Material 1 and Material 2

ΔT – Temperature change

P_t – Change in connection load due to a change in temperature, ΔT

If the temperature is increased by an amount ΔT, stresses in the through-the-thickness direction will develop in the connection due to the above-mentioned differences

in thermal expansion coefficient between the parts that constitute the joint. Temperature changes in statically indeterminate structure will usually produce stresses in its members. To visualize this in a simple manner, a model of the connection has been sketched in Figure 2.17. In this diagram, D_I is the diameter of the Influence Zone and it represents the area affected by the compressive force under both the bolt and washer. D_I is an estimated value and it was obtained from experiments previously carried out on this type of connections, using Fujifilm Prescaled Pressure Paper [Pelletier et al., 2005].

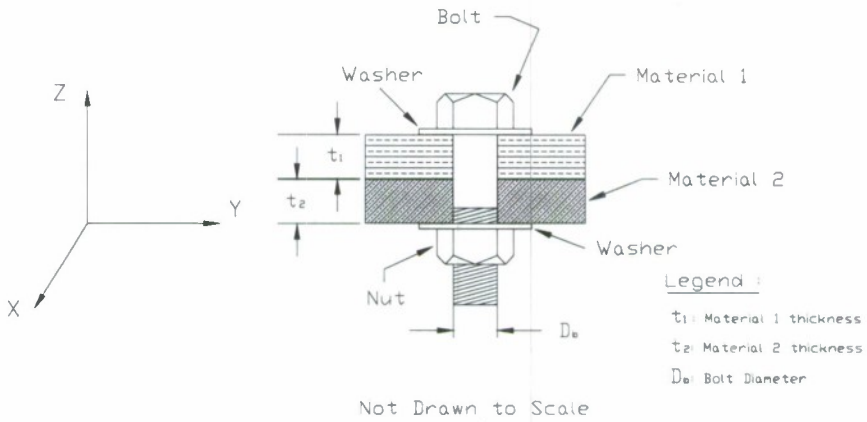

Figure 2.16 - Cross-Section of a Bolted Hybrid Connection.

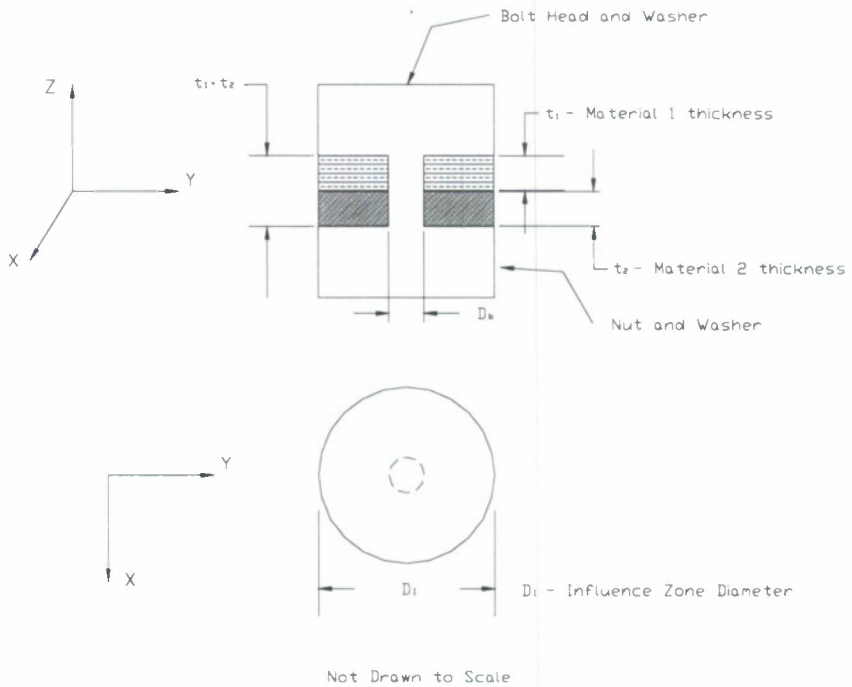

Figure 2.17 – Schematic Diagram of a Hybrid Connection

If the top part of the joint is removed, as shown in Figure 2.18, the bolt shank and both materials 1 and 2 will be free to expand in the through-the-thickness direction (Z-direction) with ΔT. Clearly, the thermal strains of these three parts will be different from each other. If δ_{tb}, that is, the thermal elongation in the bolt shank, is smaller than the combined elongation of both materials 1 and 2, $\delta_{t1} + \delta_{t2}$, then the joint will experience an increment in stress, which will be translated to an increase in bolt load. On the other hand, if δ_{tb} turns out to be larger, then clearances will develop. If the joint was loaded prior to this ΔT, stress relaxation will occur over time.

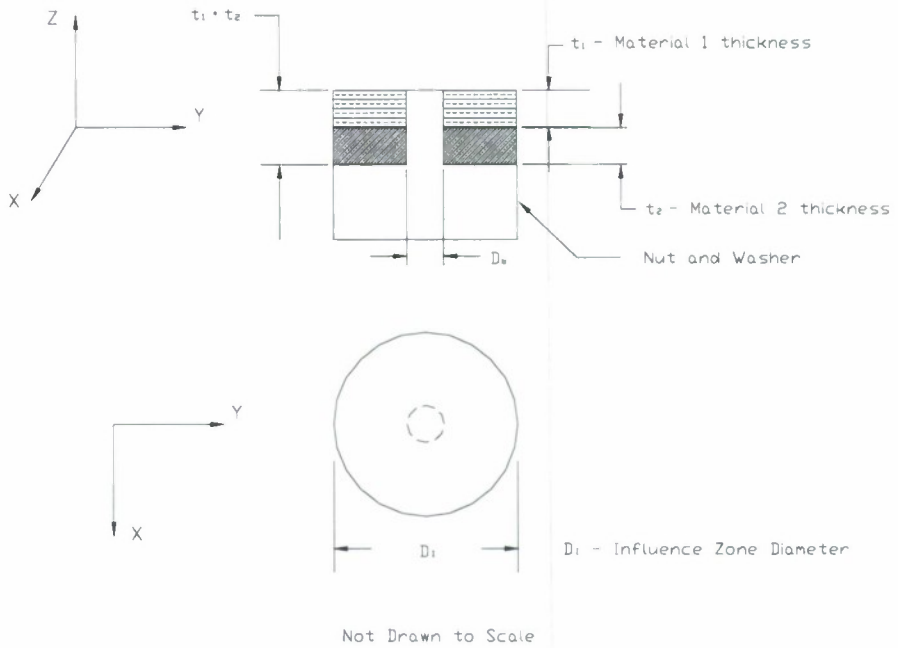

Figure 2.18 – Hybrid Connection Permitted to Expand

To maintain joint integrity, it is desired that the elongation of the bolt be equal to the sum of the elongations in materials 1 and 2, that is:

$$\delta_{tb} = \delta_{t1} + \delta_{t2} \tag{2.2}$$

where δ_{tb} is the thermal elongation in the shank of the bolt, δ_{t1} is the thermal elongation of Material 1 and δ_{t2} is the thermal elongation of Material 2.

A theoretical analysis of the effects of temperature in hybrid connection fastening two different materials, namely Material 1 and Material 2 is presented in the next paragraphs. The ultimate objective is to develop a technique that allows for the prediction in change in bolt load due to temperature and for the correction of bolt load data which has been affected by temperature fluctuations during the experimental runs.

The following two assumptions are considered in the development of this analysis:

1. The connection is free to thermally expand in the X and Y directions, as well as in the direction of interest, the through-the-thickness direction (Z direction).
2. The diameter of the bolt hole is taken to be that of the bolt itself. In reality, a tolerance must be introduced at the time of drilling. This tolerance is assumed to be negligible for the purpose of the analysis.

The area of the above mentioned Influence Zone, A_I, is calculated using the formula:

$$A_I = \pi \cdot \frac{(D_I^2 - D_b^2)}{4} \tag{2.3}$$

and that of the bolt hole is given by:

$$A_b = \pi \cdot \frac{D_b^2}{4} \tag{2.4}$$

The stiffness for materials 1 and 2 and that for the bolt are, respectively:

$$K_1 = \frac{A_I \cdot E_1}{t_1} \tag{2.5}$$

$$K_b = \frac{A_b \cdot E_b}{t_1 + t_2} \tag{2.6}$$

$$K_2 = \frac{A_I \cdot E_2}{t_2} \tag{2.7}$$

The thermal elongation or unconfined growth of the bolt, Material 1 and Material 2, due to a temperature change ΔT, are, respectively:

$$\delta_{tb} = \alpha_b \cdot (t_1 + t_2) \cdot \Delta T \tag{2.8}$$

$$\delta_{t1} = \alpha_1 \cdot (t_1) \cdot \Delta T \tag{2.9}$$

$$\delta_{t2} = \alpha_2 \cdot (t_2) \cdot \Delta T \tag{2.10}$$

The net length change of the bolt and that of both Material 1 and Material 2 is found using the equations:

$$\Delta_b = \delta_{tb} + \frac{P_t}{K_b} \tag{2.11}$$

$$\Delta_{1,2} = \delta_{t1} + \delta_{t2} - \frac{P_t}{K_1 + K_2} \tag{2.12}$$

To maintain joint integrity, the following condition must be met:

$$\Delta_b = \Delta_{1,2} \tag{2.13}$$

Substituting Equations (2.11) and (2.12) into Equation (2.13) yields:

$$\delta_{tb} + \frac{P_t}{K_b} = \delta_{t1} + \delta_{t2} - \frac{P_t}{K_1 + K_2} \tag{2.14}$$

Substituting Equations (2.8), (2.9) and (2.10) and solving for P_t gives:

$$P_t = \left[\frac{\alpha_1 \cdot t_1 + \alpha_2 \cdot t_2 - \alpha_b \cdot (t_1 + t_2)}{\frac{1}{K_b} + \frac{1}{K_1 + K_2}} \right] \cdot \Delta T \tag{2.15}$$

Equation (2.15) gives the prediction of load change, P_t, in the hybrid connection due to a temperature change, ΔT. The Influence Zone, also called the Effective Area, represents the area affected by the compressive force of the bolt and washer combination (see Figures 2.16 and 2.17). The Influence Zone was estimated using the impression left on a thin film of Fujifilm Prescaled Pressure paper [Pelletier et al., 2005]. Figure 2.19 is an example of such an impression, with its corresponding pressure distribution color chart.

The diameter of this area was estimated to be roughly twice the diameter of the bolt hole for a ½"-thick specimen loaded to 5,000 lbs. Figure 2.20 shows how P_t changes as a function of the ratio of α_1 to α_b, for different ratios of both α_2 to α_b and t_1 to t_2 and for $D_I = 2 \cdot D_b$. In Figure 2.20, Pt=P_t, t1=t_1, t2=t_2, CTE1=α_1, CTE2=α_2 and CTEb=α_b. It is obvious that P_t will be zero for $\alpha_1=\alpha_2=\alpha_b$, but it will also be zero if the right conditions in terms of material properties and geometrical considerations are met. Notice that the connection load response is, in all cases, linear in nature. The ratio variations shown in Figure 2.20 only shift the P_t curve upward or downward or affect its slope.

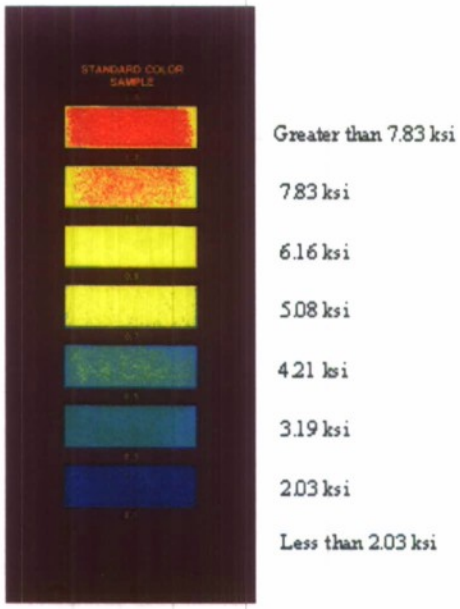

a) Fujifilm Pressure Distribution Color Chart

b)

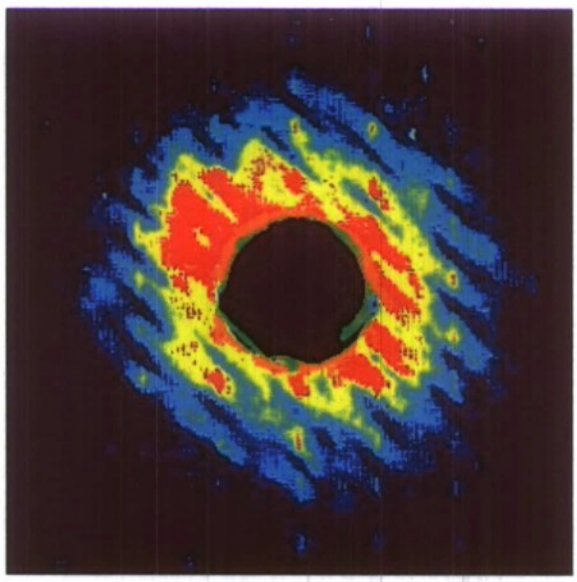

Figure 2.19 - Pressure Distribution for ½"-thick Specimen Loaded to 5,000 lbs [Pelletier et al., 2005]

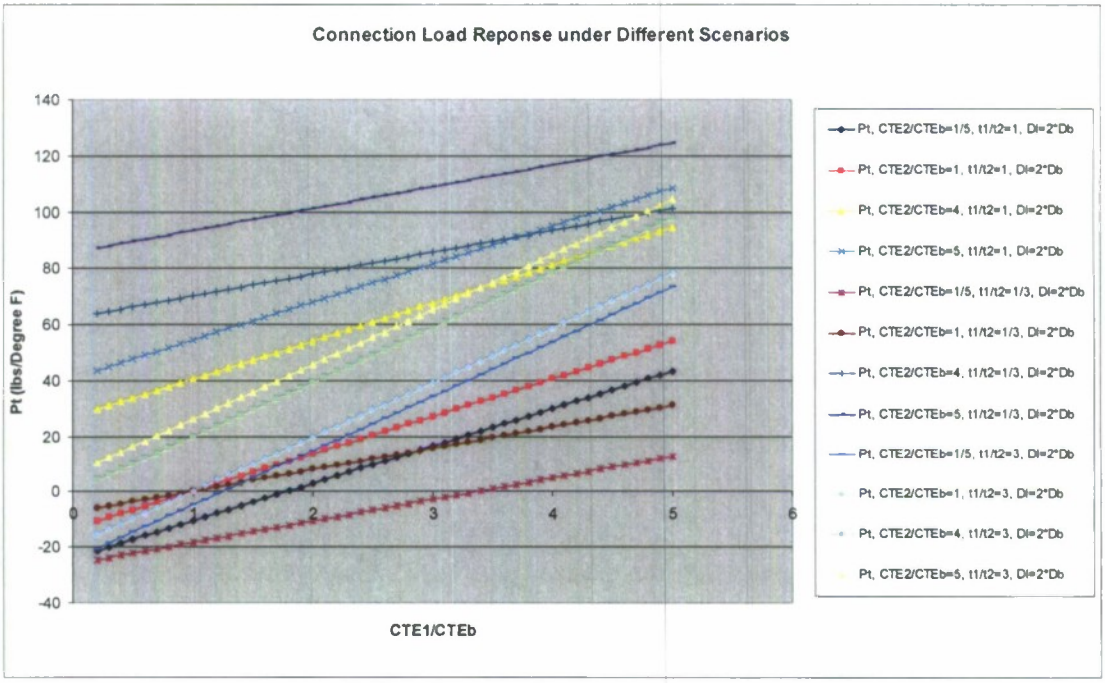

Figure 2.20 – Change in Pt for Different Ratios of α_1/α_b and α_2/α_b and for $D_I=2 \cdot D_b$

Figure 2.21 depicts the change in P_t as a function of the ratio of α_1 to α_b, for different values of D_I and for $\alpha_2/\alpha_b=4$. Varying the diameter of the Influence Zone, D_I, also affects the slope of the P_t vs. α_1/α_b curve. The general behavior presented in Figures 2.20 and 2.21, which is linear in nature, is given in the SAE system. The same conclusions can be drawn using SI units.

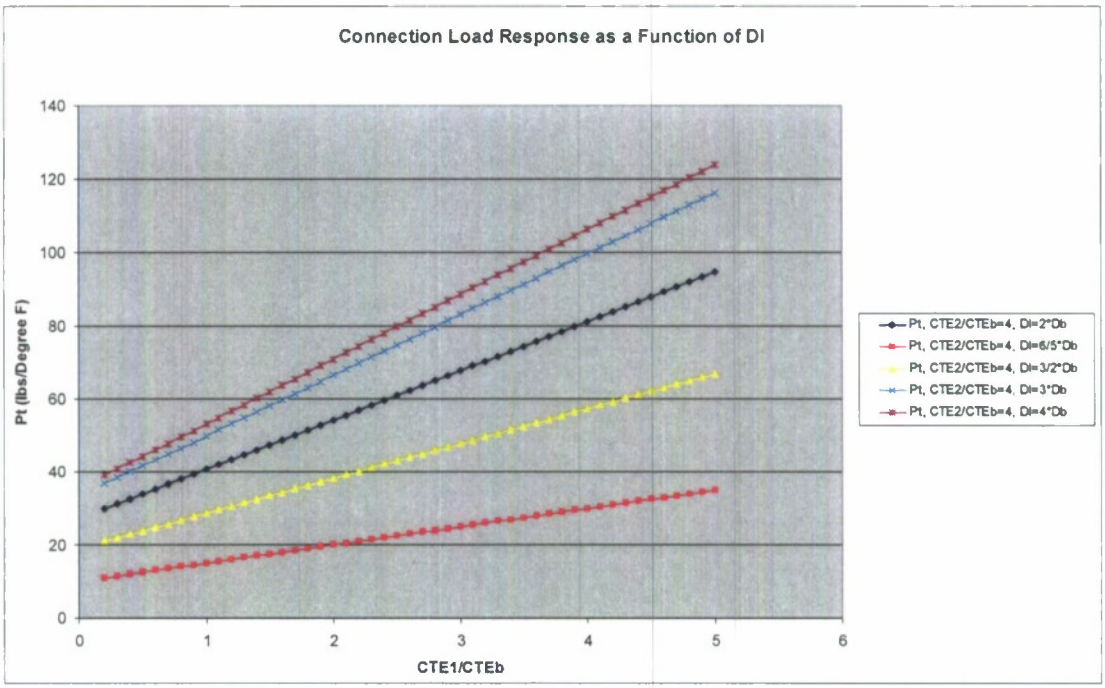

Figure 2.21 - Change in P_t as a function of α_1/α_b and D_1, for $\alpha_2/\alpha_b=4$

To illustrate how this model works, consider the hybrid aluminum to EGlass/vinyl ester bolted connection represented by Figure 2.16. Table 2.10 shows the material properties for the parts involved in the analysis of the hybrid joint. The aluminum and steel properties are readily available in the literature. The Modulus of Elasticity of the composite material, E_c, was experimentally obtained performing tension tests on 12.7 mm (½") thick specimens following the ASTM 3094 standard [Pelletier et al., 2005].

Table 2.10 - Material Properties

Material	Modulus of Elasticity (US Customary)	Coefficient of Thermal Expansion (US Customary)
Aluminum 6061-T6	$E_{Al} = 69$ GPa $(10 \cdot 10^6$ psi)	$\alpha_{Al} = 23.4 \cdot 10^{-6} \cdot \frac{1}{\circ C}$ $(13 \cdot 10^{-6} \cdot \frac{1}{\circ F})$
Steel	$E_b = 207$ GPa $(30 \cdot 10^6$ psi)	$\alpha_b = 12 \cdot 10^{-6} \cdot \frac{1}{\circ C}$ $(6.5 \cdot 10^{-6} \cdot \frac{1}{\circ F})$
EGlass/vinyl ester	$E_c = 14$ GPa $(2 \cdot 10^6$ psi)	$\alpha_c = 45.75 \cdot 10^{-6} \cdot \frac{1}{\circ C}$ $(25.42 \cdot 10^{-6} \cdot \frac{1}{\circ F})$

Figure 2.22 shows the Mathcad sheet used to demonstrate this specific example. The result shows that the load in a single bolt, hybrid aluminum to EGlass/vinyl ester connection with geometrical dimensions as given in the example and also depicted in Figures 2.16 to 2.18 will, according to this prediction, linearly vary at the rate of 51.6 lbs per degree F of temperature change. The load change per degree F, P_t, as a function of α_c is shown in Figure 2.23. Notice that this change is also linear in nature.

In the next section, the method used to analyze the bolt load data that was generated by a series of experimental tests run of hybrid connections is presented. Temperature effects on bolt load data were corrected using the GASmooth software tool developed specifically for this purpose.

2.3. Adjustment Method for Ambient Relaxation Data for Temperature Changes

Relaxation tests done at ambient conditions will suffer from data being modified by temperature shifts and unavoidable data collection noise. It is desired to develop an efficient system able to use bolt load data from an ambient experimental run and correct it for the inherent temperature variations that occurred during that run. This is done so that appropriate power law constants can be computed from ambient data without the influence of experimental noise and temperature shifts. To meet this end, a computer program was devised and hard coded under the GASmooth designation. GASmooth stands for "Genetic Algorithm Smooth", and it was written in Borland Delphi 5 at the Mechanical Engineering Department of the University of Maine.

The material properties, as presented in Table 2.10, are:

$\alpha_{Al} := 13 \cdot 10^{-6}$ 1/F $\quad \alpha_b := 6.5 \cdot 10^{-6}$ 1/F $\quad \alpha_c := 25.42 \cdot 10^{-6}$ 1/F

$E_{Al} := 10 \cdot 10^{6}$ psi $\quad E_b := 29 \cdot 10^{6}$ psi $\quad E_c := 2.0 \cdot 10^{6}$ psi

The thicknesses of the aluminum and composite plates are, respectively:

$t_{Al} := \frac{1}{2}$ in $\quad t_c := \frac{1}{2}$ in

The bolt size and the Influence Zone diameter are, respectively:

$D_b := \frac{1}{2}$ in $\quad D_I := 2 \cdot D_b$

The contact area for the aluminum and for the composite plates are, respectively:

$$A_{Al} := \pi \cdot \frac{\left(D_I^2 - D_b^2\right)}{4} \qquad A_c := \pi \cdot \frac{\left(D_I^2 - D_b^2\right)}{4}$$

The cross sectional area of the bolt is:

$$A_b := \pi \cdot \frac{D_b^2}{4}$$

The stiffness for the aluminum and composite materials and that for the bolt material (steel) are found, respectively, as:

$$K_{Al} := \frac{A_{Al} \cdot E_{Al}}{t_{Al}} \qquad K_c := \frac{A_c \cdot E_c}{t_c} \qquad K_b := \frac{A_b \cdot E_b}{t_{Al} + t_c}$$

The thermal elongation due to a temperature change or unconfined growth of the bolt, the aluminum plate and that of the composite plate, per degree F are , respectively:

$\delta_{tb} := \alpha_b \cdot (t_{Al} + t_c)$ $\quad \delta_{tb} = 6.5 \times 10^{-6}$ in/F

$\delta_{tAl} := \alpha_{Al} \cdot (t_{Al})$ $\quad \delta_{tAl} = 6.5 \times 10^{-6}$ in/F

$\delta_{tc} := \alpha_c \cdot (t_c)$ $\quad \delta_{tc} = 1.271 \times 10^{-5}$ in/F

The net length change of the bolt and that of the aluminum and the composite plates is found using the equations:

$$\Delta_b = \delta_{tb} + \frac{P_t}{K_b} \qquad (1)$$

$$\Delta_{Alc} = \delta_{tAl} + \delta_{tc} - \frac{P_t}{K_{Al} + K_c} \qquad (2)$$

To maintain joint integrity, the following condition must be met:

$$\Delta_b = \Delta_{Alc} \qquad (3)$$

Substituting equations (1) and (2) into equation (3) and solving for Pt gives:

$$P_t := \left(\delta_{tAl} + \delta_{tc} - \delta_{tb}\right) \cdot \frac{K_b \cdot (K_{Al} + K_c)}{K_{Al} + K_c + K_b} \qquad P_t = 51.592 \text{ lbs/F}$$

Figure 2.22 – Mathcad Calculation Example Print Out

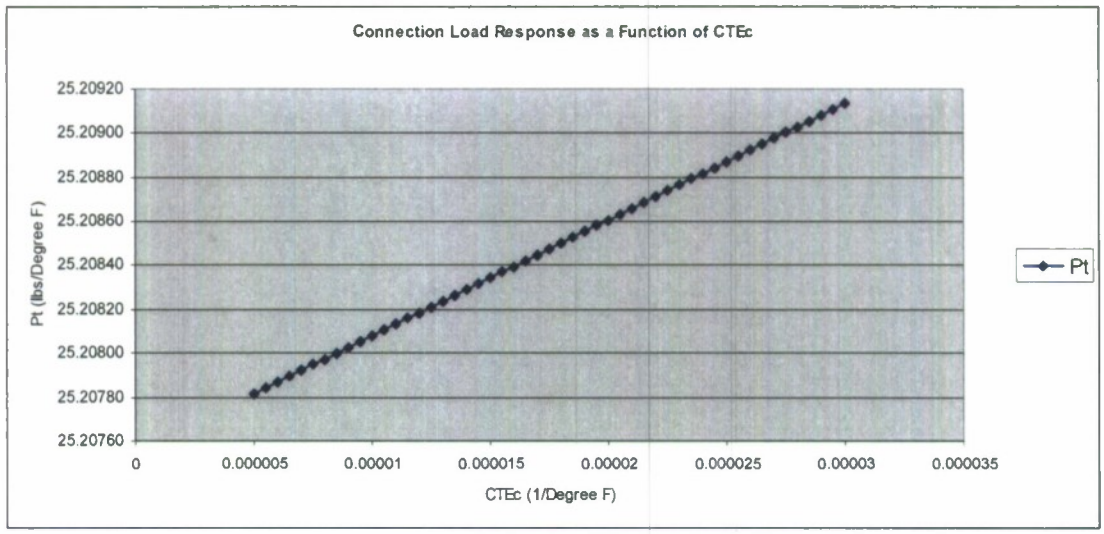

Figure 2.23 – Prediction Load Response as a Functions of CTEc

Launching the GASmooth software opens up the control dialogue box, as shown in Figure 2.24. This window allows the user to import the desired time-history data file, whether a load or a temperature or a combination of these two. Only .csv file formats can be imported in. Figure 2.25 shows a screen shot of the analysis window, which is opened by clicking on the "Analyze" button in the control window. The program allows for three types of data management: it can interpolate, smooth out using a moving average filter (MA_Filter), or temperature correct the data. All data manipulation is done graphically and by entering the following four variables, which are listed under the "GroupBox2" box:

NPTS:

Order:

Base Temp: is the temperature at which the experiment started.

Temp Factor: is the temperature correction factor for the hybrid connection, K_{pt}.

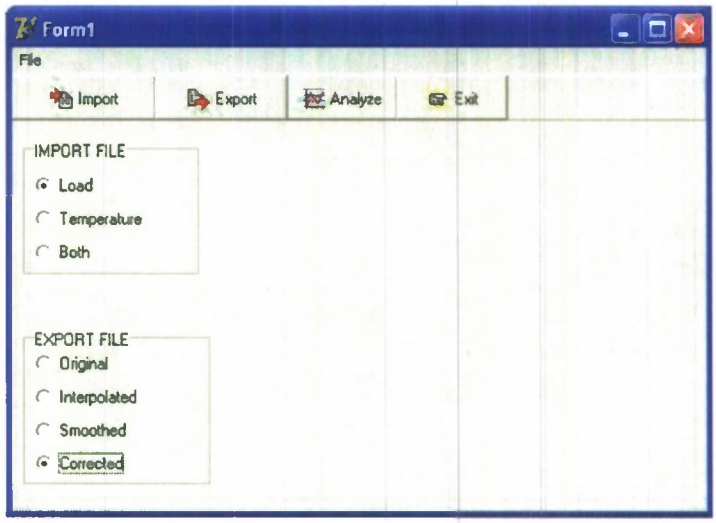

Figure 2.24 – GASmooth Control Window Screen Shot

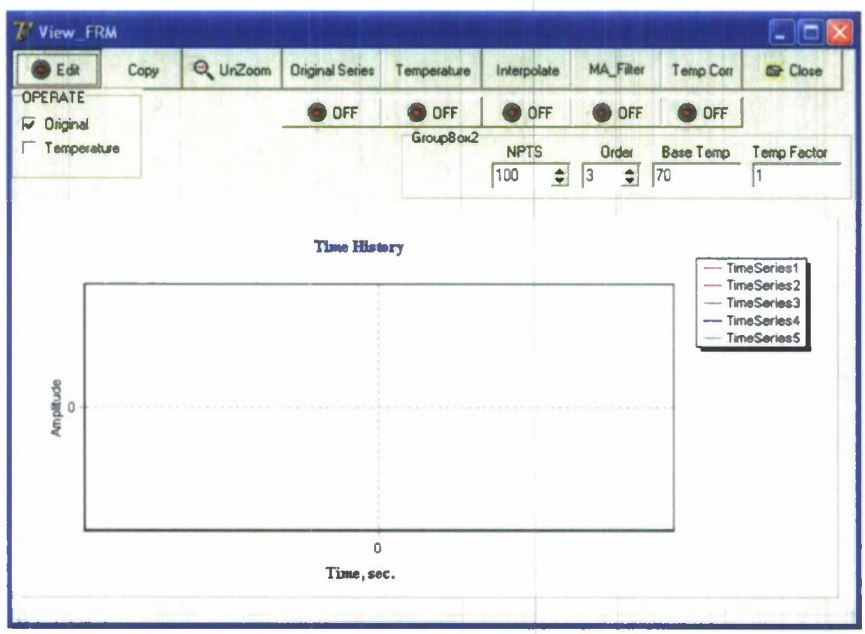

Figure 2.25 – GASmooth Analysis Window Screen Shot

Figure 2.25 also shows that the software permits the user to turn on and off the interpolated, or the filtered or the corrected data on demand. This feature is particularly useful when a quick visual comparison with the original data plot is desired. Finally, the "adjusted" data file can be exported to the desired directory by pressing the "Export' button in the control window.

GASmooth temperature corrects the data based data from a temperature transducer using the expression:

$$P_{corrected} = P_{measured} - \left[\left(T_{actual} - T_{base} \right) \cdot K_{pt} \right] \tag{2.15}$$

where:

$P_{corrected}$ is the adjusted measured bolt load.

$P_{measured}$ is the recorded bolt load.

T_{actual} is the recorded temperature when the recorded load was entered.

T_{base} is the temperature of the previous data point.

K_{pt} is the temperature correction factor for the hybrid connection.

The temperature correction factor for the hybrid connection, K_{pt}, is defined as:

$$K_{pt} = P_t / \Delta T \tag{2.16}$$

where P_t is the prediction of load change in the hybrid connection due to a temperature change, ΔT, as given by Equation (2.15). Notice that the units of K_{pt} are lbs per degree F. To correct the experimentally obtained bolt load data, appropriate values of E_c and α_c are needed. The CTE of the composite material was successfully obtained through the DMA tests presented in Section 2.1.2. The modulus of elasticity of the EGlass/vinyl ester material was experimentally obtained performing tension tests on 12.7 mm (½") thick specimens following the ASTM 3094 standard [Pelletier et al., 2005].

3. SINGLE BOLT HYBRID CONNECTION TESTS

In this chapter, the series of tests conducted to study the effects of temperature and temperature cycling on the response in the through-the-thickness direction of single bolt, metal to EGlass/vinyl ester composite connections, is presented. These environmental tests were performed to assess the effect of temperature change on the stress relaxation response of hybrid metal to composite connections. A group of six specimens, including the control, were tested. The first part of the experiment ran under room temperature conditions, and the second cycled these test articles, except the control, from room temperature to an elevated temperature of 63°C. All composite specimens were cut from EGlass/vinyl ester composite panels, fabricated at the University of Maine Crosby Laboratory, using the VARTM (Vacuum Assisted Resin Transfer Molding) process. Specific details on the test articles, materials and instrumentation used to run these experiments are also presented in this section.

3.1. Test Methodology

The tests performed in this study have been summarized in Table 3.1. Notice that although the primary focus of this study is centered in the transverse response of hybrid aluminum to EGlass/vinyl ester single bolted connections to environmental conditions, specimens joining aluminum to aluminum, steel to EGlass/vinyl ester composite and EGlass/vinyl ester composite to EGlass/vinyl ester composite were also included for reference. In all, a total of six articles were tested, as shown in Table 3.1, including the control specimen. The nominal preload levels applied are also shown in this table.

The first part of the experiment ran for 25 days and under room temperature conditions. Specimens were allowed to relax to equilibrium during this phase. The second part, which ran for 70 days, temperature cycled 5 of the 6 test articles (except the control). This was performed in a computer controlled autoclave. The temperature ranged from room temperature to 63°C (145°F). A data acquisition system was used to collect all test data generated during the entire length of the experimental run. At periodic intervals, data was collected for preliminary analysis.

Table 3.1 – Test Matrix

Specimen Name	Specimen Type	Nominal Preload (lbf)	Test Type
C/Al outside	Composite to Aluminum	5,047	Control: Relaxation* Only
C/Al inside 1	Composite to Aluminum 1	5,461	Relaxation* and Temperature Cycling†
C/Al inside 2	Composite to Aluminum 2	6,086	Relaxation* and Temperature Cycling†
Al/Al inside	Aluminum to Aluminum	4,795	Relaxation* and Temperature Cycling†
C/St inside	Composite to Steel	5,166	Relaxation* and Temperature Cycling†
C/C inside	Composite to Composite	4,985	Relaxation* and Temperature Cycling†

*Relaxation: specimens are left to relax for 25 days

†Temperature Cycling: Specimens are temperature cycled five times from room temperature to 145°F ± 3°F every 7 days.

Figure 3.1 shows an overview of the test specimen architecture and the scheme used for testing. All test specimens shared the geometry shown in Figure 3.1. Figure 3.2 shows a photograph of the aluminum to EGlass/vinyl ester composite control specimen. Figure 3.3 shows a photograph of the 5 test articles that underwent the temperature cycles inside the autoclave.

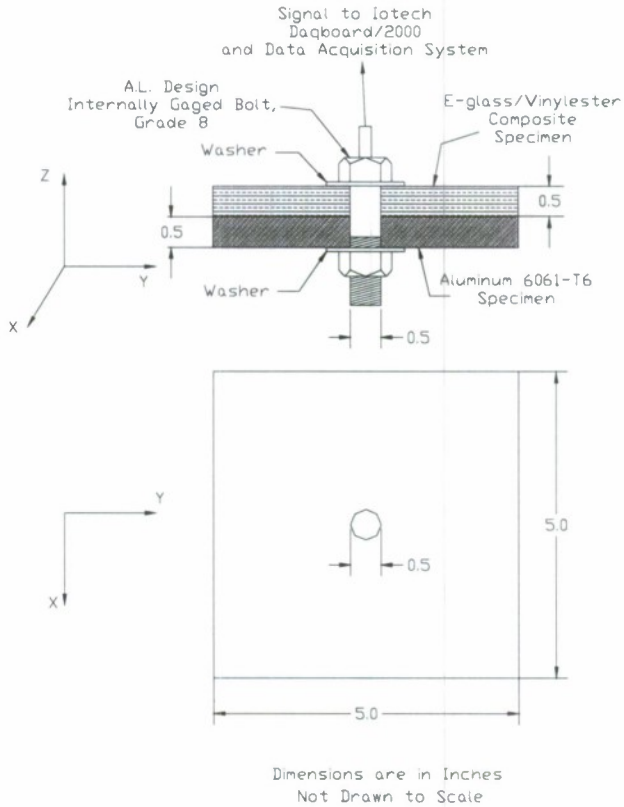

Figure 3.1 – Single Bolt Hybrid Connection Test Specimen Schematic

Figure 3.2 – Hybrid Aluminum to EGlass Vinyl ester Composite Control Specimen

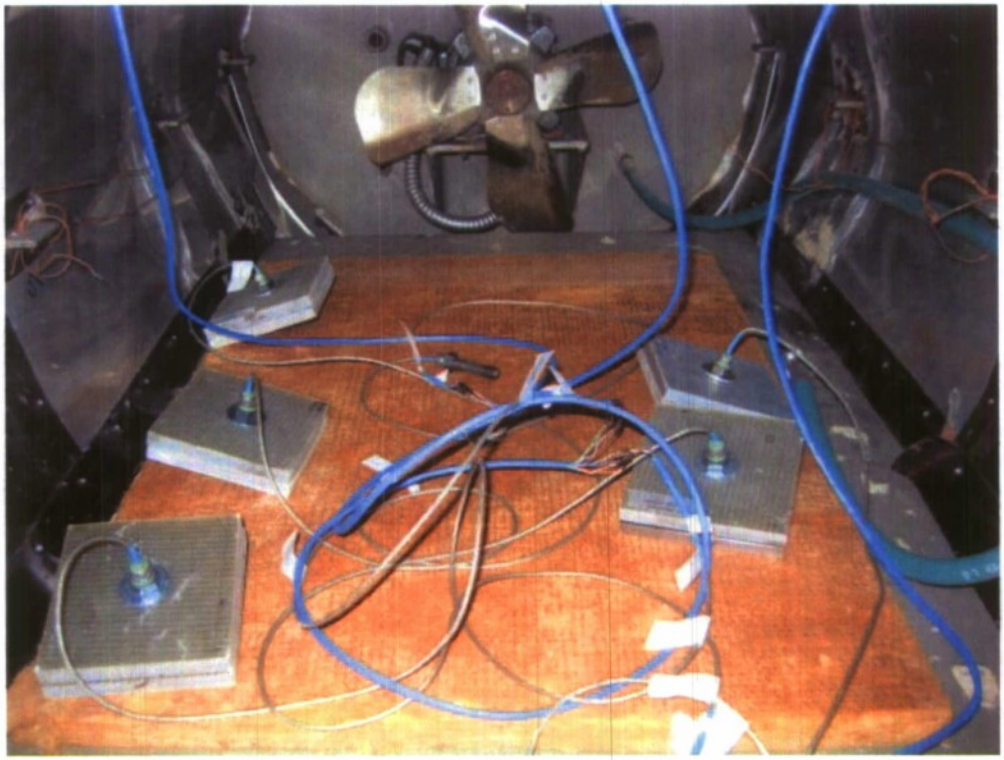

Figure 3.3 – Autoclave Test Setup

The ½" thick EGlass/vinyl ester composite specimens have a quasi-isotropic lay-up and their side length has been made equal to 10 times their thickness. They have a hole in the center equal to the diameter of the bolt, d. The plates are bolted together using internally gaged 1/2 –inch diameter bolts (AL Design Model ALD-BOLT-.5" X 2" LONG), used to monitor the load in the connection. These bolts, supplied by A.L. Design Inc., are used to measure load during the tests and they were tightened using a Blackhawk dial torque wrench with a maximum capacity of 175 ft lb. The load relaxation and the temperature data are collected using an lOTech data acquisition system with a 16-bit resolution and a computer code called DAFQI. The DAFQI program was created at UMaine, and a module was written specifically to run the stress relaxation tests.

3.1.1. Single Bolt Test Articles

The geometry of the single bolt test specimen was chosen to insure that the plate was wide enough to observe the entire pressure distribution at the composite/metal

interface of the bolts due to the stress intensification below the bolt head. It was determined using a finite element model of the geometry used in these tests, that pressure effects can be seen at a radial distance of, at most, 3 times the bolt diameter from the center of the bolt line. Choosing a test article that is 10 times the bolt diameter along its length enables the entire pressure distribution to be confined well within the specimen's geometrical limits. Metal plates of either 6061-T6 aluminum or A-36 steel, of the same dimensions as the composite plate, are bolted to the composite specimens. All composite specimens were cut from the same panel of EGlass/vinyl ester composite. They were also cut and drilled using diamond coated, water lubricated tooling.

3.1.2. Single Bolt Test Procedures

Once the specimens have been cut, holes drilled, and the bolts connected to the power supply and data acquisition system, the assembled test articles are finally ready to be loaded to the desired preload. The internally gaged bolts contain full bridge strain gages that are used to read the applied load. They were all calibrated to allow direct reading of the bolt load by the data acquisition system.

In order to load a bolted connection, the connection is held relatively stationary during tightening. The specimens are tightened in the following manner. The first specimen is placed in a tightening fixture to hold it in place. Nickel based Locktite anti-seize is applied lightly to the end of the bolt. The dial torque wrench is then used to apply load to the bolts. A data file is opened, and the load is monitored through the monitoring feature of the DAQFI software. Once the bolt is tightened to the desired preload, the log button is hit in the software, and a single data point is logged. This process is repeated for each test article. Once all bolts have been tightened, the run button is activated in the DAQFI software, and the computer is left to collect data at prescribed increments. The software is written to append new data set to previous data set, unless the program is completely shut down and restarted. For each single bolt connection fixture, a plot of load and temperature vs. time is made. The data is then analyzed for temperature effects using the GASmooth software package.

3.2. Material Specifications

Materials used in testing are described in this section. The composite specimens were made from Dow Derakane 8084 vinyl ester epoxy resin reinforced with EGlass fiber. The aluminum and steel used was a standard grade 6061-T6 and ASTM A-36 plate, respectively. What follows are some of the material properties of the various materials used.

3.2.1. Metallic Components

The metallic plates are fabricated of aluminum Grade 6061 – T6 and steel grade A36. Table 3.2 lists some of the properties in US Customary and SI units of the aluminum alloy whereas Table 3.3 lists those for steel A36. Properties of importance for this study are the modulus of elasticity and the coefficient of thermal expansion (CTE). Note that the CTE of aluminum is nearly double that of steel.

Table 3.2 - Aluminum 6061-T6 Properties (matweb.com)

Physical Properties	SI	US Customary
CTE, linear 68°F	$23.6 \cdot 10^{-6}$/°C	$13.1 \cdot 10^{-6}$/°F
Density	2.7 g/cc	0. 0975 lb/in^3
Mechanical Properties	**SI**	**US Customary**
Hardness, Brinell	95	95
Tensile Strength, Ultimate	310 MPa	45 ksi
Tensile Strength, Yield	275 MPa	40 ksi
Elongation @ break	12%	12%
Poisson's Ratio	0.33	0.33
Modulus of Elasticity	69 GPa	10,008 ksi
Shear Modulus	26 GPa	3,771 ksi
Shear Strength	205 MPa	29,733 psi
Fatigue Strength	95 MPa	13,779 psi

Table 3.3 – ASTM Steel A36, Plate Properties (matweb.com)

Physical Properties	SI	US Customary
CTE [Gere and Timoshenko]	$12.0 \cdot 10^{-6}$/°C	$6.5 \cdot 10^{-6}$/°F
Density	7.85 g/cc	0.284 lb/in^3
Mechanical Properties	**SI**	**US Customary**
Hardness, Brinell	95	95
Tensile Strength, Ultimate	400 MPa	60 ksi
Tensile Strength, Yield	250 MPa	36 ksi
Elongation @ break	20%	20%
Poisson's Ratio	0.260	0.260
Modulus of Elasticity	200 GPa	29,000 ksi
Shear Modulus	79.3 GPa	11,500 ksi
Shear Strength	205 MPa	29,733 psi

3.2.2. Composite Specimens

The composite specimens used in this study were fabricated at the Hybrid Structures Laboratory, University of Maine, using a VARTM process. They consist of Dow Derakane 8084, which is an epoxy vinyl ester resin. The composite is reinforced with an EGlass knit cloth procured from Brunswick Technology, Inc (St. Gobain). The cloth is either a 24 oz. 0/90 cross-ply, or a 24 oz. ±45 bi-axial. Properties of Dow Derakane 8084 are listed in Table 3.4, while the EGlass cloth properties are listed in Table 3.5.

Table 3.4 – Dow DERAKANE 8084 Epoxy Vinyl ester Resin (Dow Chemical Company)

Physical Properties	SI	US Customary
Viscosity	350 cps	73.1 $(lbf \cdot s)/ft^2$
Specific Gravity	1.02	1.02
CTE, linear 20°C (matweb.com)	8 – 36 E-6/°C	4.44-20 E-6/°F
Mechanical Properties	**SI**	**US Customary**
Barcol Hardness	30	30
Tensile Modulus	3.17 GPa	$4.6x10^5$ psi
Tensile Strength, Yield	69 - 76 MPa	10 – 11,000 psi
Elongation @ break	10 - 12 %	10 - 12 %
Flexural Modulus	3.03 GPa	$4.4x10^5$ psi
Flexural Strength	110 - 124MPa	16 – 18,000 psi
Heat Distortion Temperature	82 °C	180 °F

Table 3.5 – EGlass Cloth Properties Isotropic (matweb.com)

Physical Properties	SI	US Customary
Extensional Modulus E_1^f	7.24E+10 Pa	1.05E+07 psi
Shear Modulus G_{12}^f	3.03E+10 Pa	4.40E+06 psi
Poisson's ratio η_{12}^f	2.00E-01	2.00E-01
Tensile Strength $+S_1^f$	1.86E+09 Pa	2.70E+05 psi
Compressive Strength $-S_1^f$	-1.10E+09 Pa	-1.60E+05 psi
Density ρ^f	2.55E-02 kg/ $m^2 \cdot s^2$	9.40E-02 lb/in^2
End Area	4.33E-07 m^2	6.71E-04 in^2
CTE linear 20°C	5E-6/°C	2.78E-6/°F
CTE linear 250°C	5.4E-6/°C	3E-6/°F

The lay-up used for the test specimens is quasi-isotropic, with stacking sequence given by $([(\pm 45)_f,(0/90)_f]_4)_s$. They were cut from the same ½" thick panel. The panel was fabricated with approximate dimensions of 50" x 24". Test coupons are then mapped out of each panel and cut to the specifications given in Section 3.1.

3.2.3. Composite Material Tests

Material verification tests were performed to quantify strength and stiffness of the composite materials used in the stress relaxation tests. Tension (ASTM 3094) and compression (ASTM 3410) were carried out on ½"-thick specimens cut from the EGlass/vinyl ester composite panels used in the stress relaxation studies [Pelletier et al., 2005]. The results of these tests are summarized in Table 3.6.

Table 3.6 – Tensile and Compressive Properties of the EGlass/vinyl ester Composite [Pelletier et al., 2005]

Tensile Strength	39,000 psi (269 MPa)
Tensile Modulus	2.0 Msi (14 GPa)
Compressive Strength	40,250 psi (277.5 MPa)
Compressive Modulus	2.7 Msi (18.6 GPa)

3.3. Instrumentation Details

Several sensors are used during testing to monitor data such as load in the bolted connection, maximum pressure distribution in the connection, ambient temperature and humidity. The data acquisition program is also used to monitor and record this data, in conjunction with the various sensors. What follow in this section is a description of the sensors and a description of the pertinent parts of the DAQFI data acquisition program.

3.3.1. Internally Gaged Bolts

The model number of the internally gaged bolt used in all the test specimens is ALD-BOLT-.5" X 2" LONG. This type of bolt is designed to measure dynamic or static tension, compression or bending loads. Their load capacity is 9,220 lbs. Figure 3.4 shows a summary of the bolt specifications.

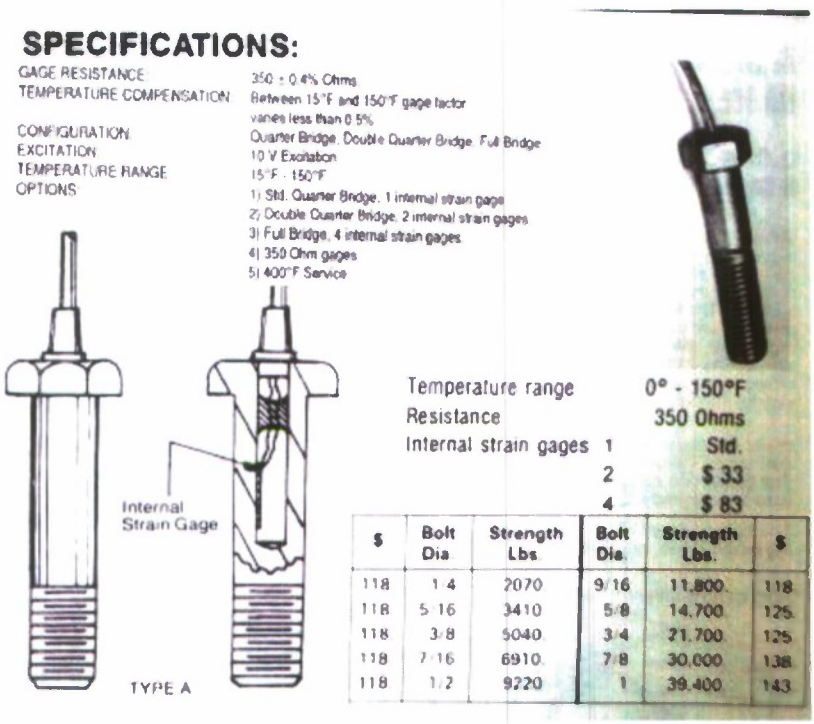

$	Bolt Dia	Strength Lbs	Bolt Dia.	Strength Lbs.	$
118	1/4	2070	9/16	11,800	118
118	5/16	3410	5/8	14,700	125
118	3/8	5040	3/4	21,700	125
118	7/16	6910	7/8	30,000	138
118	1/2	9220	1	39,400	143

Figure 3.4 - Internally Gaged Bolts Spec. Sheet (aldesigninc.com)

The bridge excitation was provided by a BK power supply and the output was connected to the IoTech interface configured in differential mode. A 10 volt power supply was used for the bridge excitation of the load bolts. The output wires were both connected to successive channels on the IoTech hub, and the hub is connected to the computer through the use of a DaqBoard/2000.

Each bolt has an internal 350 ohm full bridge strain gage mounted to the inside of the bolt that is used to measure the applied tension load in the bolt. The output voltage difference is read across the green and white wires of the bolt. Calibration factors for each bolt are given in Table 3.7.

Table 3.7 – Internally Gaged Bolts Calibration Factors

Bolt Number	Size	Serial Number	Calibration Factor (lbs/mV)
1	1/2"	220642	455.0582
2	1/2"	20011107	456.0101
3	1/2"	20011108	567.0741
4	1/2"	20011109	433.3666
5	1/2"	20011110	443.2593
6	1/2"	20011105	574.7479

3.3.2. Humidity Sensor

During testing, humidity was monitored using a HIH-3610 series sensor, manufactured by Honeywell. Figure 3.5 shows a diagram of the chip and mounting dimensions. This sensor has a very low current draw of 200 μA when operating at 5 Vdc. It can operate on power supplies from 4 Vdc to 5.8 Vdc. For these experiments, it was operated at 5 Vdc, since this was the calibration voltage for the sensor. It can operate from between –40°F to 185°F, and between 0 and 100% RH. In that range, it is accurate to ±2% RH.

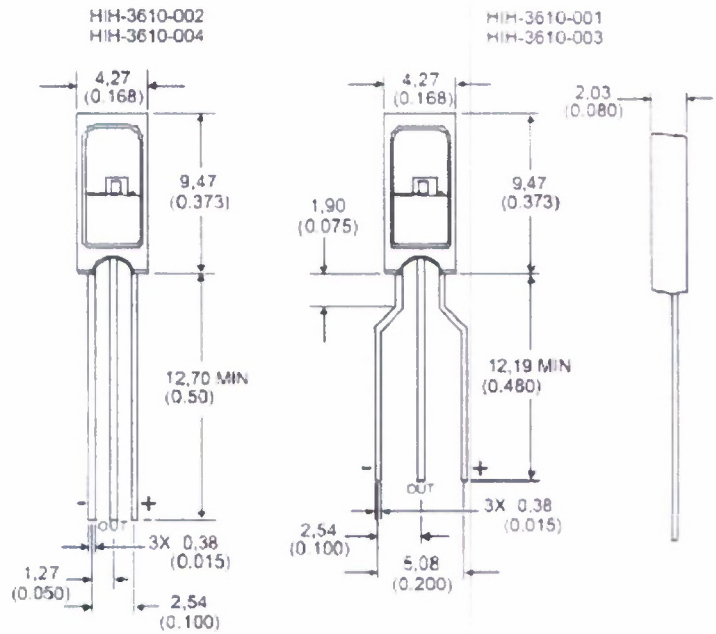

Figure 3.5 – Diagram of HIH -3610 Series Humidity Sensor, mm (in) (Honeywell.com)

3.3.3. Temperature Sensor

The temperature sensor used to monitor room temperature and the temperature cycles during the testing was a LM34CZ chip, manufactured by National Semiconductor. Figure 3.6 shows the overall layout and dimensions of the LM34CZ temperature sensor. It has a linear relationship between output voltage and Fahrenheit temperature, with a +10 mV/°F scale factor. It runs over a temperature range of –50 °F to 300 °F, with an accuracy of ±1½°F. The sensor can operate with an excitation from 5 to 30 volts. A 15 V excitation was used during the experiments. Also, to reduce AC noise, it was needed to bridge a resistor of 9kΩ between V_{OUT} and GND.

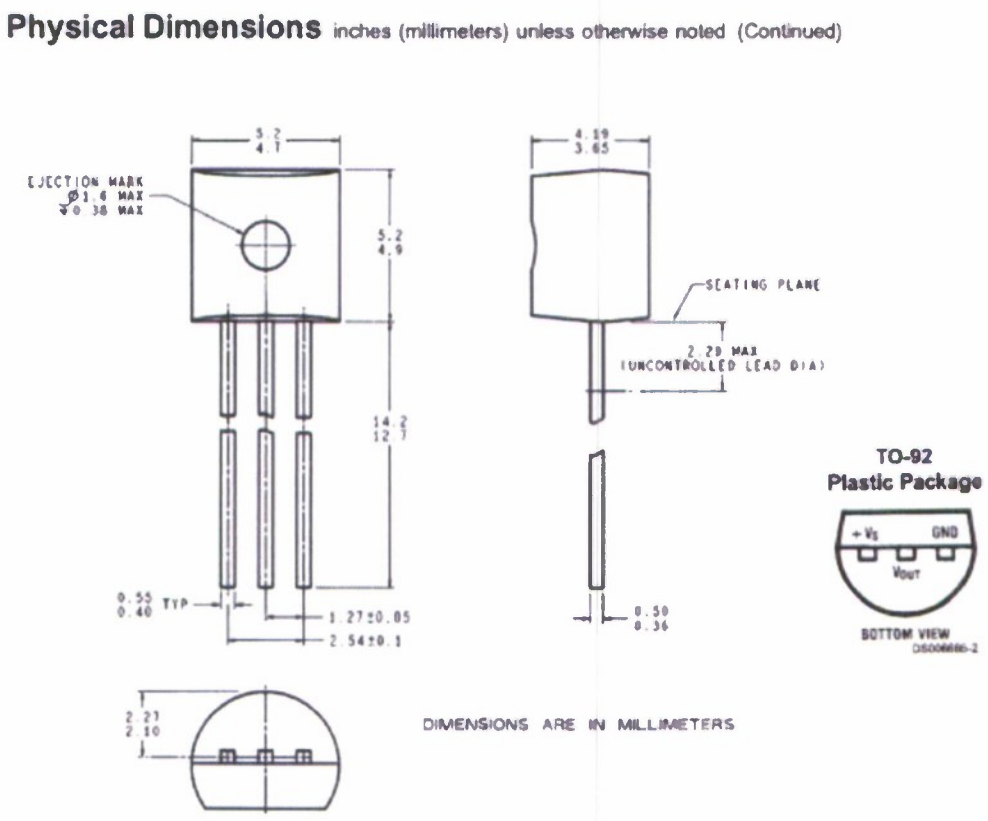

Figure 3.6 – Dimensions of the LM34 Temperature Sensor (National.com)

3.3.4. Temperature Controlled Chamber

A large computer controlled autoclave was used to temperature cycle all the test specimens, except the control. Both humidity and temperature sensors were place in the autoclave chamber. A photograph of the inside of this autoclave is shown in Figure 3.3. A total of 5 temperature cycles were run, ranging from room temperature to 63°C (145°F±3°F). The time span between cycles was 7 days. This allowed the test articles time to go through primary creep and into the secondary creep stage before going through the next cycle.

3.3.5. Power Supply

The power supply used in these experiments was a model number 1652, manufactured by BK Precision®. It features a triple output DC power supply, with a digital display. It has two variable power supplies, ranging from 0 to 24 volts, and have a 0.5 amp current capacity. The two variable power supplies are run at a constant 10 volts, and are used as the power source for the internally gaged bolts.

3.3.6. Data Acquisition System

A schematic of the data acquisition system employed to run the experiments is shown in Figure 3.7. It is based upon an IoTech Daqboard/2000 plug-in card. The 16-bit resolution, along with an ability to set an internal gain of 64, provided the necessary resolution with which to accurately read the loads in the internally gaged bolts

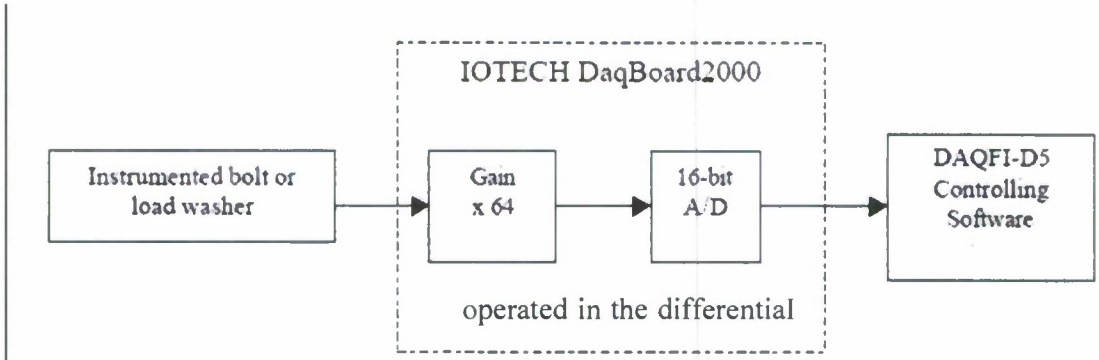

Figure 3.7 – Data Acquisition System Schematic

3.3.6.1. DaqBoard/2000

The DaqBoard/2000, made by IOtech, is used to collect the voltage output from the hubs, and send it to the computer. The board plugs into a PCI slot on a computer, and enables 8 channels of differential data (16 if single ended) to be read per board. Two boards are connected to each computer, enabling 16 channels to be read in differential mode by each computer. The card has a 16-bit resolution, and when used at a range of ±10 V and a gain of 64, corresponds to a voltage resolution of 0.002384 mV.

3.3.6.2. Delphi 5 Data Acquisition Program

The DAQFI-D5 software, written at the University of Maine, controls the data acquisition system. A special software routine as described in Pelletier et al. [2005] was written specifically for the stress relaxation testing. The data configuration and setup screens for the stress relaxation testing are shown in Figures 3.8 and 3.9. The screen shown in Figure 3.8 is where input data such as the number of channels being used, the number of averages, and whether the test is being run in single ended or differential mode is specified. The creep study testing was run in differential mode, as per sensor requirements. A channel can be turned on or off at this screen. The number of averages allows the user to gain more precise data by allowing the program to record several readings at one instant in time, and average them together to obtain a single data point.

Figure 3.9 shows the configuration screen for each individual sensor. Calibration factors are entered in this section of the program. Tabulated values for these calibration factors are given in Table 3.7. The second area on this screen is the voltage offset. The voltage bias, taken with no load applied to the connection, is entered into the voltage offset section of this configuration screen. Accordingly, the resulting load is:

$$(V_{in} - V_{offset}) \cdot \text{Calibration} \tag{3.1}$$

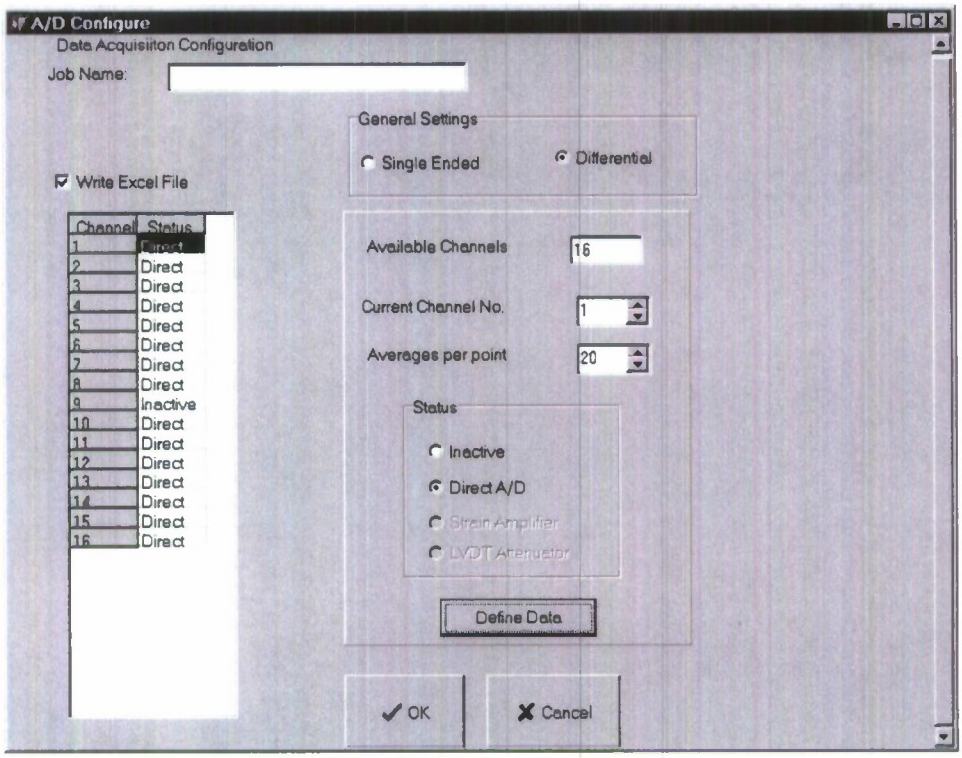

Figure 3.8 – DaqFi-D5 Configuration A

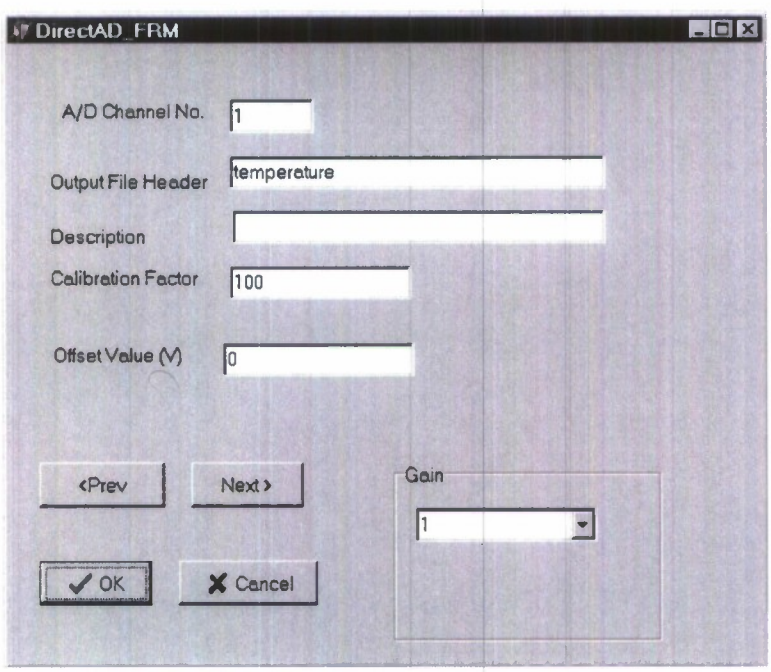

Figure 3.9 – DaqFi-D5 Configuration B

All other information on these two screens is used as a header for the data file. This is information such as a description of the data file, and a description of each channel.

Figure 3.10 shows the actual stress relaxation data recording form. The data recording schedule is shown on the left side of the screen, and is hard coded into the program. Below that is a place to select the name and location of the output data file. Under that is a box labeled Run Test. This is where the program can be started or stopped. This box also dynamically lists which data taking cycle the program is currently on.

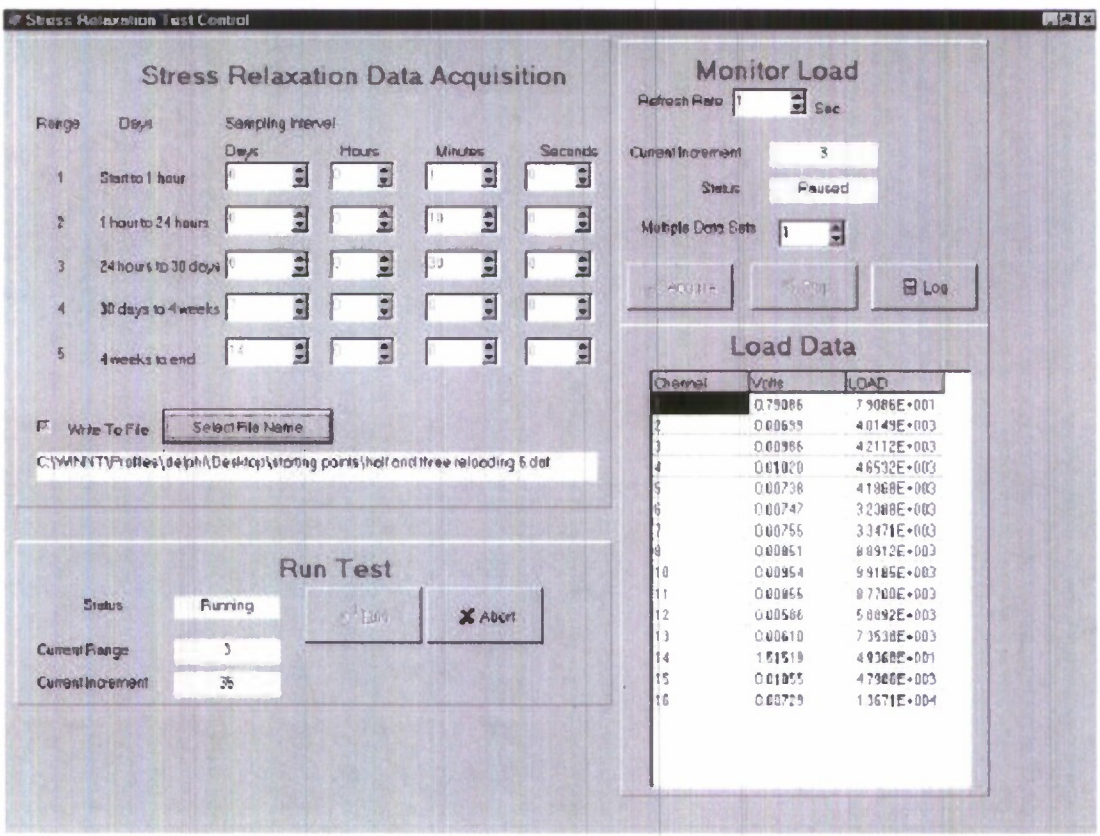

Figure 3.10 – DaqFi-D5 Stress Relaxation Program

On the right side of the screen, there is a place that displays both the output voltage for each channel, as well as the load on each channel. This is active when the program is taking data, but can also be activated in a manual mode. The refresh rate controls the data rate in manual mode. Below that is where the monitor can be turned on

or off while the program is not in the run mode. The monitor allows the user to observe the load being applied to the sensors as the bolts are being tightened.

There is also a log button located on this screen. It allows the user to log a single data point, with a time stamp, during the setup phase, as the bolts are initially tightened. Without this feature, some critical initial data would be lost, as the automated data acquisition system cannot be started until all bolts are tightened to the desired load. With this log button, one bolt can be tightened, a data point can be logged, and the initial load on every channel can be recorded. The data acquisition can then be initiated in the run mode when all bolts have been tightened to the desired load level.

4 TEST RESULTS

The results of the tests performed on single bolt, hybrid connection specimens are presented in this chapter. The focus is centered in two main investigations: the effects of temperature in the primary creep response of the 6 specimens tested, and the response of deliberately executing temperature cycles on 5 of these 6 specimens, the 6th being the control subject. This last specimen was placed outside the autoclave chamber used to run the temperature cycles. In the first phase, all specimens were preloaded to the levels prescribed in Table 3.1 and were left to stress relax for 600 hours (25 days) at room temperature. The obtained data was then reduced and analyzed using the model presented in Chapter 2. The proposed model was then compared to those suggested by Shivakumar and Crews [1982] and Pelletier et al. [2005].

In the second phase of testing, a total of 5 specimens were temperature cycled 5 times in an autoclave chamber. The maximum target temperature was chosen to be 62.5°C ± 1.5°C (144.5°F ± 3°F) and it was maintained at that level for 1 hour, after which it was allowed to return to room temperature condition. Specimens were then left to stress relax for one week to allow them to reach equilibrium condition before the next cycle was performed.

Figure 4.1 shows a graphical representation of the data obtained during the entire single bolt, hybrid connection experiment. The following observations can be made:

1. The bolt load is displayed in KiloNewtons, the time in hours, the temperature in degrees Celsius and the relative humidity in percentage for the entire experimental run.
2. The two testing phases are clearly visible in this figure.
3. The first phase spans from the beginning to day 25 (600 hours). All the specimens were left to stress relax, undisturbed, at room temperature. They were initially preloaded to the nominal levels presented in Table 3.1. The data acquisition program was set to record data according to the schedule presented in

Table 4.1. In this 25-day period, all specimens reach an equilibrium condition in which little additional relaxation occurs.

4. The second phase starts at day 28 (672 hours) and stops at about day 92 (2,208 hours). Five specimens, except the control subject, were temperature cycled a total of 5 times in a computer controlled autoclave chamber. These cycles consisted in increasing the testing temperature from room temperature to 62.5°C ± 1.5°C (144.5°F ± 3°F), for a period of 1 hour after which it was slowly returned to room temperature. The maximum temperature attained is theoretically below the composite's glass transition temperature, T_g. The specimens were then allowed to stress relax forone week to let them reach an equilibrium condition before the start of the next cycle. The data acquisition system was automatically reset for every temperature cycle performed.
5. A data acquisition system malfunction can also be seen in this figure, causing it to cease the collection of data after the first temperature cycle was performed, around day 28 (672 hours). It resulted in a gap of about a week-worth of data. Therefore, the first temperature cycle spans for about 2.5 hours only.
6. The relative humidity has a clear tendency of increasing from day 28 (672 hours) to the end of the test, at around 2,200 hours. It is believed that this is the result of entering the more humid months of the spring and early summer.
7. The relative humidity sharply decreases when a temperature cycle is performed. This is attributed to the fact that the amount of water vapor the air can hold increases with temperature. Therefore, relative humidity decreases with increasing temperature if the actual amount of water vapor stays the same.
8. The composite bolted to composite and composite bolted to aluminum specimens show the highest susceptibility to relative humidity shifts. This response is believed to be related to their ability to absorb the increasing environmental moisture present, especially after running the temperature cycles. The composite bolted to steel specimen does not display the same behavior, possibly due to the larger Modulus of Elasticity of the steel plate compared to that of the composite plate. During the relaxation stage, little effects are detected from relative humidity fluctuations.

9. The data turns noisy as the test enters day 75 (~1,800 hours) for all except the C/Al 1 specimen (first of two composite bolted to aluminum specimens placed in the autoclave). The origin of this noise is uncertain, but it is believed it could be related to RF interference caused by a cavitation experiment run nearby at the time this noise was recorded. This could explain why the control specimen displays the largest noise amplitudes as it was placed relatively close to the cavitation apparatus, while the rest of the specimens remained in the autoclave chamber.
10. The data shown in Figure 4.1 will be broken down and further explained in subsequent sections.

Table 4.1 – Data Acquisition Recording Schedule

Data Acquisition Schedule	
Start to 1 hr.	every minute
1 hr. to 24 hrs.	every 10 minutes
24 hrs. to 30 days	every 30 minutes
30 days to 4 weeks	every 7 days
4 weeks to end	every 14 days

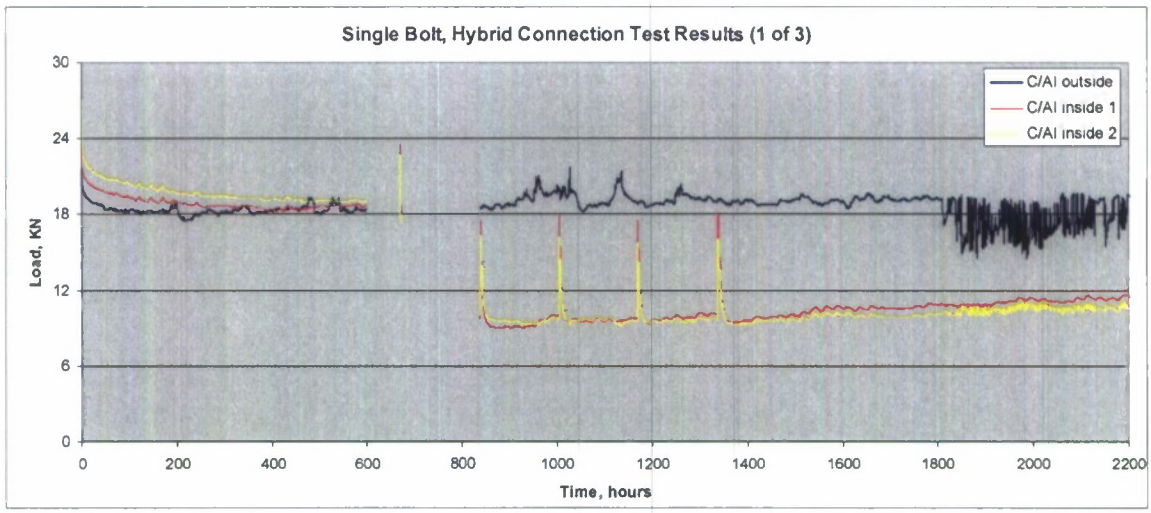

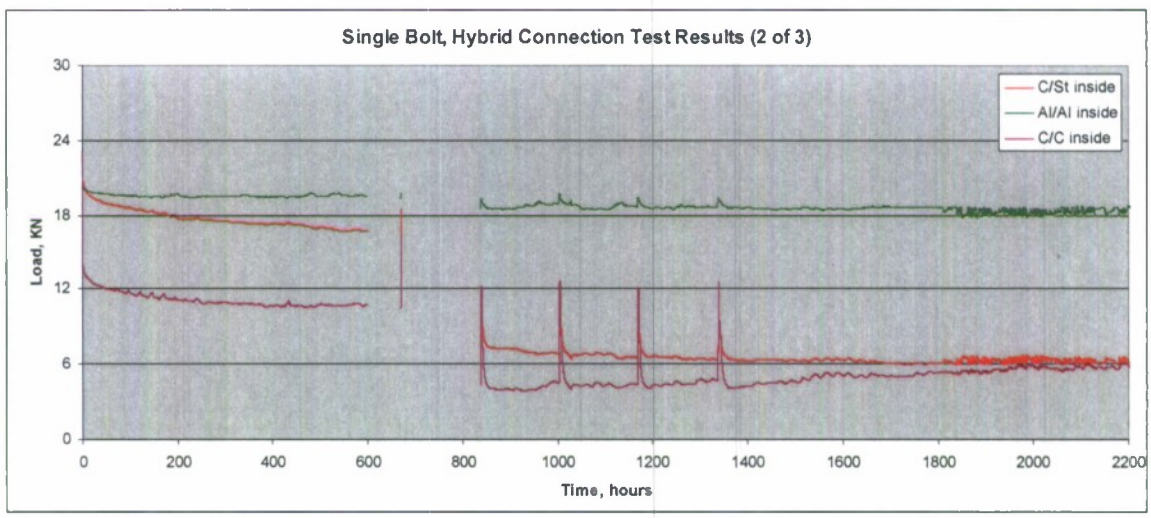

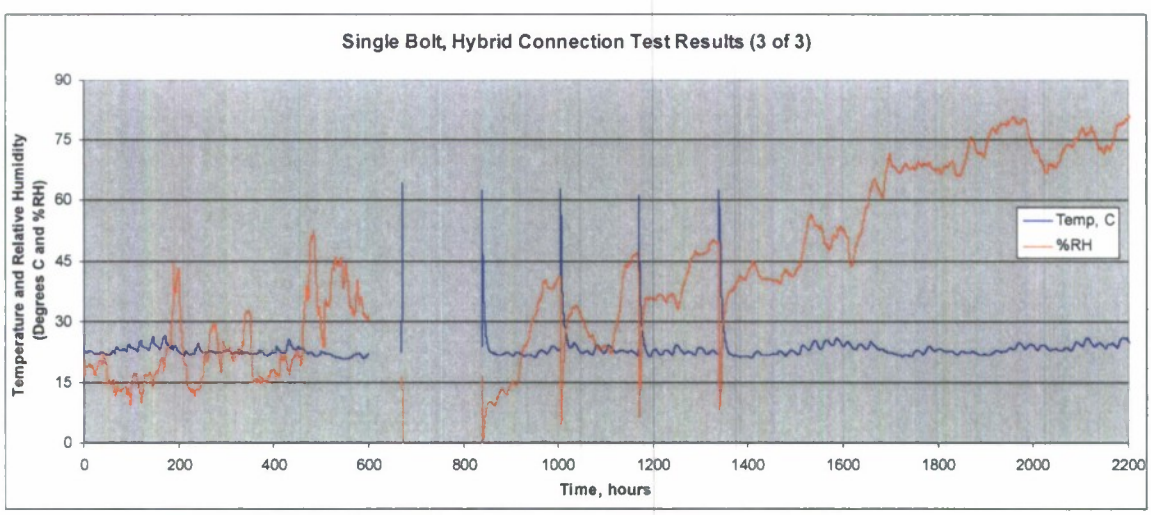

Figure 4.1 – Hybrid Connection Test Results

4.1. Undisturbed Stress Relaxation Results

The result of the first phase of the experiment, the undisturbed stress relaxation of all test articles, is shown in Figure 4.2. This stage ran for a total of 25 days. The following conclusions can be drawn from this figure:

1. It can clearly be seen that the stress relaxation of both hybrid and non-hybrid connections is temperature dependent. Even small ambient temperature shifts were capable of significantly affecting bolt load readings. There are a few areas in Figure 4.2 where the dependence of stress relaxation data on temperature is best shown. An increment in temperature between 2°C and 4°C (4°F and 8°F) from a very constant room temperature of 22°C (71°F) can be seen at the 72, 98, 122, 148, 172, 243 and 434 hour marks. These temperature spikes caused an increase in bolt load evident in all specimens except in both the control (Eglass/vinyl ester bolted to aluminum) and the aluminum bolted to aluminum specimens, which seemed to be more sensitive to relative humidity shifts instead. The reason for such response is uncertain.
2. It can also be appreciated that the bolt load has very little dependence on ambient environmental relative humidity fluctuations in the tested range. These results confirm those obtained by Pelletier et al. [2005], for the ½" thick aluminum to Eglass/vinyl ester composite single bolt hybrid connection tests.

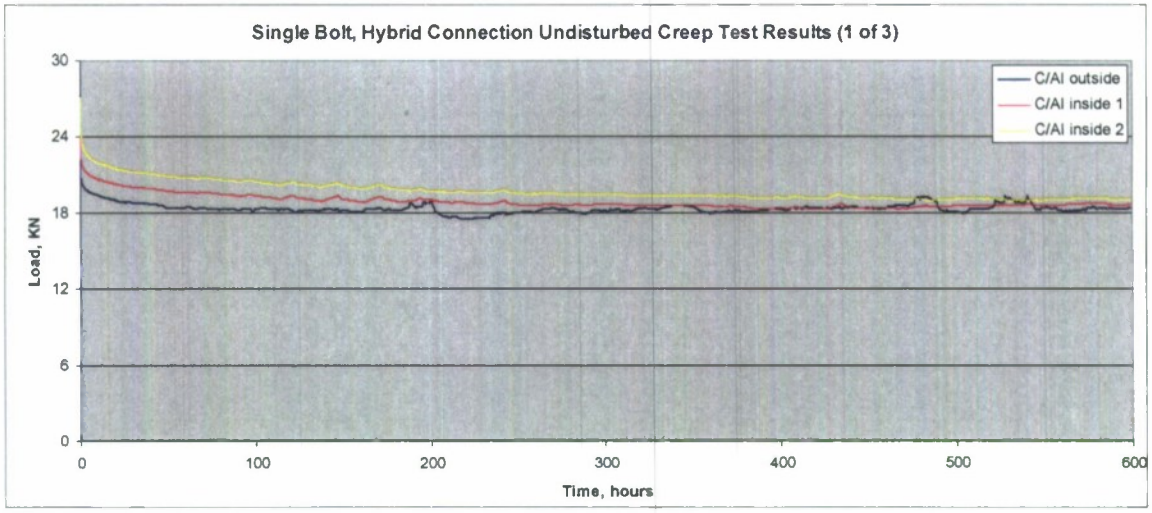

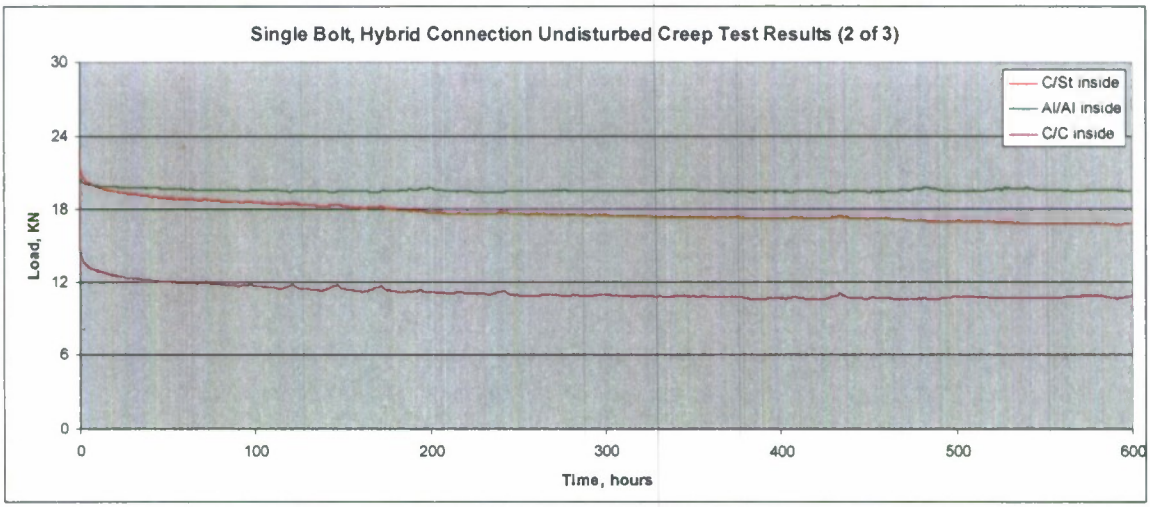

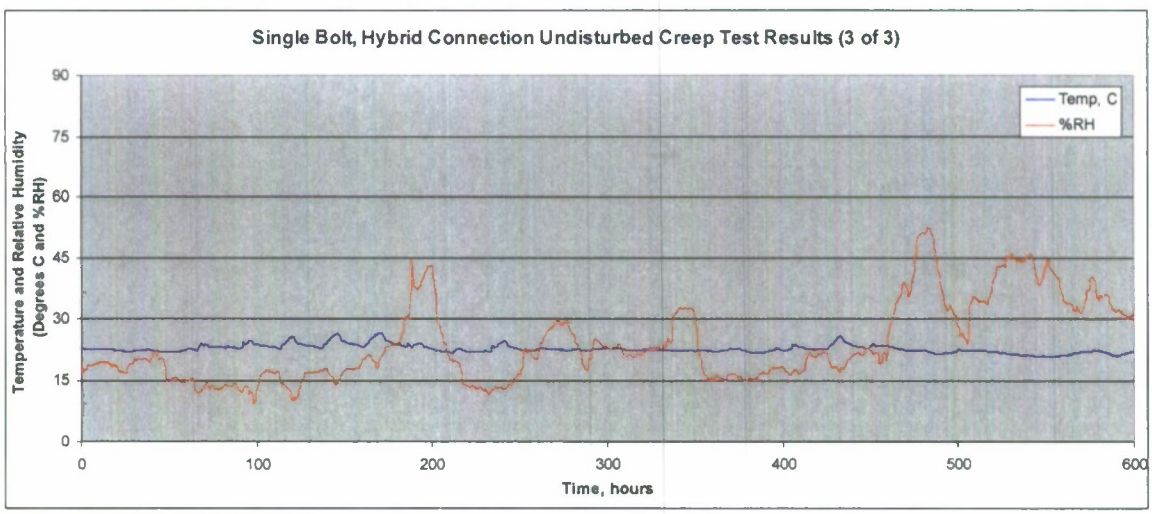

Figure 4.2 – Undisturbed Stress Relaxation Results for All Specimens

The increase in bolt load when there is an increase in temperature is mainly due to the higher CTE value of the materials fastened compared to the CTE of the single steel bolt. The CTE for the aluminum and composite materials is, respectively, twice and four times that of the steel material used in the fastening bolts. Therefore, the differential thermal strains will cause differential stresses in the connection. For example, in the test article constructed by joining a steel plate to a composite plate using a steel bolt, the temperature dependence is also evident, although to a lesser degree. The reason is the relatively smaller amount of composite material compared to steel material in the construction of the joint. Figure 4.2 also shows that when the temperature finally returned to normal, so did the load in the connections. In other words, the bolt load returned to what was expected after the temperature had returned to more "normal" levels.

A computer program was specifically written to temperature correct the stress relaxation data generated by the single bolt, hybrid connection specimens used in this study. The program was also instrumental in obtaining the curve fits to the experimental data, which was done prior to computing the stress relaxation constants (see Section 2.3). The coefficient of thermal expansion for the EGlass/vinyl ester composite material used in the hybrid connection test was experimentally found and reported in Section 2.1. The procedure to obtain the temperature correction factor, K_{pt}, was presented in Sections 2.2 and 2.3. The temperature correction factors used in this section for the different specimens are reported in Appendix C.

Figure 4.3 is a screen shot of temperature correcting the stress relaxation data of the "C/Al inside 2" specimen, an EGlass/vinyl ester to aluminum single bolt hybrid connection, generated during the first phase of the test. Notice in Figure 4.3 that the GASmooth program satisfactorily smoothes (green curve) and corrects (blue curve) the raw data (red curve) for temperature fluctuations. From the start of the run at day 0 to about day 1.5, the correction departs from the raw data. It is still unclear what is causing such an outcome. It is believed this must be related to how the GASmooth code processes the first data points. An alternate method for smoothing and correcting the experimental data was then developed based on the GASmooth application for comparison purposes.

The GASmooth application was first used to correct the data of all specimens. The only factor that changed from one specimen to another was the "Temp Factor" in Figure 4.3, to account for the different joint construction. Then, the alternate method for smoothing and correcting the data was implemented and its results compared to those obtained using the GASmooth program.

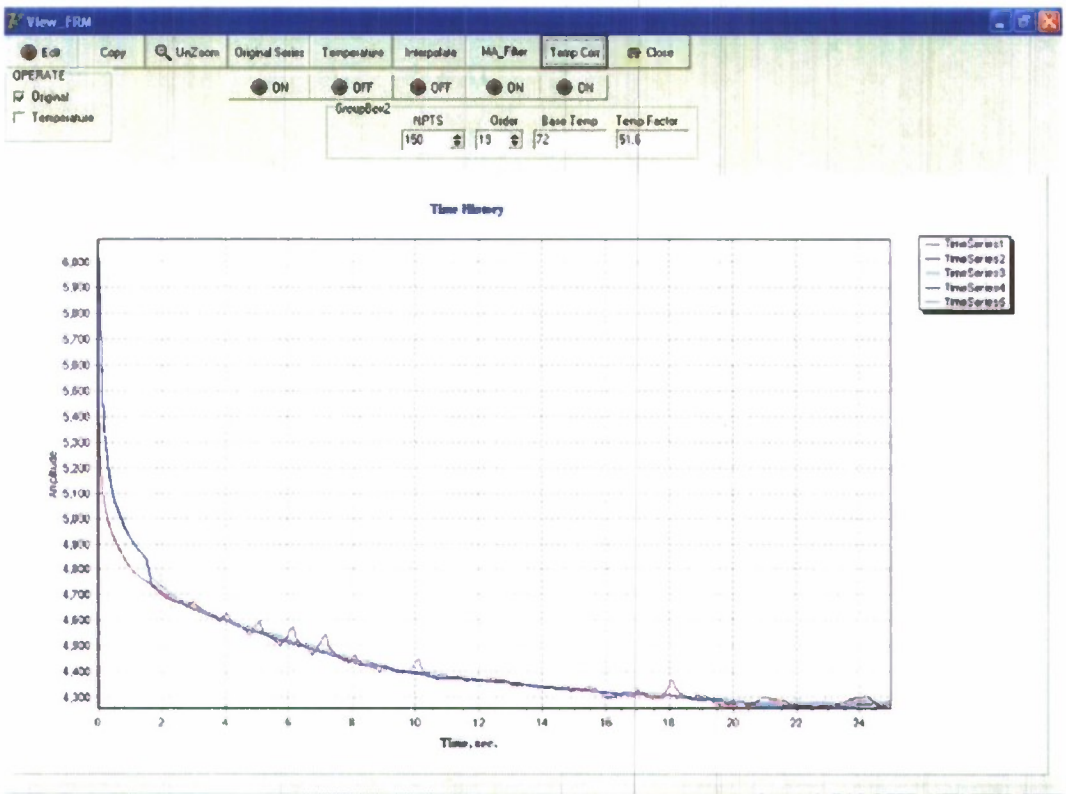

Figure 4.3 – Correcting the C/Al inside 2 Specimen Data for Temperature Shifts using GASmooth

The GASmooth procedure goes as follows:

1. Each specimen's raw data is compiled in a .csv file. This file contains the specimen's time, bolt load and temperature histories, in days, pounds and degrees F, respectively.
2. The newly generated .csv file is then imported into the GASmooth application. The appropriate temperature correction factor ("Temp Factor", in the GASmooth application window), which is dependent on the specimen's constituents, and the NPTS, Order and Base Temp factors are entered next.

The different temperature factors used for the different specimens tested are given in Appendix C.

3. The actual experimental bolt load data is plotted by pressing on the "Original Series" button (red curve in Figure 4.3).
4. Pressing on the "MA_Filter" button generates the smoothed curve (green curve in Figure 4.3). GASmooth applies a moving average algorithm to produce it.
5. The temperature corrected curve (blue line in Figure 4.3) is generated last by pressing on the "Temp Corr" button. It is necessary to create the smoothed curve first before the temperature corrected plot can be generated.
6. Next, the corrected .csv data file is exported back and converted to the SI System of units for further manipulation.

The alternate procedure processes the raw data from the experiments directly. Smoothing and correcting follows the same idea as in the GASmooth application, but is performed using spread sheets instead.

A graph is generated plotting the dimensionless ratio P_t/P_0 vs. Time + 1, in hours, where P_t and P_0 are, respectively, the corrected bolt load at any time and the actual bolt preload at Time = 0. The included time bias of 1 hour allows obtaining a power law curve fit that can be solved at Time = 0. This equation has the general form:

$$\frac{P_t}{P_0} = \beta \cdot (t+1)^{-\alpha 1} \tag{4.1}$$

In this equation, β and $\alpha 1$ are the stress relaxation constants. Notice that this equation is basically the same as the one proposed by Pelletier et al. [2005] in their work, and presented as:

$$\frac{P}{P_0} = \beta \cdot t^{-\alpha} \tag{4.2}$$

where P and P_0 are, respectively, the load in the connection at any time (in days) and the actual bolt preload at Time = 0. Equation (4.2) did not take into consideration the correction of the experimental data for the effects of temperature. It is, therefore, the result of finding the best fit to the raw experimental data, a power law curve. The authors

did compute the two relaxation constants, namely β and α, and needed to include a time bias of 0.0069 days (10 minutes) for its solution at Time = 0. Therefore, Equation (4.2) is basically identical to Equation (4.1), except that the time bias is different.

The work presented by Shivakumar and Crews' [1982] concluded that the best fit to their experimental effort on bolt clamp-up relaxation when no hygrothermal shift is considered was given by the expression:

$$\frac{P_t}{P_0} = \frac{1}{1 + F_1 \cdot t^n} \tag{4.3}$$

where P_t and P_0 is again the load at time t and the initial clamp-up load, respectively, F_1 is a material dependent constant and n is the viscoelastic power law constant for the material.

In an effort to find alternate methods for predicting the actual stress relaxation data generated by the type of connection tested in the work presented herein, a third equation was introduced, which will be evaluated in conjunction with Equations (4.1) and (4.3). It has the form:

$$\frac{P_t}{P_0} = (t+1)^{-\alpha 2} \tag{4.4}$$

where P_t and P_0 are the load in the connection at time t and the initial load, respectively, and α2 is the power law relaxation constant. Equation (4.4) is a modified version of Equation (4.1). It excludes the relaxation constant β to force the initial state to be at the value of the preload P_0. Therefore, Equations (4.1), (4.3) and (4.4) will be evaluated using the two correcting methods.

4.2 Relaxation Constant Quantification for Equations (4.1), (4.3) and (4.4)

Table 4.2 shows the relaxation constants computed with the aid of the GAsmooth application. It also displays, in this order, the following information;

1. C to Al Group % Difference. This is the % difference within the group of composite bolted to aluminum specimens.
2. Group % Difference no C/Al outside. The composite bolted to aluminum control specimen was excluded due to the poor quality of its output data.

3. Total % Difference. This is the % difference for the entire specimen population.
4. Total % Difference no C/C inside. This is the % difference of all specimens excluding the composite bolted to composite subject.
5. Total % Difference no Al/Al inside. This is the % difference of all specimens excluding the aluminum bolted to aluminum specimen due to the poor quality of its output data.
6. C to Al Group Average. This is the relaxation constant average for the group of composite bolted to aluminum specimens.
7. Group Average no C/Al outside.
8. Total Average for the entire specimen population.
9. Total Average no C/C inside. The composite bolted to composite specimen is excluded for the computation of this value.
10. Total Average no Al/Al inside. The aluminum bolted to aluminum specimen is excluded for the computation of this value.

The final form for the equations with these constants plugged in is presented in Table 4.3. Similarly, the relaxation constants as computed using the alternate correcting technique are displayed in Table 4.4, together with their averages and percent differences. The final form for their corresponding equations is shown in Table 4.5.

Table 4.2 – GASmooth-Obtained Relaxation Constants for Equations (4.1,4.2 & 4.4)

	GASmooth Technique				
	Equation (4.1)		Equation (4.3)		Equation (4.4)
Specimen Type	β	α1	n	F1	α2
Fig 3_4 C to Al Control*	1.0182	0.0702	0.2245	0.1250	0.0675
C to Al outside	0.8922	0.016	0.0769	0.1467	0.0364
C to Al inside1	0.9446	0.0356	0.1741	0.1098	0.0458
C to Al inside2	0.946	0.0476	0.1912	0.1297	0.0576
C to C inside	0.7779	0.0811	0.1541	0.4312	0.1261
C to St inside	1.0039	0.049	0.2449	0.0780	0.0483
Al to Al inside	0.9517	0.0076	0.075	0.0633	0.0165
C to Al Group % Difference	13.1910	125.7541	97.9429	28.7206	59.8653
Group % Difference no C/Al outside	7.4995	65.4064	25.2885	16.5865	38.3054
Total % Difference	26.7580	165.7272	106.2207	148.7890	153.7167
Total % Difference no C/C inside	13.1910	165.7272	106.2207	148.7890	153.7167
Total % Difference no Al/Al inside	26.7580	134.0886	104.4127	138.7174	110.4000
C to Al Group Average	0.9503	0.0424	0.1667	0.1278	0.0518
Group Average no C/Al outside	0.9696	0.0511	0.1966	0.1215	0.0570
Total Average	0.9335	0.0439	0.1630	0.1548	0.0569
Total Average no C/C inside	0.9594	0.0377	0.1644	0.1088	0.0454
Total Average no Al/Al inside	0.9305	0.0499	0.1776	0.1701	0.0636

* Pelletier et al. [2005]

Table 4.3 – Final Form for Equations (4.1), (4.3) and (4.4) by the GSmooth Method

	GASmooth Technique		
Specimen Type	Equation (4.1)	Equation (4.3)	Equation (4.4)
Fig3_4 C to Al Control*	$\frac{P_t}{P_0} = 1.0182 \cdot (t+1)^{-0.0702}$	$\frac{P_t}{P_0} = \frac{1}{1 + 0.1250 \cdot t^{0.2245}}$	$\frac{P_t}{P_0} = (t+1)^{-0.0675}$
C to Al outside	$\frac{P_t}{P_0} = 0.8922 \cdot (t+1)^{-0.0160}$	$\frac{P_t}{P_0} = \frac{1}{1 + 0.1467 \cdot t^{0.0769}}$	$\frac{P_t}{P_0} = (t+1)^{-0.0364}$
C to Al inside1	$\frac{P_t}{P_0} = 0.9446 \cdot (t+1)^{-0.0356}$	$\frac{P_t}{P_0} = \frac{1}{1 + 0.1098 \cdot t^{0.1741}}$	$\frac{P_t}{P_0} = (t+1)^{-0.0458}$
C to Al inside2	$\frac{P_t}{P_0} = 0.9460 \cdot (t+1)^{-0.0476}$	$\frac{P_t}{P_0} = \frac{1}{1 + 0.1297 \cdot t^{0.1912}}$	$\frac{P_t}{P_0} = (t+1)^{-0.0576}$
C to C inside	$\frac{P_t}{P_0} = 0.7779 \cdot (t+1)^{-0.0811}$	$\frac{P_t}{P_0} = \frac{1}{1 + 0.4312 \cdot t^{0.1541}}$	$\frac{P_t}{P_0} = (t+1)^{-0.1261}$
C to St inside	$\frac{P_t}{P_0} = 1.0039 \cdot (t+1)^{-0.0490}$	$\frac{P_t}{P_0} = \frac{1}{1 + 0.0780 \cdot t^{0.2449}}$	$\frac{P_t}{P_0} = (t+1)^{-0.0483}$
Al to Al inside	$\frac{P_t}{P_0} = 0.9517 \cdot (t+1)^{-0.0076}$	$\frac{P_t}{P_0} = \frac{1}{1 + 0.0633 \cdot t^{0.0750}}$	$\frac{P_t}{P_0} = (t+1)^{-0.0165}$

* Pelletier et al. [2005]

Table 4.4 – Alternate Method-Obtained Relaxation Constants for Equations (4.1), (4.3) and (4.4)

	Alternate Technique				
	Equation (4.1)		Equation (4.3)		Equation (4.4)
Specimen Type	β	α1	n	F1	α2
Fig3_4 C to Al Control*	0.9498	0.0626	0.2089	0.1484	0.0706
C to Al outside	0.8957	0.0171	0.1157	0.1198	0.0373
C to Al inside1	0.9155	0.0305	0.1631	0.1186	0.0467
C to Al inside2	0.8953	0.0384	0.1624	0.1547	0.0587
C to C inside	0.6551	0.0512	0.0975	0.5972	0.1287
C to St inside	0.9475	0.0389	0.2006	0.1006	0.0487
Al to Al inside	0.9478	0.0069	0.0914	0.0580	0.0167
Group % Difference	5.9075	114.1782	57.4245	26.4392	61.7238
Group % Difference no C/Al outside	5.9075	68.9581	25.0471	26.4392	40.7502
Total % Difference	36.7250	160.2878	78.2551	164.5693	154.0578

Total % Difference no C/C inside	5.9075	160.2878	78.2551	90.8965	123.4822
Total % Difference no Al/Al inside	36.7250	160.2878	78.2551	164.5693	154.0578
Group Average	0.9141	0.0372	0.1625	0.1354	0.0533
Group Average no C/Al outside	0.9202	0.0438	0.1781	0.1406	0.0587
Total Average	0.8867	0.0351	0.1485	0.1853	0.0582
Total Average no C/C inside	0.9253	0.0324	0.1570	0.1167	0.0465
Total Average no Al/Al inside	0.8765	0.0398	0.1580	0.2066	0.0651

* Pelletier et al. [2005]

Table 4.5 – Final Form for Equations (4.1), (4.3) and (4.4) by the Alternate Method

	Alternate Technique		
Specimen Type	Equation (4.1)	Equation (4.3)	Equation (4.4)
Fig 3_4 C to Al Control*	$\frac{P_t}{P_0} = 0.9498 \cdot (t+1)^{-0.0626}$	$\frac{P_t}{P_0} = \frac{1}{1+0.1484 \cdot t^{0.2089}}$	$\frac{P_t}{P_0} = (t+1)^{-0.0706}$
C to Al outside	$\frac{P_t}{P_0} = 0.8957 \cdot (t+1)^{-0.0171}$	$\frac{P_t}{P_0} = \frac{1}{1+0.1198 \cdot t^{0.1157}}$	$\frac{P_t}{P_0} = (t+1)^{-0.0373}$
C to Al inside1	$\frac{P_t}{P_0} = 0.9155 \cdot (t+1)^{-0.0305}$	$\frac{P_t}{P_0} = \frac{1}{1+0.1186 \cdot t^{0.1631}}$	$\frac{P_t}{P_0} = (t+1)^{-0.0467}$
C to Al inside2	$\frac{P_t}{P_0} = 0.8953 \cdot (t+1)^{-0.0384}$	$\frac{P_t}{P_0} = \frac{1}{1+0.1547 \cdot t^{0.1624}}$	$\frac{P_t}{P_0} = (t+1)^{-0.0587}$
C to C inside	$\frac{P_t}{P_0} = 0.6551 \cdot (t+1)^{-0.0512}$	$\frac{P_t}{P_0} = \frac{1}{1+0.5972 \cdot t^{0.0975}}$	$\frac{P_t}{P_0} = (t+1)^{-0.1287}$
C to St inside	$\frac{P_t}{P_0} = 0.9475 \cdot (t+1)^{-0.0389}$	$\frac{P_t}{P_0} = \frac{1}{1+0.1006 \cdot t^{0.2006}}$	$\frac{P_t}{P_0} = (t+1)^{-0.0487}$
Al to Al inside	$\frac{P_t}{P_0} = 0.9478 \cdot (t+1)^{-0.0069}$	$\frac{P_t}{P_0} = \frac{1}{1+0.0580 \cdot t^{0.0914}}$	$\frac{P_t}{P_0} = (t+1)^{-0.0167}$

* Pelletier et al. [2005]

Tables 4.2 and 4.4 indicate that the alternate smoothing and correcting technique implemented seems to yield better results than the GASmooth application, according to the % differences displayed, which tend to be smaller when the alternate method is used. In general, the discrepancies shown in these two tables are related to the two articles that performed poorly: the composite bolted to aluminum control specimen and the aluminum bolted to aluminum.

The graphical results are presented in the next section. They corroborate what is observed by inspection of the numerical results presented in the above tables.

4.3 Graphical Results for the First Testing Phase, Relaxation Only

In the following figures, the following notation convention has been adopted (see the legend in the figures):

1. The experimental dimensionless curve is given by "P/Po". This is the actual curve.
2. Equation (4.1) is "Eqn1 Pt/Po".
3. Shivakumar and Crews' [1982] Equation (4.3), is "Eqn3 Pt/Po".
4. Equation (4.4) is "Eqn2 Pt/Po".
5. Equation (4.5), developed by Pelletier et al. [2005], is "Pelletier P/Po".

Pelletier et al. [2005] found that the best fit to the stress relaxation data of the control specimen tested and reported in Figure 3.4 of their work is given by the power law Equation (4.2). The constants β and α where found to be 0.77 and 0.0608, respectively. Therefore, Equation (4.2) has the final form of:

$$\frac{P}{P_0} = 0.77 \cdot t^{-0.0608} \tag{4.5}$$

As it was mentioned earlier, this equation cannot be solved at Time = 0. Therefore, the authors introduced an offset of 0.0069 days (10 minutes), which, in turn, over estimates the initial bolt preload, P_0. Table 4.6 compares Equation (4.5) with the power law fit equations obtained by the GASmooth and the alternate methods.

Table 4.6 – Pelletier et al. [2005] Figure 3.4 Control Specimen Power Law Fit Equation Comparison

	Pelletier et al. [2005] Fig. 3.4 Control Specimen GASmooth Technique
Equation (4.1)	$\frac{P_t}{P_0} = 1.0182 \cdot (t+1)^{-0.0702}$
Equation (4.3)	$\frac{P_t}{P_0} = \frac{1}{1 + 0.1250 \cdot t^{0.2245}}$
Equation (4.4)	$\frac{P_t}{P_0} = (t+1)^{-0.0675}$
	Alternate Technique
Equation (4.1)	$\frac{P_t}{P_0} = 0.9498 \cdot (t+1)^{-0.0626}$
Equation (4.3)	$\frac{P_t}{P_0} = \frac{1}{1 + 0.1484 \cdot t^{0.2089}}$
Equation (4.4)	$\frac{P_t}{P_0} = (t+1)^{-0.0706}$
Pelletier's Equation (4.5)	$\frac{P}{P_0} = 0.77 \cdot t^{-0.0608}$

Figures 4.4 and 4.5 show how the output of Equations (4.1), (4.3), (4.4) and (4.5) compare to the real data, using the GASmooth application and an alternate technique to smooth and correct the data.

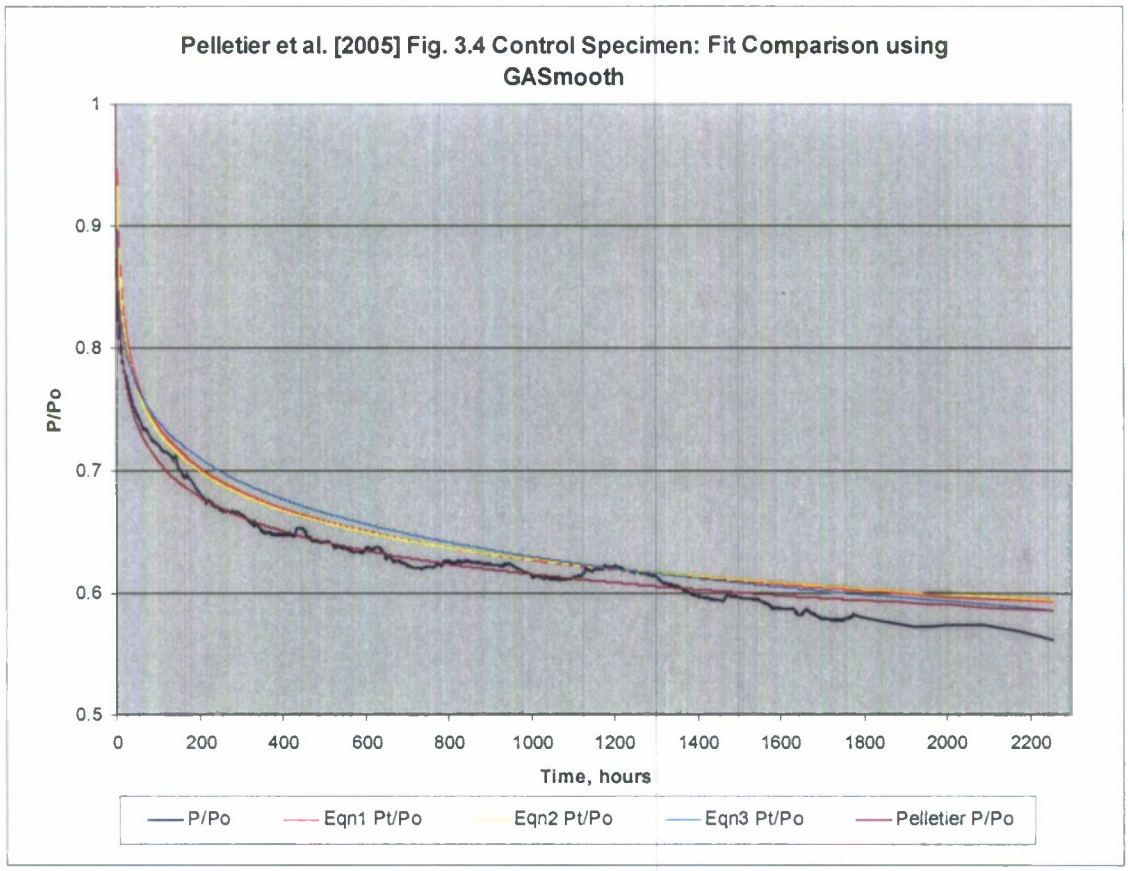

Figure 4.4 – Fit Comparison Using the GASmooth Application for the Control Specimen Shown in Figure 3.4 of Pelletier et al. [2005] Work.

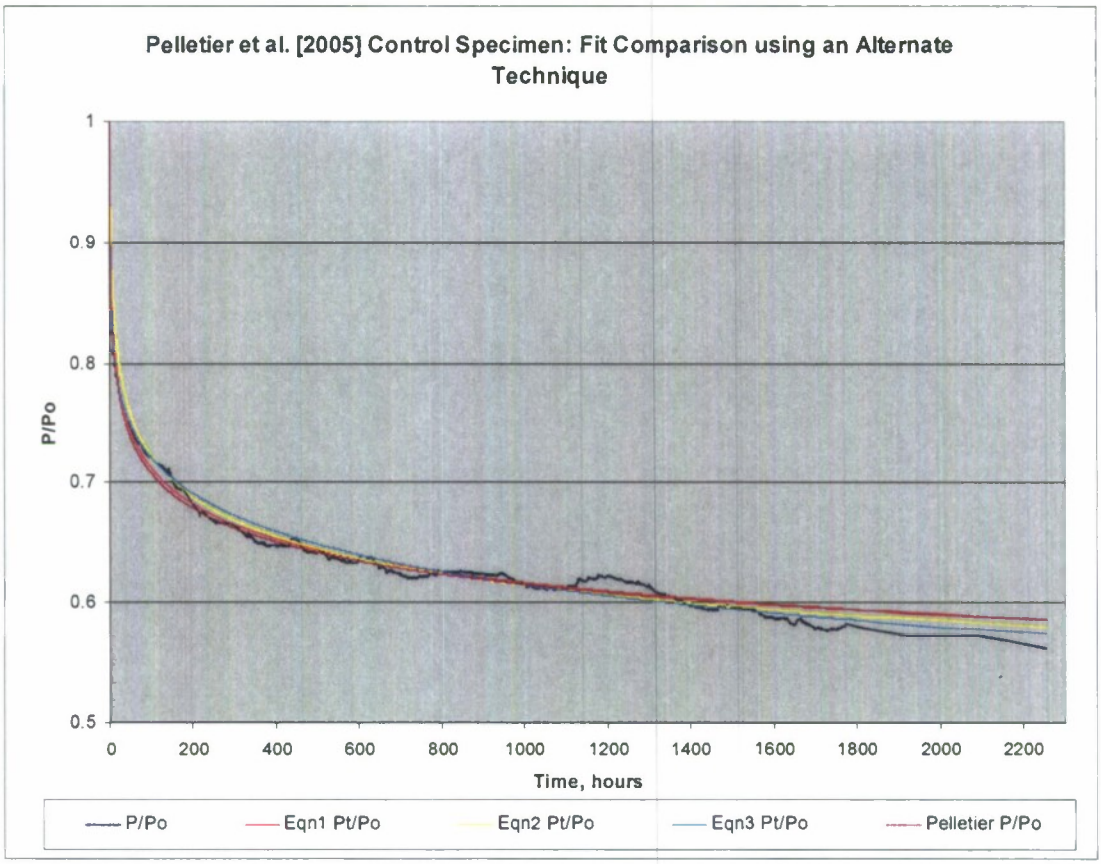

Figure 4.5 – Fit Comparison Using an Alternate Method for the Control Specimen Shown in Figure 3.4 of Pelletier et al. [2005] Work.

Notice that Equation (4.5), "Pelletier P/Po", gives the best results in Figure 4.4. Equations (4.1), (4.3) and (4.4) significantly over estimate the load in the bolt over the entire experimental run. Figure 4.5 shows the result of using the alternate method to smooth and correct the data. This alternate technique seems to work better than the GASmooth at smoothing and correcting. Equation (4.3) seems to work the best. It also predicts the actual load at Time = 0.

Composite bolted to Aluminum Control Specimen

Figures 4.6 and 4.7 compare the results obtained for the control specimen tested in the present work. The control specimen (composite bolted to aluminum, or "C to Al control") data shown in these two figures turned out to be notably noisier than that of the rest of the specimens tested, with the exception of the aluminum bolted to aluminum ("Al to Al inside"), which also seemed to be more sensitive to relative humidity shifts than to temperature variability. The reason for such behavior is uncertain. Equation (4.4) performs significantly worse than Equations (4.1) and (4.3) in both figures, which yield the best results. Also, the difference between the two techniques used is imperceptible.

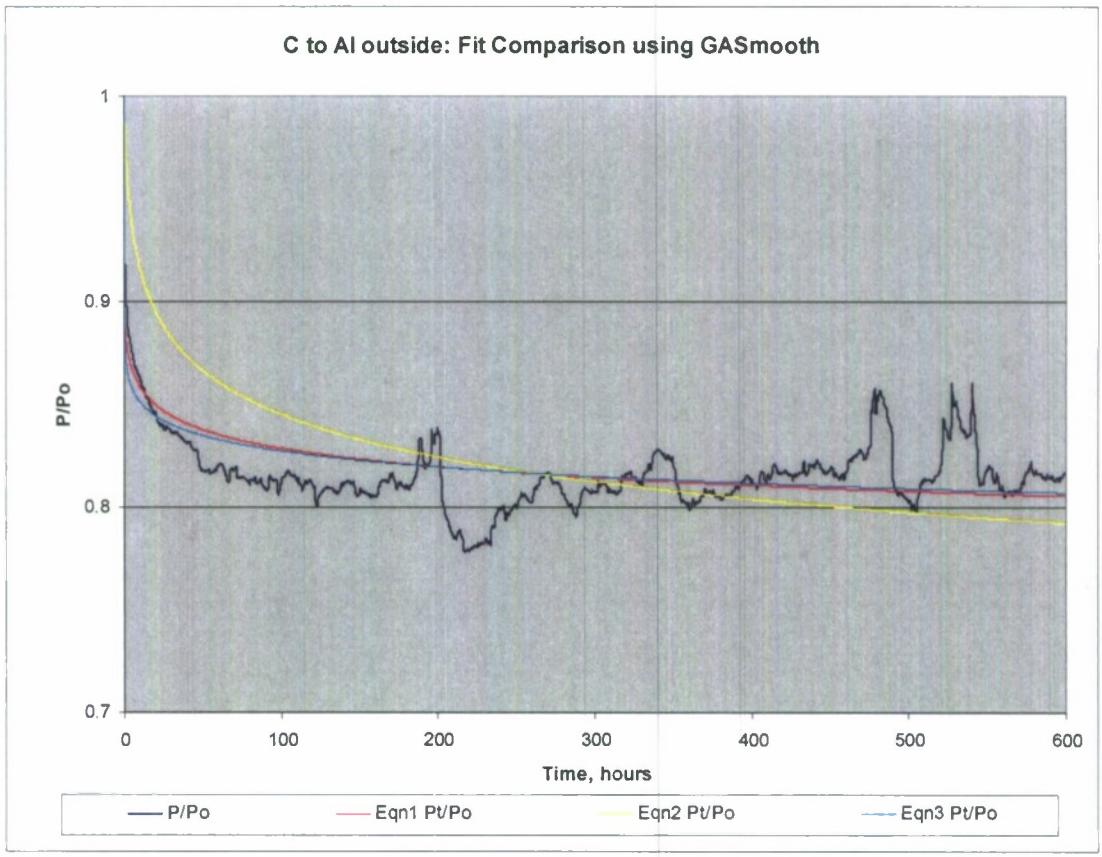

Figure 4.6 – Control Specimen Fit Comparison Using GASmooth

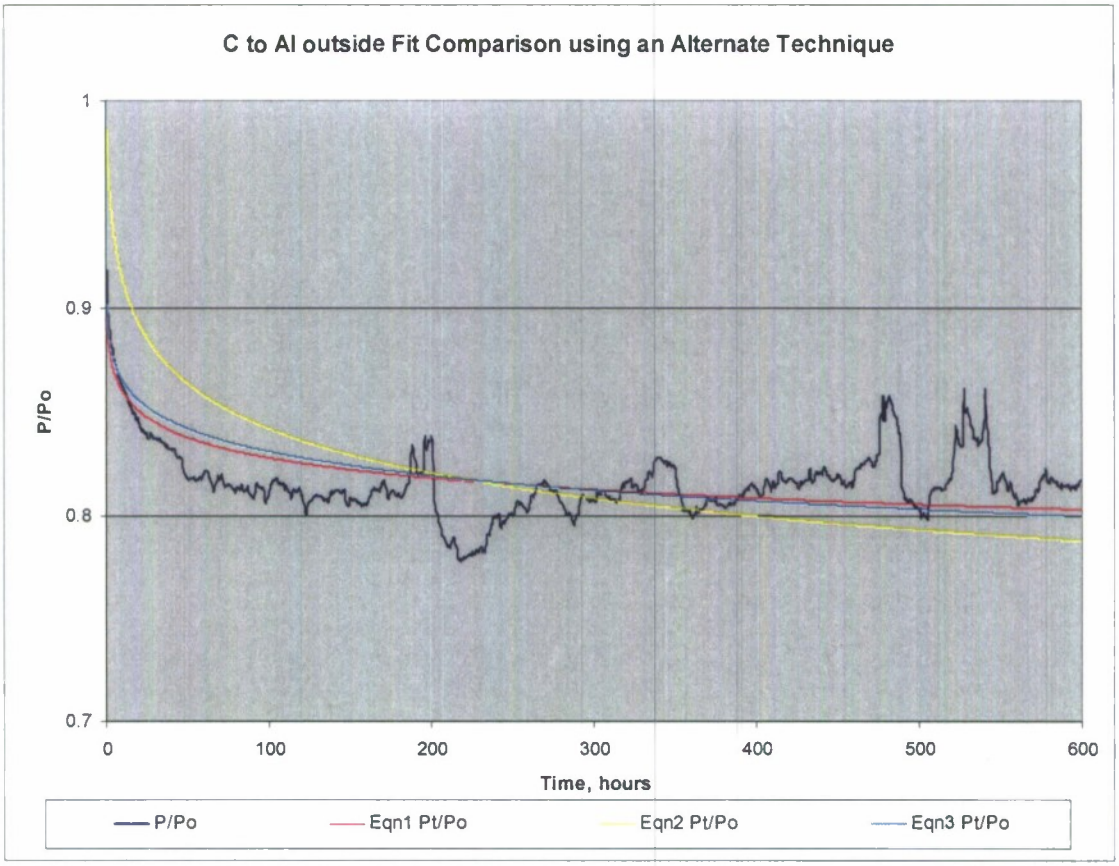

Figure 4.7 – Control Specimen Fit Comparison Using an Alternate Technique

Composite bolted to Aluminum Specimen #1

Figures 4.8 and 4.9 show how these two techniques compare to each other when the first specimen of composite bolted to aluminum is considered.

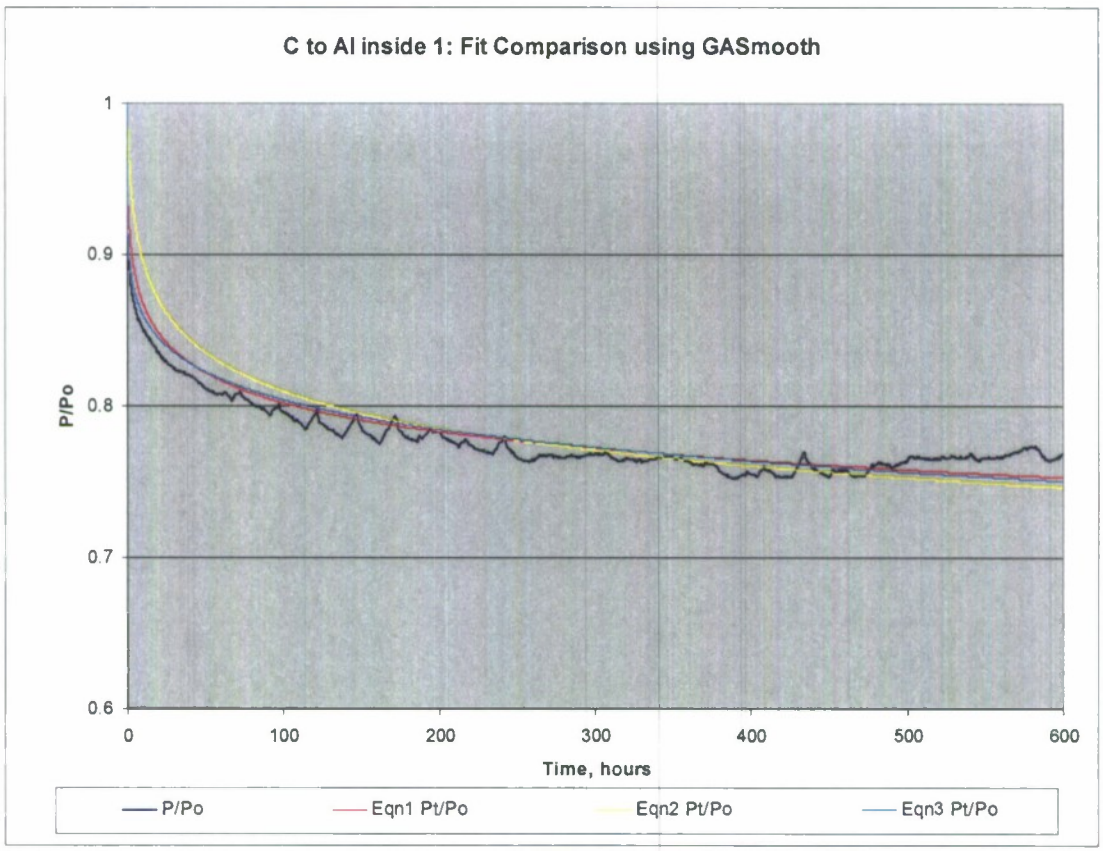

Figure 4.8 – Composite Bolted to Aluminum #1 Fit Comparison Using GASmooth

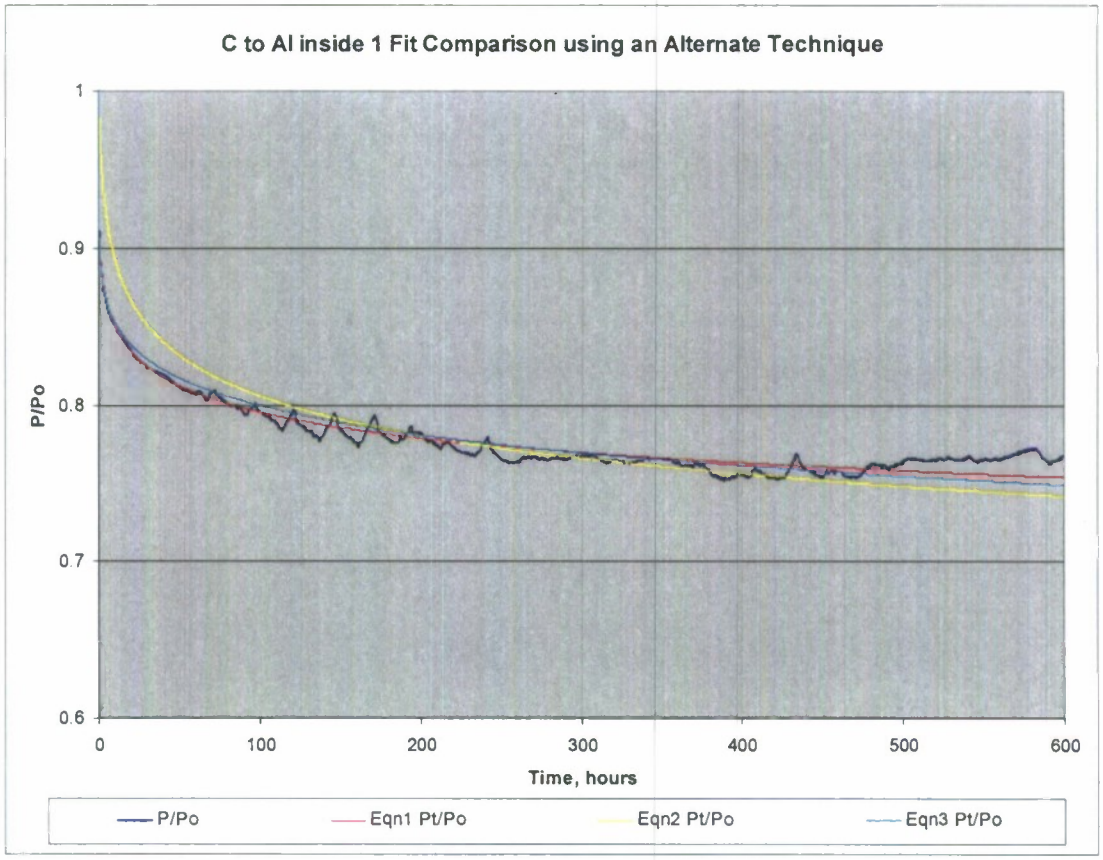

Figure 4.9 – Composite Bolted to Aluminum #1 Fit Comparison Using an Alternate Technique

Once again the alternate technique used seems to fit the data more closely. Equations (4.1) and (4.3) work substantially better that Equation (4.4). Notice also that the data is cleaner and that it clearly shows the effects of the temperature fluctuations.

Composite bolted to Aluminum Specimen #2

Figures 4.10 and 4.11 show the second composite bolted to aluminum specimen, with the two techniques compared to each other. Notice that the raw data represented by the P/Po curve is very similar to that of the first composite bolted to aluminum specimen. Again, the alternate fitting technique works better that the GASmooth application. And again equations (4.1) and (4.3) fit the data more closely that equation (4.4).

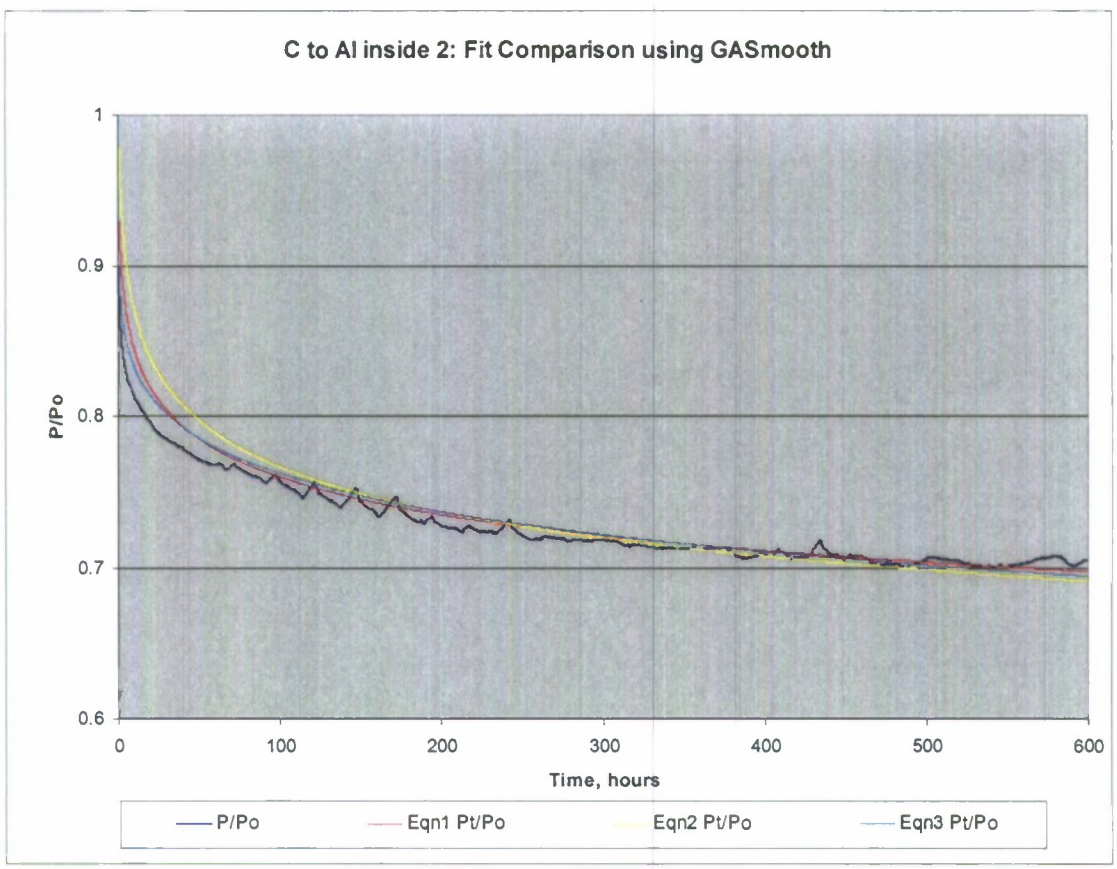

Figure 4.10 – Composite Bolted to Aluminum #2 Fit Comparison Using GASmooth

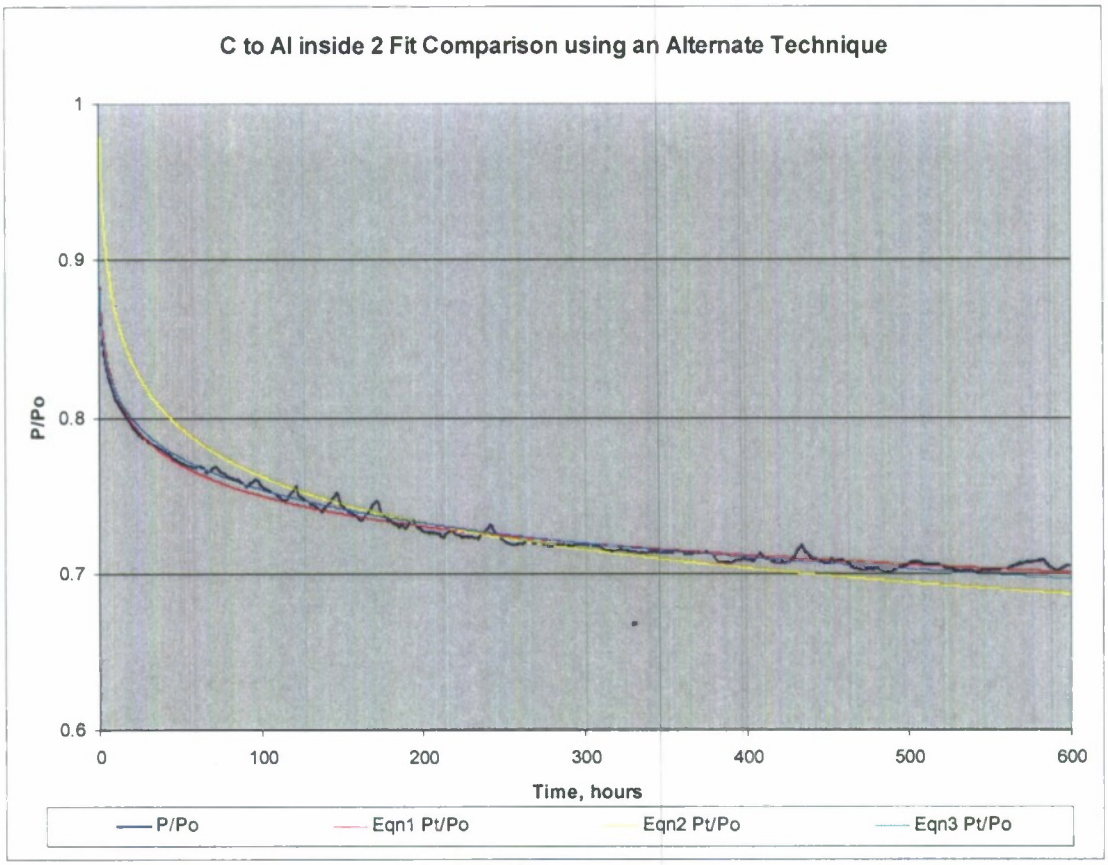

Figure 4.11 – Composite Bolted to Aluminum #2 Fit Comparison Using an Alternate Technique

Composite bolted to Composite Specimen

Figures 4.12 and 4.13 show the only composite bolted to composite specimen tested in the present work. The sharp drop in bolt load is explained by the fact that this joint is made up of two composite plates bolted together, making the viscoelastic nature of the composite material the principal cause for this creep-related plunge. Once again, the alternate correcting technique fits the raw data considerably more closely than the GASmooth technique used. Equations (4.1) and (4.3) yield very good results once more.

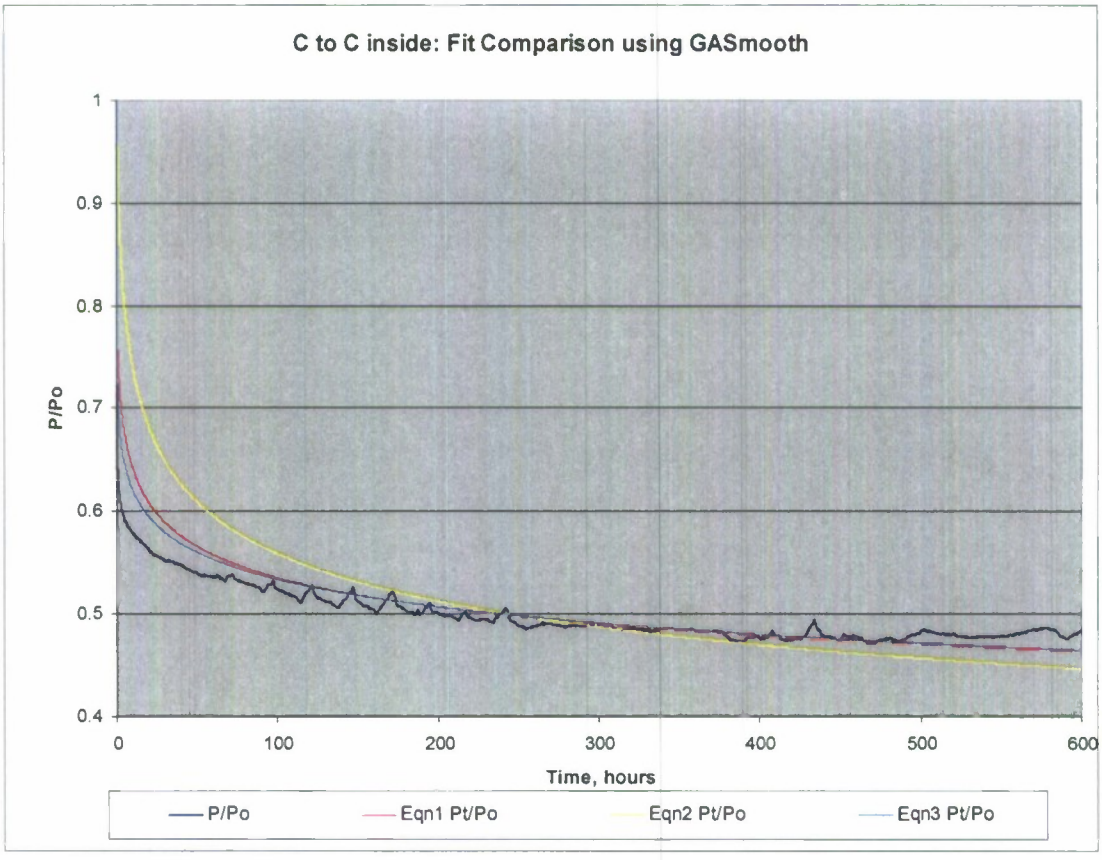

Figure 4.12 – Composite Bolted to Composite Fit Comparison Using GASmooth

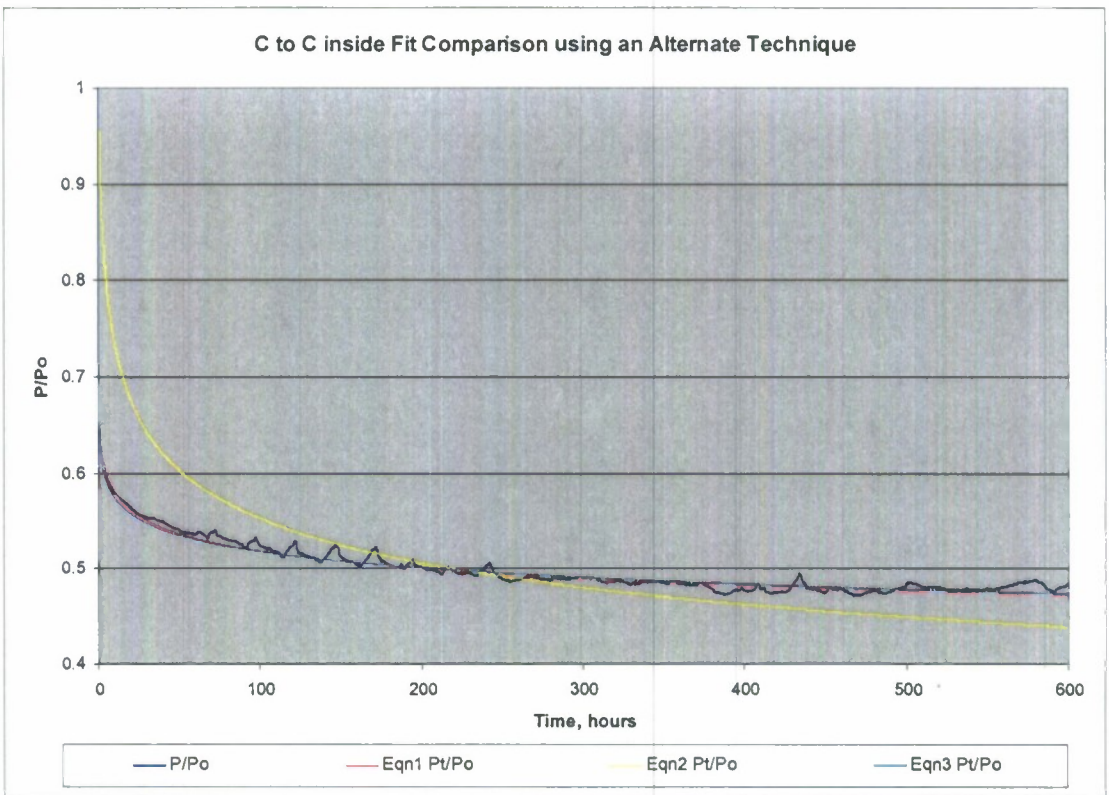

Figure 4.13 – Composite Bolted to Composite Fit Comparison Using an Alternate Technique

Composite bolted to Steel Specimen

Figures 4.14 and 4.15 show the stress relaxation data of the composite bolted to steel specimen tested. Notice that the three fits obtained by GASmooth means are comparable and do not deviate much from each other. Also, the differences between the results obtained by implementing the two techniques are very similar for this test specimen. It is believed that this behavior is related to the lower CTE value of the steel material in this test article. Equation (4.3) is the one that fits the data more closely in both figures. In Figure 4.14 it over estimates the load in the bolt during the first 75 hours of the test. This does not occur when the alternate technique is used. It can be concluded that the alternate technique in conjunction with equations (4.1) and (4.3) is again more appropriate than the GASmooth technique as it can be argued that under estimating the load in the bolt is equivalent as entering a factor of safety.

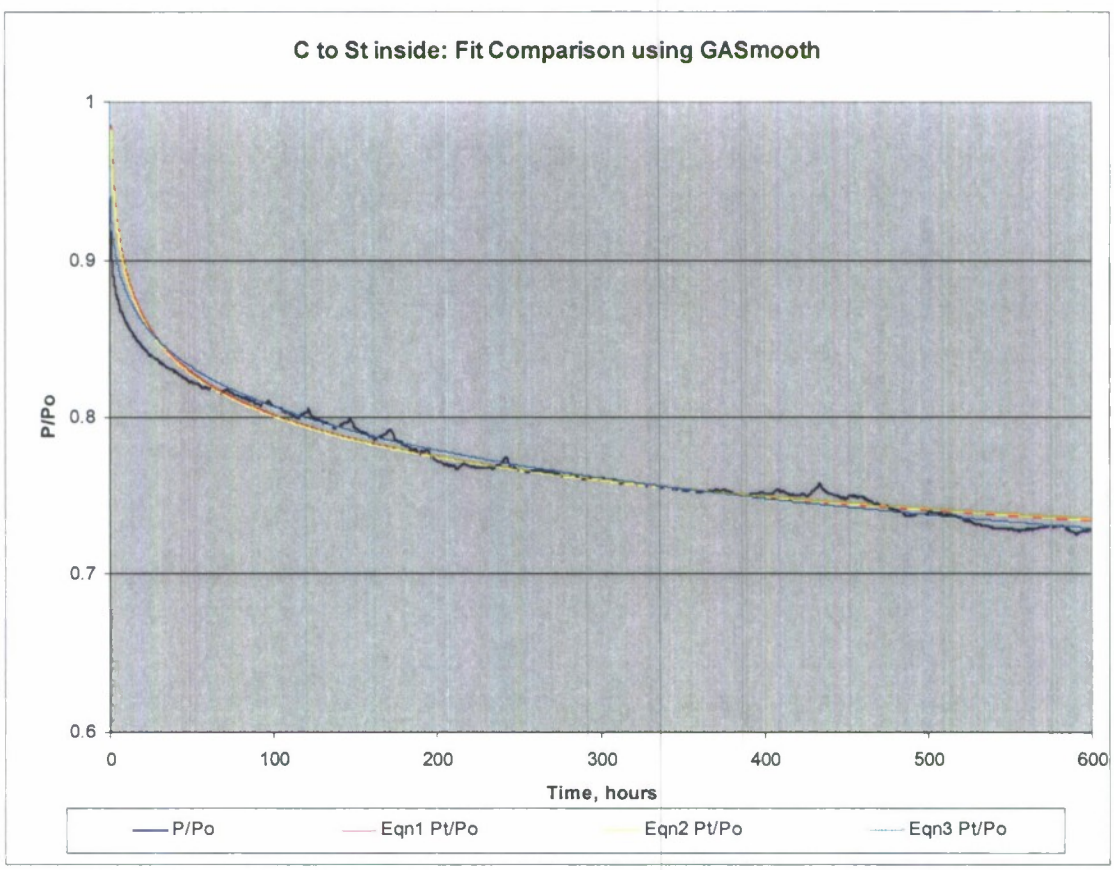

Figure 4.14 – Composite Bolted to Steel Fit Comparison Using GASmooth

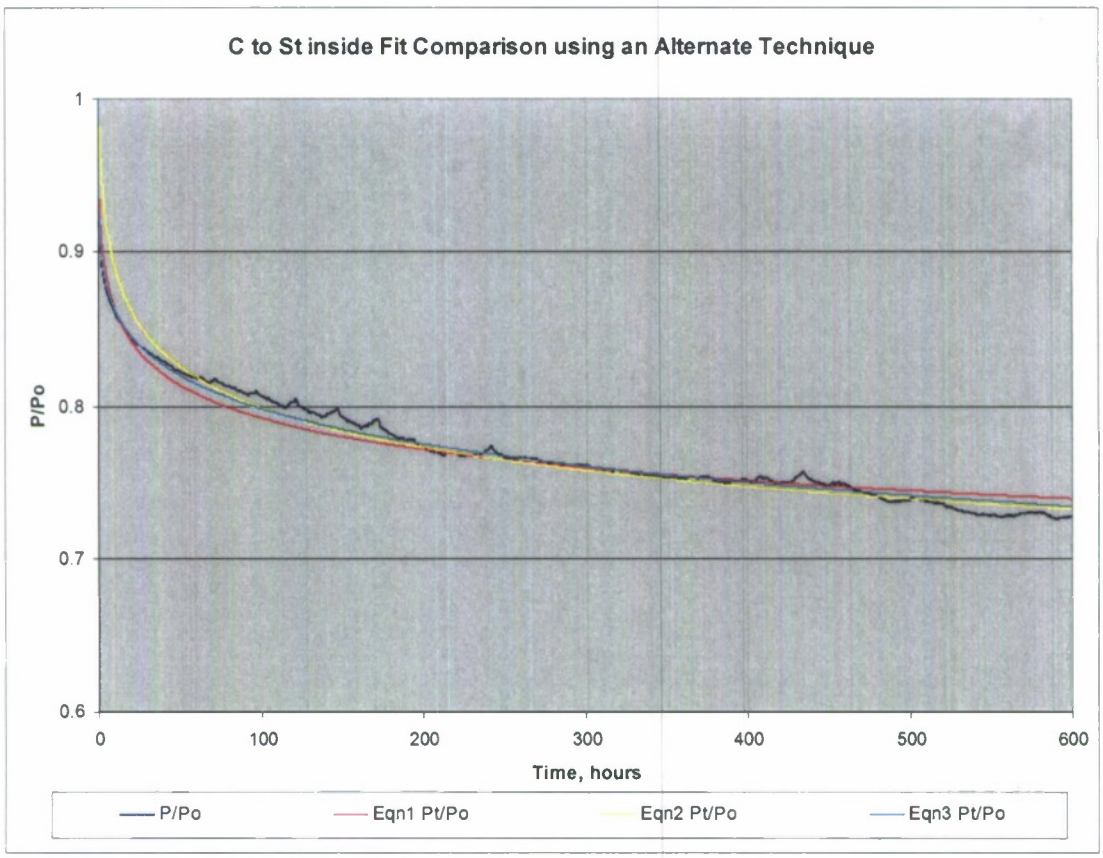

Figure 4.15 – Composite Bolted to Steel Fit Comparison Using an Alternate Technique

Aluminum bolted to Aluminum Specimen

The aluminum bolted to aluminum specimen fit results are shown in Figures 4.16 and 4.17. This was the only metal to metal specimen tested in the present work. It is uncertain, as in the case of the composite bolted to aluminum control specimen, the reason why the quality of the output data turned out to be significantly noisier than that of the rest of the tested articles. It is believed that the connections to the load sensor was,, similarly to that of the control, corrupted. One detail can be readily seen from these figures, and it is the fact that the rate of bolt load loss in this specimen is significantly smaller than that of the rest of the subjects tested, as expected.

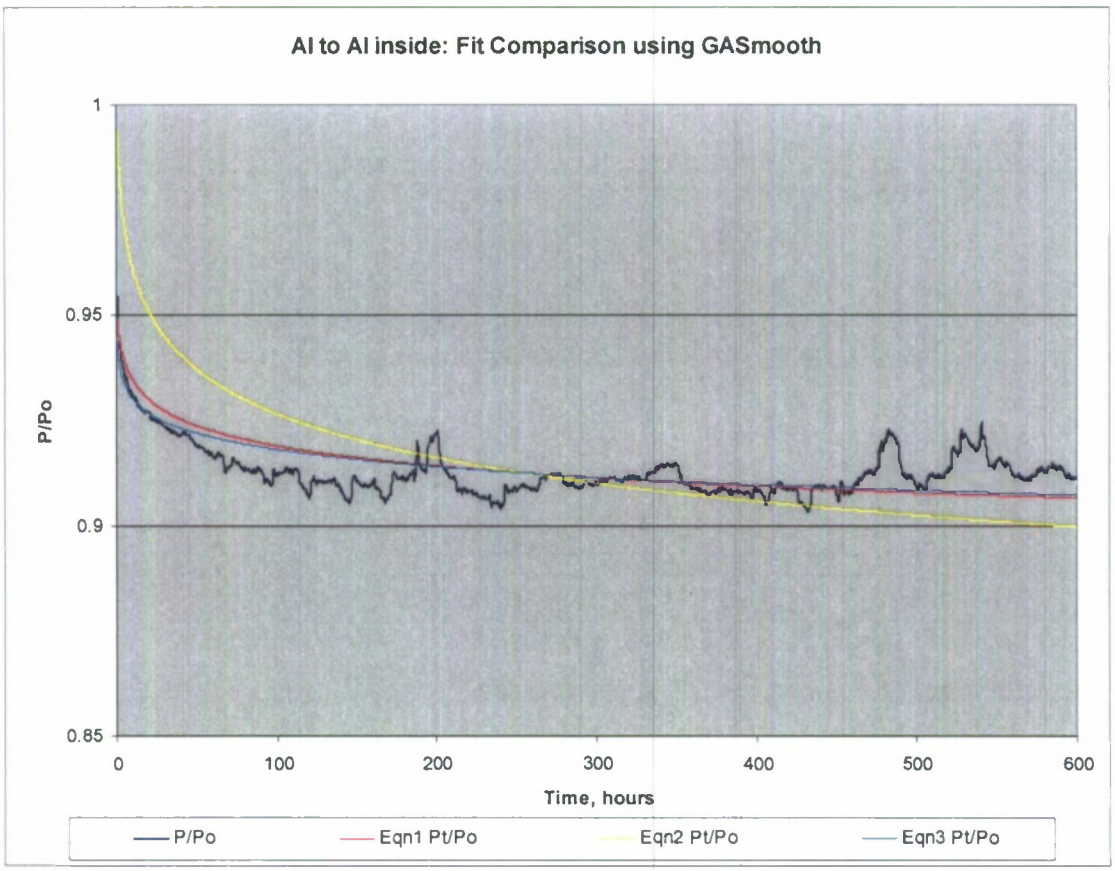

Figure 4.16 – Aluminum Bolted to Aluminum Fit Comparison Using GASmooth

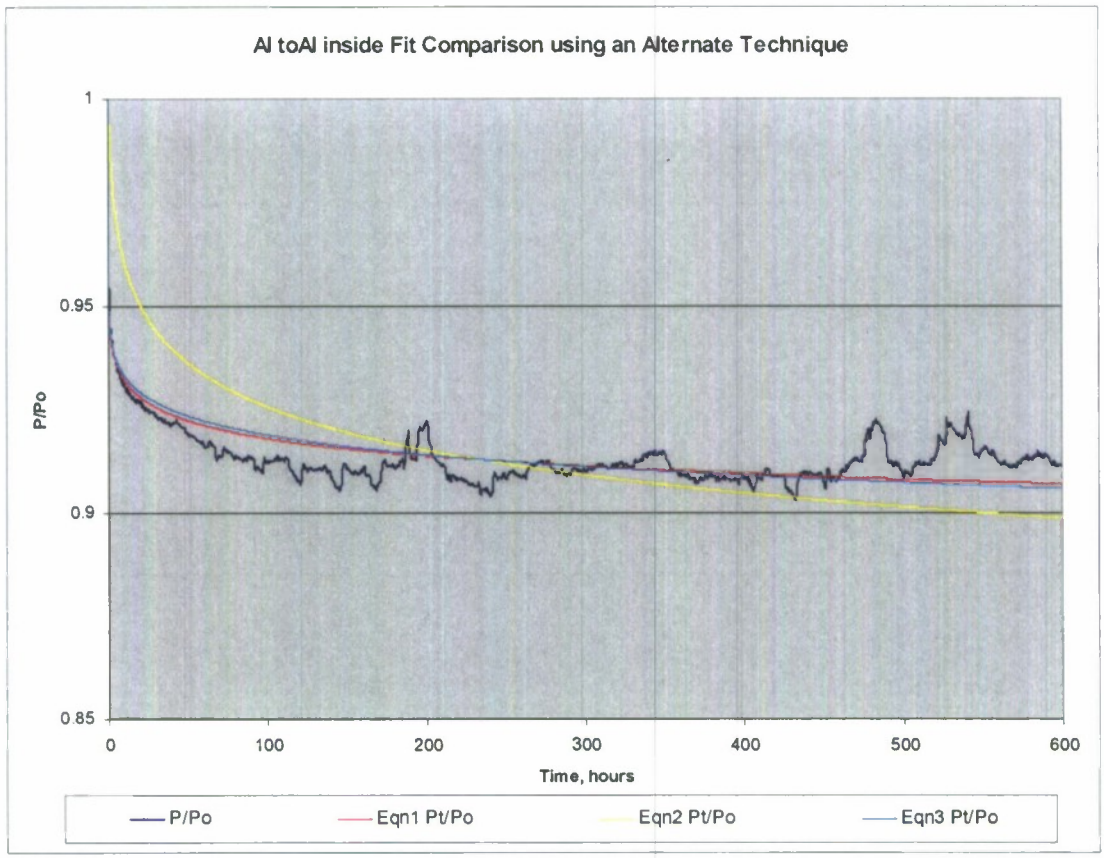

Figure 4.17 – Aluminum bolted to Aluminum Fit Comparison using an Alternate Technique

The graphical results presented here confirm the numerical ones obtained in the previous section. The alternate method for smoothing and correcting the raw experimental data, in conjunction with Equations (4.1) and (4.3) yield the best results. The GASmooth application appears to process the first data point inefficiently, leading to the deviations from the actual data as seen in Figure 4.3. It is believed that if the GASmooth code for smoothing and correcting is refined to avoid such deviations, the end result will be comparable to that of the alternate method.

4.4. Effects of Temperature Cycling

In phase two of the test all samples, except the control, were temperature cycled 5 times. These cycles ran from room temperature to 62.5°C ± 1.5°C (144.5°F ± 3°F) in a

computer controlled autoclave chamber. The time between cycles was set to 7 days to allow the test articles to reach equilibrium. Figure 4.18 shows the 5 temperature cycles in isolation. The result of a one week-long data acquisition malfunction can also be observed in the data gap occurring right after the first temperature cycle, and was the result of a power outage. A closer look at Figure 4.18 reveals a substantial loss of bolt load after this first temperature cycle. Unfortunately, the relaxation data which would enable to quantify this bolt loss was lost in that gap. In any case, this large loss of load occurs to those specimens in which a composite plate, or plates in the case of the composite bolted to composite test article, is used to assemble the connection. The aluminum bolted to aluminum connection, for example, seems to be very little affected by this first temperature cycle, as expected. It is believed this first cycle pre-conditioned the composite material by changing its internal structure. Its effect can therefore be regarded as post-curing the composite material. The large bolt load drop seen in the figure is attributed to the composite material approaching its T_g. The experimental value obtained for the T_g of the composite material was about 78°C (172.4°F). During the first cycle, the maximum temperature reached 64°C (about 147°F). At this point, the curvature of the strain (%) vs. temperature (°C) curve obtained by the DMA is already changing (see Figure 2.7), which could account for what happened. Also, the T_g is the intersection point of two tangents traced on the strain vs. temperature curve and it can slightly vary depending on the way those tangents are traced.

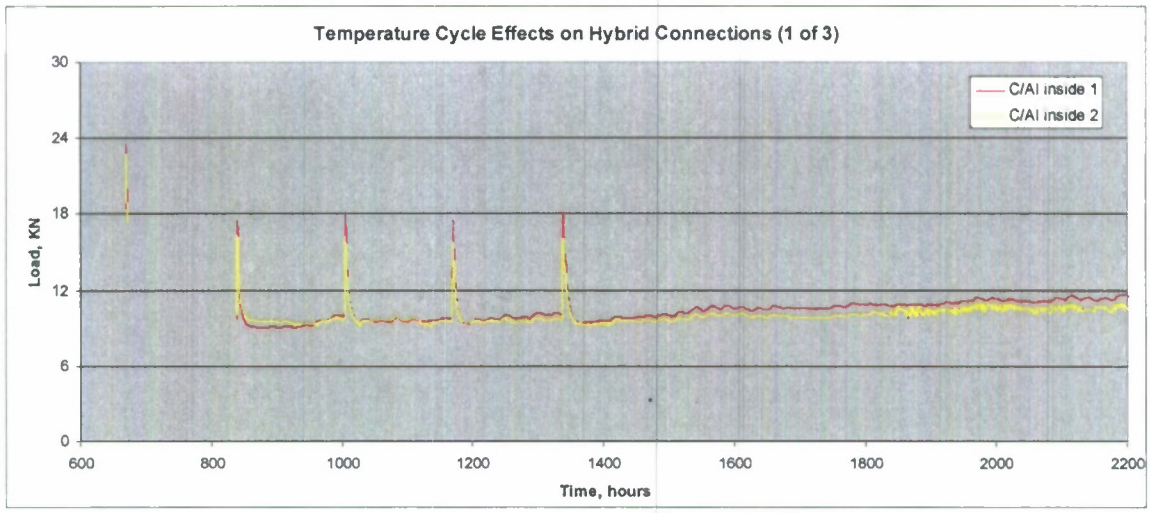

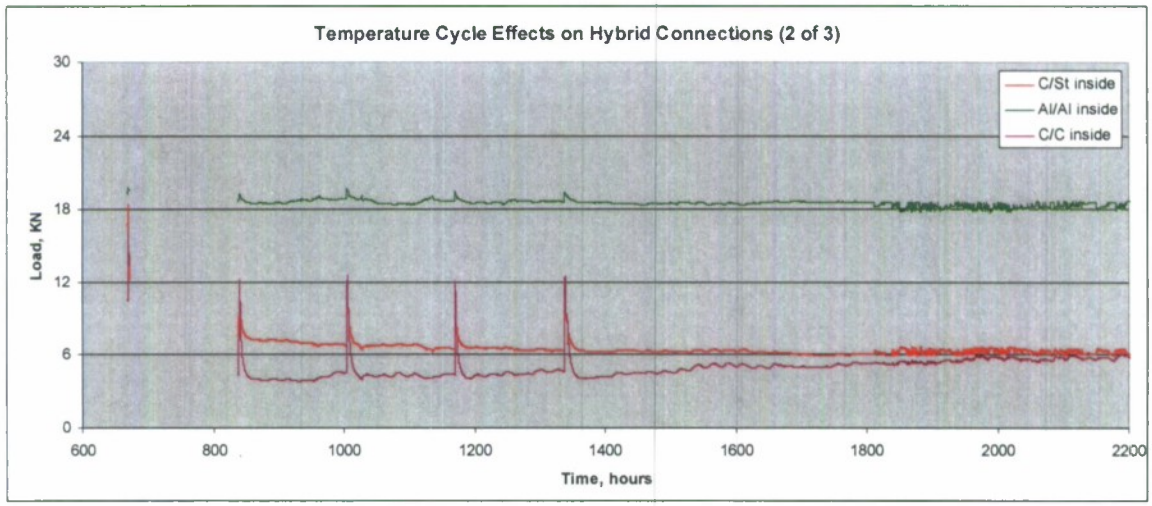

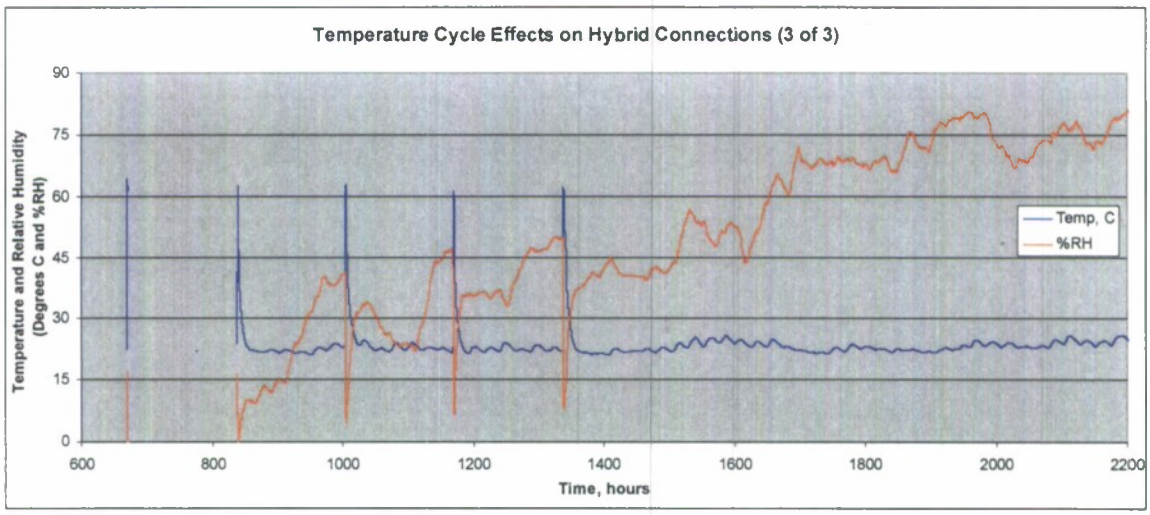

Figure 4.18 – Temperature Cycle Effects on Hybrid Connections

The effect of the subsequent four temperature cycles is consistent across the board for all the specimens tested. The difference in behavior between the "Al/C inside 1" and "AL/C inside 2" specimens is mainly due to the fact that this two coupons were initially loaded to 24.3 and 27.1 KiloNewtons, respectively.

Figure 4.18 also shows the onset of an upward drift starting at about 1500 hours into the test run for the "C/Al inside 1", "C/Al inside 2" and "C/C inside" specimens. This upward drift seems to follow the increase of relative humidity in the chamber where these test articles were placed. On the other hand, the "C/St inside" and "Al/Al inside" specimens appear to be impervious to this increase in relative humidity. The differential response of these test articles to relative humidity fluctuations is best explained by the coupled effect of the material properties and the composite's ability to absorb moisture. The high Modulus of Elasticity of the steel coupled with its low CTE causes this type of connection to be resistant to humidity shifts.

Table 4.7 numerically shows the observed difference between the first temperature cycle and the subsequent four. Attention should be placed on the % Load Increase, as it quantifies the load change due to that particular temperature cycle. Notice that, for all specimens, the first cycle % Load Increase is substantially lower than that of the following four cycles, which then become consistent. The outcome presented in Table 4.7 reaffirms the basis for the argument of a first temperature cycle post-cure effect.

Table 4.7 - Phase 2 Results

Initial Preload, KN	24.29	27.07	21.33	22.17	22.98
1st Temperature Cycle	C/AL inside 1	C/AL inside 2	AL/AL inside	C/C inside	C/St inside
Start Temp (°C)	22.00	22.00	22.00	22.00	22.00
Max. Temp (°C)	64.10	64.10	64.10	64.10	64.10
Temp Increase (°C)	42.09	42.09	42.09	42.09	42.09
% Temp Increase	191.32	191.32	191.32	191.32	191.32
Max Load, KN	23.51	22.62	19.70	16.16	18.42
Start Load, KN	18.29	18.96	19.28	10.44	16.70
End Load, KN	18.26	17.36	19.46	13.23	12.14
Load Increase, KN	5.22	3.67	0.41	5.73	1.72
% Load Increase	28.57	19.34	2.15	54.87	10.30
2nd Temperature Cycle					

Start Temp (°C)	23.56	23.56	23.56	23.56	23.56
Max. Temp (°C)	62.27	62.27	62.27	62.27	62.27
Temp Increase (°C)	38.71	38.71	38.71	38.71	38.71
% Temp Increase	164.31	164.31	164.31	164.31	164.31
Max Load, KN	17.48	16.34	19.25	12.15	11.38
Start Load, KN	9.63	10.06	18.51	4.29	7.44
End Load, KN	9.93	9.71	18.81	4.52	6.76
Load Increase, KN	7.85	6.27	0.74	7.86	3.94
% Load Increase	81.49	62.36	4.00	183.42	52.95
3rd Temperature Cycle					
Start Temp (°C)	22.98	22.98	22.98	22.98	22.98
Max. Temp (°C)	62.64	62.64	62.64	62.64	62.64
Temp Increase (°C)	36.57	36.57	36.57	36.57	36.57
% Temp Increase	172.58	172.58	172.58	172.58	172.58
Max Load, KN	18.06	16.16	19.65	12.60	10.79
Start Load, KN	9.93	9.71	18.81	4.52	6.76
End Load, KN	9.68	9.50	18.60	4.32	6.46
Load Increase, KN	8.06	6.39	0.82	8.18	4.03
% Load Increase	81.92	66.39	4.43	178.73	59.62
4th Temperature Cycle					
Start Temp (°C)	21.30	21.30	21.30	21.30	21.30
Max. Temp (°C)	60.95	60.95	60.95	60.95	60.95
Temp Increase (°C)	37.07	37.07	37.07	37.07	37.07
% Temp Increase	186.14	186.14	186.14	186.14	186.14
Max Load, KN	17.50	15.73	19.36	12.08	10.30
Start Load, KN	9.68	9.50	18.60	4.32	6.46
End Load, KN	10.03	9.68	18.52	4.60	6.29
Load Increase, KN	7.79	6.19	0.79	7.81	3.84
% Load Increase	80.76	65.51	4.12	179.66	59.49
5th Temperature Cycle					
Start Temp (°C)	21.83	21.83	21.83	21.83	21.83
Max. Temp (°C)	62.11	62.11	62.11	62.11	62.11
Temp Increase (°C)	40.28	40.28	40.28	40.28	40.28
% Temp Increase	184.52	184.52	184.52	184.52	184.52
Max Load, KN	18.03	16.01	19.33	12.51	10.20
Start Load, KN	10.03	9.68	18.52	4.60	6.29
End Load, KN	9.79	9.54	18.43	4.39	6.29
Load Increase, KN	7.99	6.33	0.81	7.90	3.91
% Load Increase	79.68	65.41	4.35	171.79	62.11
% Load Increase Average Cycles 2-5	80.96	64.92	4.23	178.40	58.54

Figure 4.19 shows the graphical result of the first temperature cycle for all the specimens, which ran for a little over 2.5 hours. The autoclave chamber did not reach the preset maximum temperature cleanly due to controlling problems. The figure clearly shows that the "C/C inside" specimen is the most sensitive to the temperature spike. This is attributed to the large CTE value of the composite material compared to that of the steel bolt. On the other hand, the "Al/Al inside" specimen modestly feels the cycle due to its lower CTE. Notice also the response differential between the two composite bolted to aluminum specimens. Although their behavior mirror each other, the temperature cycle of the article loaded to a smaller preload, the "C/Al inside 1", has a distinctively greater effect than that of the second composite bolted to aluminum ("C/Al inside 2") specimen. The reason is that the "C/Al inside 1" retained about 75.3% of its preload at the start of the cycle, whereas the "C/Al inside 2" retained only about 70%. This result is in agreement with the findings presented in the work of Pelletier et al. [2005], which stated that the more preload retained by a connection, the more sensitive it becomes to temperature shifts. Also identified in the figure is the rapid loss of bolt load in all specimens except the "Al/Al inside" once the maximum load gain has been reached for the attained temperature. This loss of load is mainly due creep and relaxation occurs even maintaining the temperature constant. Appendix D presents the graphical output for the following four temperature cycles run. In those, creep related load loss is not observed in any of the specimens tested. The onset of relaxation occurs the moment the temperature initiates its descend to room temperature.

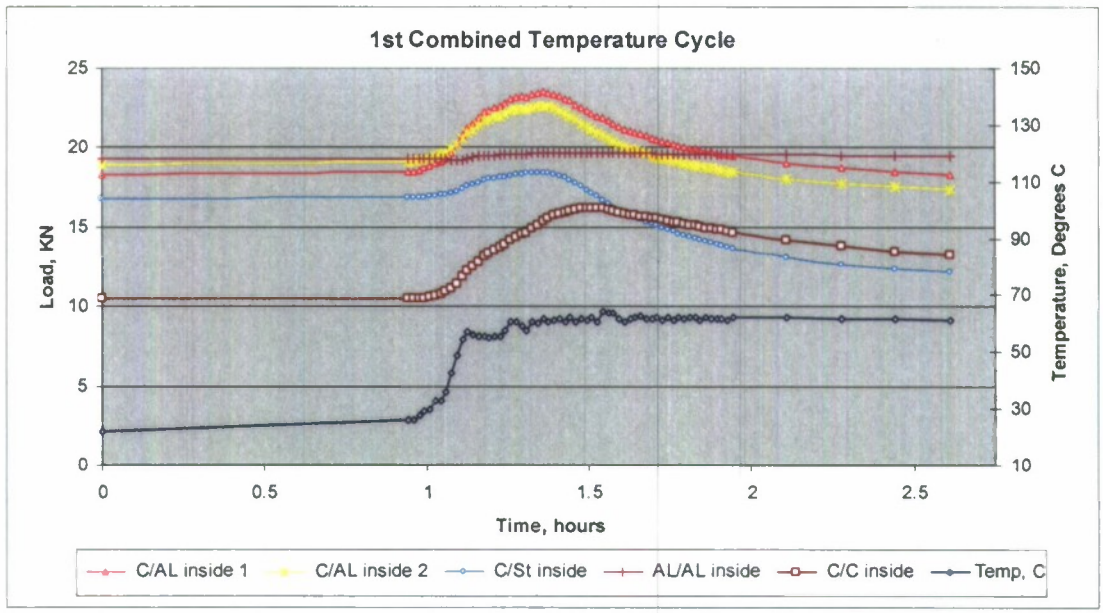

Figure 4.19 – Specimen Response to the First Temperature Cycle

From these interpretations it is concluded that temperature shifts have a clear impact on the response of hybrid connections primarily due to the different CTE values of the material constituents. Quantifying such responses depends on an appropriately obtained temperature correction factor, which in turn depends on such variables like material properties and the important Influence Zone or contact area between the two mating parts of the connection. Sections 2.2 and 2.3 present the procedure followed to compute the temperature factor for the different connection type tested. Tables 4.8 to 4.11 show the relationship between the correction factor and the Influence Zone diameter, D_I, for the composite bolted to aluminum, the composite bolted to steel, the composite bolted to composite and the aluminum bolted to aluminum specimens, respectively.

Table 4.8 – Temperature Correction Factor Correlation with D_I for the Composite Bolted to Aluminum Specimens

$D_I = xD_b$	TFact, KN/°C
2.5	0.471
2.25	0.447
2	0.413
1.75	0.365
1.5	0.295
1.3	0.211
1.275	0.198
1.25	0.184

Table 4.9 – Temperature Correction Factor Correlation with D_I for the Composite Bolted to Steel Specimen

$D_I = xD_b$	TFact, KN/°C
2.5	0.396
2.25	0.387
2	0.373
1.75	0.352
1.5	0.314
1.3	0.257
1.275	0.247
1.25	0.235

Table 4.10 – Temperature Correction Factor Correlation with D_1 for the Aluminum Bolted to Aluminum Specimen

$D_1 = xD_b$	TFact, KN/°C
2.5	0.510
2.25	0.456
2	0.391
1.75	0.312
1.5	0.221
1.3	0.138
1.275	0.127
1.25	0.116

Table 4.11 – Temperature Correction Factor Correlation with D_1 for the Aluminum Bolted to Aluminum Specimen

$D_1 = xD_b$	TFact, KN/°C
2.5	0.260
2.25	0.251
2	0.239
1.75	0.219
1.5	0.187
1.3	0.148
1.275	0.137
1.25	0.129

The results presented in this section establish the importance of post curing the composite material used in this type of connections. In general, the selected composite material should be post cured above its service temperature to avoid the dramatic loss of load that carries the first temperature cycle.

5. SUMMARY, CONCLUSIONS AND RECOMMENDATIONS

The primary effects of temperature on the stress relaxation response of hybrid connections were studied experimentally in the effort presented in this report. To this end, six single lap, single bolted connection specimens were fabricated and tested. Three of them were made by joining a composite plate to an aluminum plate. The fourth connected a composite plate to a steel plate. The fifth consisted in joining two composite plates together, and the sixth connection used two aluminum plates bolted to each other. The selected fastener to join all six articles was a set of instrumented steel bolts. The composite chosen came from a ½" thick EGlass/Vinyl ester plate. Aluminum 6061-T6 and structural steel A36 plates of the same thickness were the other two materials selected to fabricate the connections. The investigation presented herein focuses first, on the effects of room temperature and its inherent variations in the primary stress relaxation response, and second, on the effects of deliberate temperature cycles in this type of connection. Specific plans were devised to analyze the effects of temperature change in these connections. First, a model was developed with the sole purpose of incorporating the existing Coefficient of Thermal Expansion mismatch between all the joint parts in the scheme of the analysis. Second, tests were planned and conducted to obtain the CTE property value of the EGlass/Vinyl ester composite material used in the hybrid connections. Third, a series of tests were designed and carried out on the connection specimens to observe their stress relaxation dependency on temperature, and fourth, a computer program, GASmooth, and an alternate technique were used to reduce the data generated by the hybrid connection tests.

The coefficient of thermal expansion, CTE, and the glass transition temperature, T_g, of the composite material used in the tests was found to be $45.8 \cdot 10^{-6}$/°C ($25.4 \cdot 10^{-6}$/°F) and 78.33°C (173°F), respectively. The Modulus of Elasticity and the CTE of the connection materials was entered, in addition to the geometrical variables, in the model developed to account for the coefficient of thermal expansion mismatch between the connection parts. The goal was to obtain a temperature correction factor to correct the raw data obtained from the tests

The experiment performed to study the effects of temperature on single bolt hybrid connections ran for a period of 3 months (around 2,200 hours). Two test phases were considered. The first test stage ran over a period of 25 days (600 hours). The initial preload for the specimens tested is given in Table 3.1. All test articles were left to stress relax at room temperature, undisturbed. In the second phase, the test specimens, except for the control, were temperature cycled a total of 5 times. These cycles were performed every 7 days and consisted in increasing the testing temperature from room temperature to 62.5°C ± 1.5°C (144.5°F ± 3°F), for a period of 1 hour after which it was slowly returned to room temperature. The maximum temperature attained was theoretically below the composite's glass transition temperature, T_g. The specimens were then allowed to stress relax for one week to let them reach an equilibrium condition before the start of the next cycle.

The following conclusions and recommendations are provided from the test results obtained:

1. The bolt load dependence on temperature has been confirmed for a second time. The degree of this dependence is strongly influenced by the CTE and the Modulus of Elasticity of the constituent materials of the connection, as expected. The evidence is shown in Figures 4.2 and 4.19. In these two figures, the composite bolted to steel ("C/St inside") and the aluminum bolted to aluminum ("Al/Al inside") specimens display a less sensitive reaction to temperature shifts compared to that of the rest of the test articles. Such response is attributed to the relatively small CTE figure for both steel and aluminum compared to that of the EGlass/vinyl ester composite used in the connections. On the other hand, the composite's Modulus of Elasticity is significantly smaller than that of both metals. This explains why temperature fluctuations have a greater effect in the composite bolted to aluminum specimens than in the composite bolted to steel specimen. It also explains the gentler rate of bolt load loss in the composite bolted to steel and aluminum bolted to aluminum specimens.
2. Similarly to the temperature effects on the response of the specimens tested, relative humidity swings have a stronger influence on the composite bolted to aluminum and composite bolted to composite specimens than on the composite

bolted to steel or aluminum bolted to aluminum test coupons. The same reasons that explain the specimens' behavior to temperature variability apply when the relative humidity changes. In this case, the ability of the composite material to absorb ambient moisture is responsible for the increase in bolt load in those specimens. Figures 4.1 and 4.2 show that a moderate increase in relative humidity towards the end of the first test stage seemed to slow down the stress relaxation progression of the composite bolted to aluminum and the composite bolted to composite specimens, whereas the relaxation of the composite bolted to steel and aluminum bolted to aluminum specimens was unaltered. Moreover, the same observation can be made during the second testing phase, where the increase of relative humidity is more evident.

3. A sound procedure to obtain the coefficient of thermal expansion, CTE, of a composite material using a DMA was presented in Section 2.1. The CTE for the EGlass/vinyl ester composite was found to be 45.75×10^{-6}/°C (25.42×10^{-6}/°F). This material property became fundamental for the proper analysis of the temperature effects on the relaxation history of the tested specimens.
4. The composite material's CTE was entered in a model developed to account for the CTE mismatch between all the hybrid connection parts. This model presented in Section 2.2, was instrumental in finding the connection-specific correction factor needed to smooth and correct the raw data for temperature effects.
5. Two techniques were used to reduce the raw data generated by the experiments. The GASmooth Windows-based application and an alternate technique were implemented to smooth and correct the bolt load data. Three different power law expressions were used to analyze the bolt load with respect to time in an attempt to seek alternate and simpler means to fit the data. The goal was to avoid hard-to-explain relaxation coefficients. These expressions were presented in Section 4.1 as Equations (4.1), (4.3) and (4.4). Pelletier et al. [2005] Equation (4.2) was also cross referenced with the above equations for Figure 3.4 presented by the authors. In general, it was found that Equations (4.1) and (4.3) together with the alternate technique for smoothing and correcting fit the data the best.

6. The temperature cycles run during the second phase of the experimental program here presented confirmed the importance of post curing the composite material above its service temperature. As shown in Figure 4.18 and also in Table 4.7, the first temperature cycle carried with it a dramatic loss of bolt load. Subsequent temperature cycles did not further alter the response of the test articles.

The author of the work presented herein recommends to further study the environmental effects on the stress relaxation of hybrid connections using alternate analysis techniques. The GASmooth application has been proved a powerful instrument, but it requires code revision to more effectively reduce stress relaxation data. The use of environmental chambers would also be advisable in an effort to compare tight controlled circumstances to normal operating conditions. Alternate load cells should also be considered when investigating the behavior of these hybrid connections. Klett et al. [2005] performed indirect measurements of bolt preload with several types of washer load cells and a strain gaged bolt. To compare the different load cells, the bolt preload was monitored for a steel to steel bolted specimen with both a washer load cell and the bolt load cell. After torquing, the preload did not change significantly with time for the washer load cell, which would be expected for steel plates. However, the bolt load cell indicated the preload continued to drop to 86% of the initial bolt preload after 70 hours. They concluded that although the bolt load cell would be desirable for use in static and fatigue joint tests from a simplicity standpoint, it was unsuitable for monitoring bolt preload due to this drift or creep of the load cell itself. An Interface washer load cell, Model LW2550-30K, was chosen instead for use in the static and fatigue joint testing to monitor the loss of bolt preload.

REFERENCES

A.L. Design, Inc. - Designers and Manufacturers of Custom and Standard Load Cells, A.L. Design, Inc., www.aldesigninc.com, copyright 1999-2006

ASTM Designation D 2990-01 [2001], "Standard Test Method for Tensile, Compressive, and Flexural Creep and Creep-Rupture of Plastics," Vol. 8.02, 202-221

ASTM Designation E 328-02 [2002], "Standard Test Method for Stress Relaxation for Materials and Structures," Vol. 3.01, pp. 379-390

ASTM Designation F 1276-99 [1999], "Standard Test Method for Creep Relaxation of Laminated Composite Gasket materials," Vol. 9.02, pp. 414-418

ASTM Designation E 831-08 [2006], "Standard Test Method for Linear Thermal Expansion of Solid Materials by Thermomechanical Analysis,"

Bathgate, R. G., Wang, C. H. and Pang, F. [1997], "Effects of Temperature on the Creep Behaviour of Woven and Stitched Composites," Composite Structures, vol. 38, No. 1-4, pp. 435-445

Benkhedda, A., Tounsi, A. and Adda Bedia, E. A. [2008], "Effect of Temperature and Humidity on Transient Hygrothermal Stresses During Moisture Desorption in Laminated Composite Plates," Composite Structures, Vol. 82, pp. 629-635.

Caccese, V., Mewer, R. and Vel, S. S. [2004], "Detection of Bolt Load Loss in Hybrid Composite/Metal Bolted Connections," Engineering Structures, vol. 26, pp. 895-906.

Cain, J. J., Post, N. L., Lesko, J. J., Case, S. W. [2006], "Post-Curing Effects on Marine VARTM FRP Composite Material Properties for Test and Implementation," Transaction of the ASME, vol. 128, pp. 34-40

Chen, H. –S. and Kung, H. K. [2002], "A Hygrothermal Sensitivity Evaluation on the Clamp-up Torque of Bolted Composite Joint," 17th Annual Technical Conference American Society for Composites, October 21-23, 2002

"Derakane Epoxy Vinyl Ester Resins," Form no. 125-00016-396X SMG, March 1996, The Dow Chemical Company, pp. 16-17.

Fox, D.M. [1994], "Bolted Joint Studies in GRP", Master of Science Thesis, Massachusetts Institute of Technology, 124 pp.

Findley, W. N., James, L. S. and Onaran, K. [1976], Creep and Relaxation of Nonlinear Viscoelastic Materials, Dover Publications, Inc., New York

Honeywell Home, Honeywell International Inc., www.honeywell.com, copyright 2003

Ireman, T. [1998], "Three-dimensional stress analysis of bolted single-lap composite joints," Composite Structures, Vol. 43, pp. 195-216

Kabche, J. –P., Caccese, V., Berube, K. A., Thompson, L. and Walls, J. [2005], "Structural Response of a Hybrid Composite-to-Metal Bolted Connection Under Uniform Pressure Loading," Composite Structures, vol. 78, pp. 207-221

Katouzian, M., Brueller, O.S., Horoschenkoff, A. [1995], "Effect of Temperature on the Creep Behavior of Neat and Carbon Fiber Reinforced PEEK and Epoxy Resin", Journal of Composite Materials, Vol. 29, No. 3, pp. 372-387.

Kim, W., and Sun, C.T., [2002] "Modeling Relaxation of a Polymeric Composite During Loading and Unloading", Journal of Composite Materials, Vol. 36, No. 6, pp. 745-755.

Klett, L. B., Herling, D. R., Eberhardt, J. J. and Sklad, P. S. [2005], "Attachment Techniques for Heavy Truck Composite Chassis Members", Progress Report, FY 2005, Oak Ridge National Laboratory Contract No. DE-AC05-00OR22725 and DE-AC06-76RL01830.

MatWeb, Online Material Data Sheet, Automation Creations, Inc., www.matweb.com, Copyright 1996-2003

National Semiconductor, The Sight and Sound of Information, National Semiconductor Corporation, www.national.com, copyright 2003

Pelletier, K. N., Caccese, V. and Berube, K. A. [2005], "Influence of Stress Relaxation in Hybrid Composite/Metal Bolted Connections", Report No. UM-MACH-RPT-01-02, Prepared for the Office of Naval Research under Grant No. N00014-01-1-0916

Pang, F. and Wang, C. H. [1999], "Activation Theory for Creep of Woven Composites," Composites: Part B, vol. 30, pp. 613-620

Shivakumar, K.N., and Crews, J. H., [1982], "Bolt Clamp-up Relaxation in a Graphite/Epoxy Laminate", NASA, TM 83268, 30pp.

Sun, H-T., Chang, F-K, and Quing, X., [2002], "The Response of Composite Joints with Bolt Clamping Loads, Part II: Model Verification", Journal of Composite Materials, Vol. 36, No. 1, pp. 69-92.

Weerth, D. E. and C. Ortloff [1986], "Creep Considerations in Reinforced Plastic Laminate Bolted Connections," Army Symposium on Solid Mechanics – Lightening the Force, Oct. 1986, pp. 137-154

APPENDICES

Appendix A. Additional DMA Test Results

Figures A.1 to A.5 show the graphical results for the CTE and T_g obtained for samples 2 to 6 of the EGlass/vinyl ester composite. Figures A.6 to A.8 show the three baselines obtained using a quartz article. Lastly, Figures A.9 and A.10 show the CTE results of two control runs using a copper specimen.

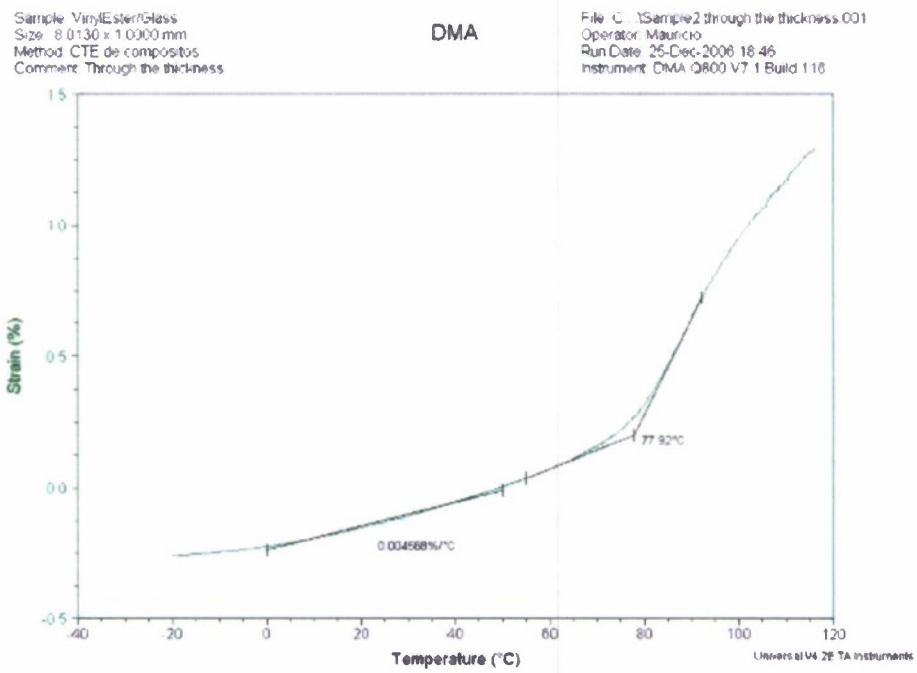

Figure A.1 – Sample 2 Obtained from -20°C to 120 °C

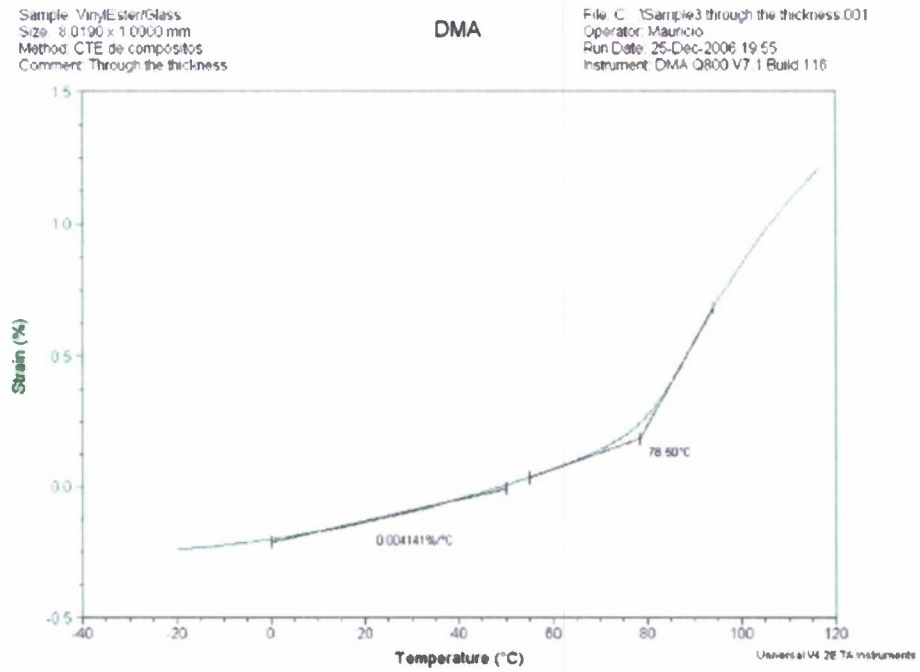

Figure A.2 – Sample 3 Obtained from -20°C to 120 °C

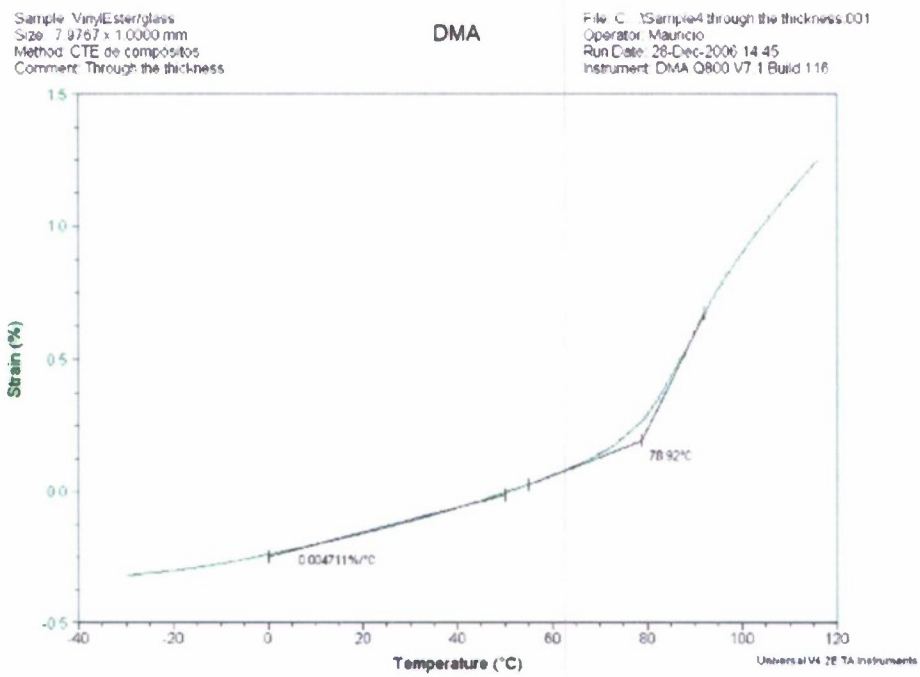

Figure A.3 – Sample 4 Obtained from -30°C to 120 °C

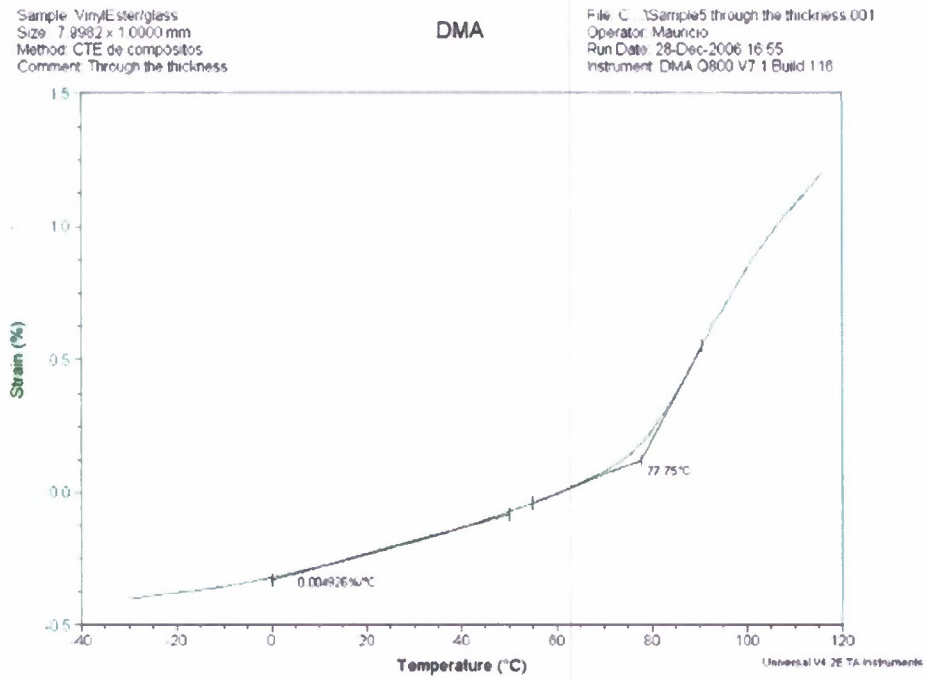

Figure A.4 – Sample 5 Obtained from -30°C to 120 °C

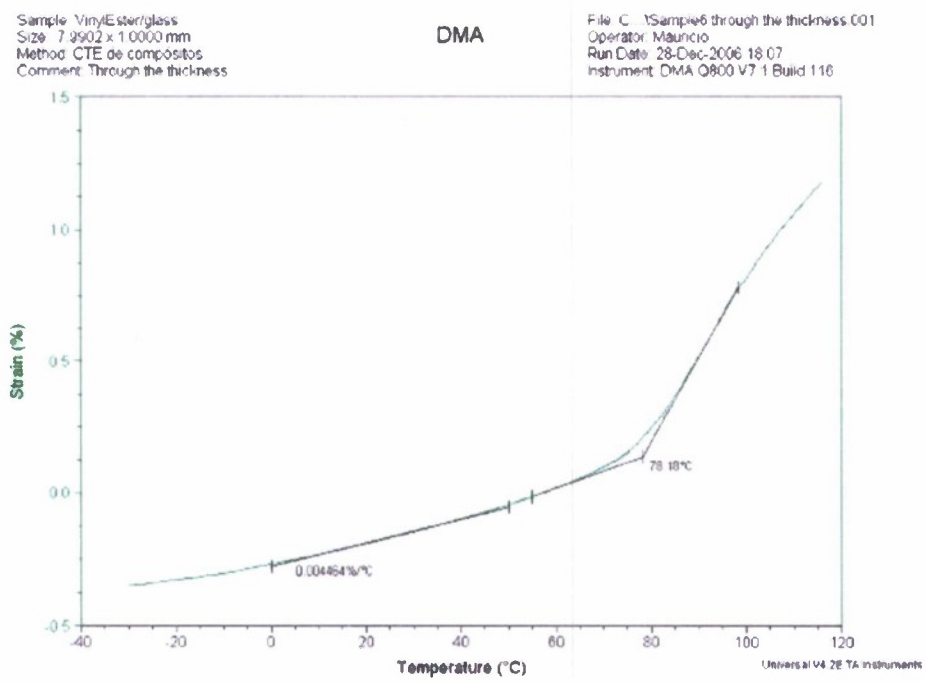

Figure A.5 – Sample 6 Obtained from -30°C to 120 °C

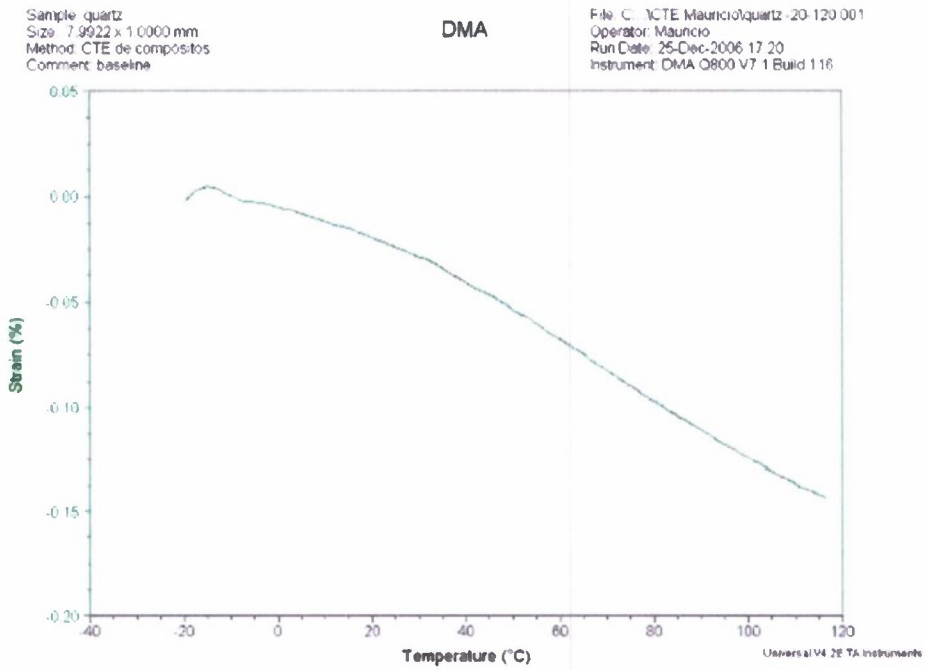

Figure A.6 – Quartz Baseline Obtained from -20°C to 120 °C

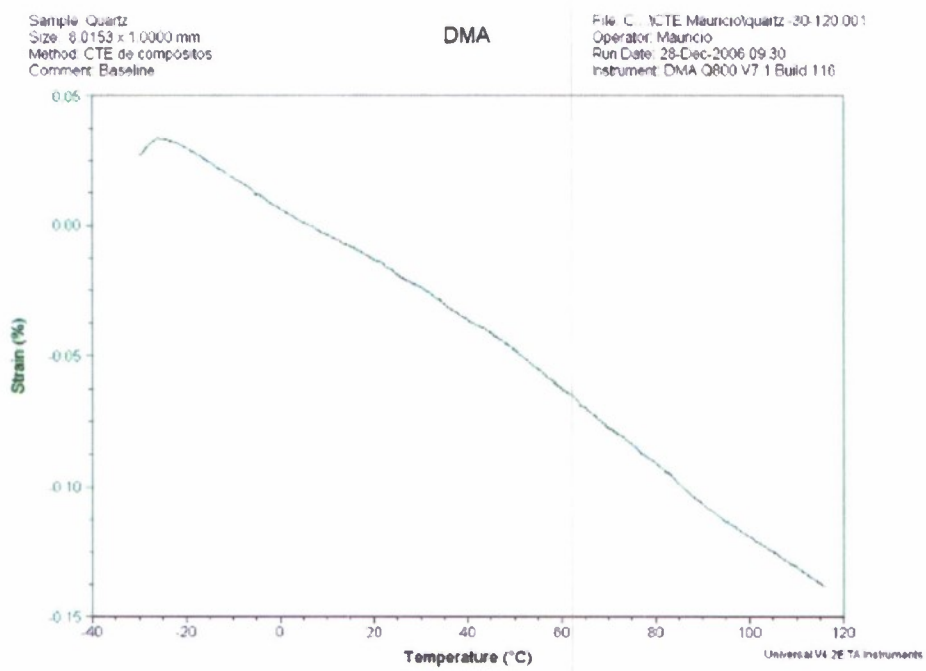

Figure A.7 – Quartz Baseline Obtained from -30°C to 120 °C

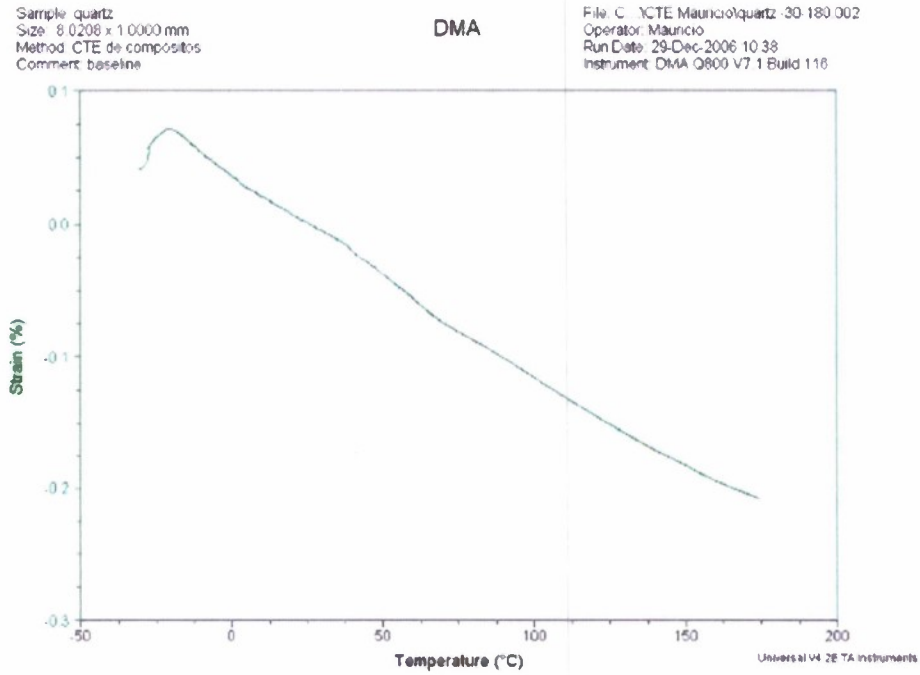

Figure A.8 – Quartz Baseline Obtained from -30°C to 180 °C

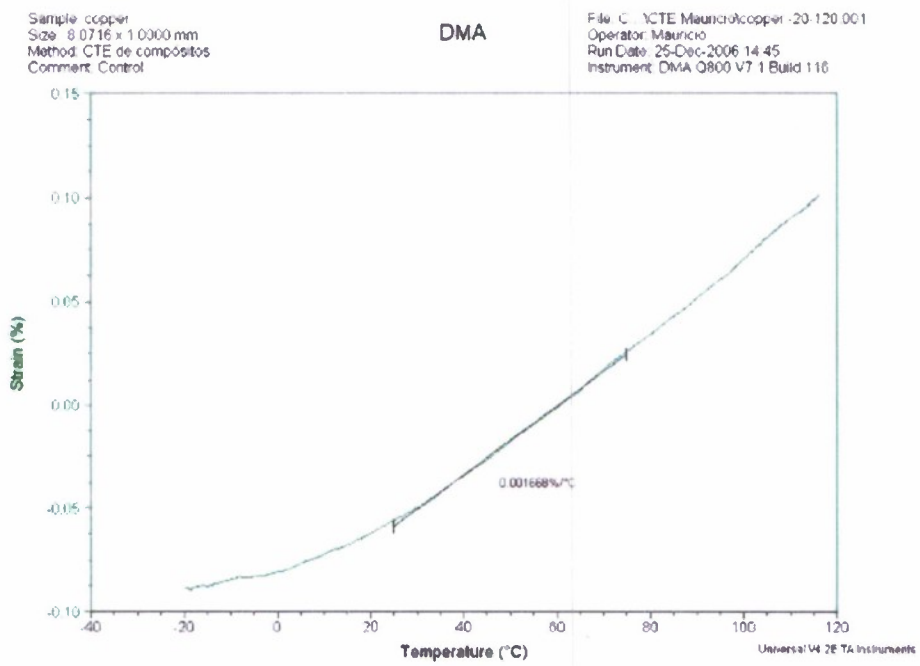

Figure A.9 – Copper Control CTE Obtained from -20°C to 120 °C

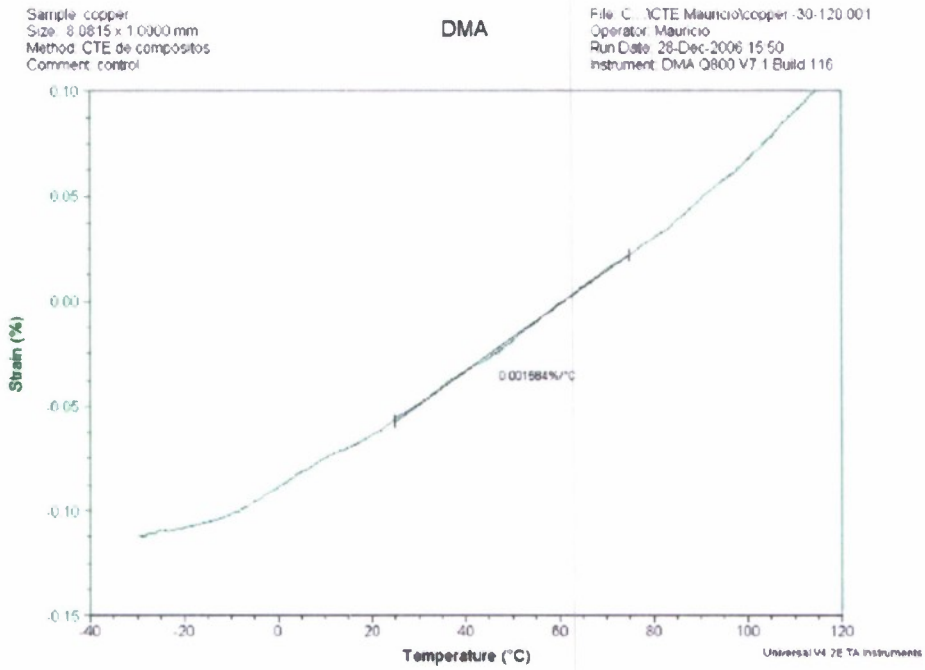

Figure A.10 – Copper Control CTE Obtained from -30°C to 120 °C

Appendix B. Additional TMA Test Results

The graphical results for specimens 1b to 1d are displayed in Figures B.1 to B.3. These figures also include the method to obtain the through-the-thickness CTE for these coupons. Similarly, Figures B.4 to B.6 show the in-plane CTE for specimens 2a to 2c and Figures B.7 to B.9 that for specimens 3a to 3c.

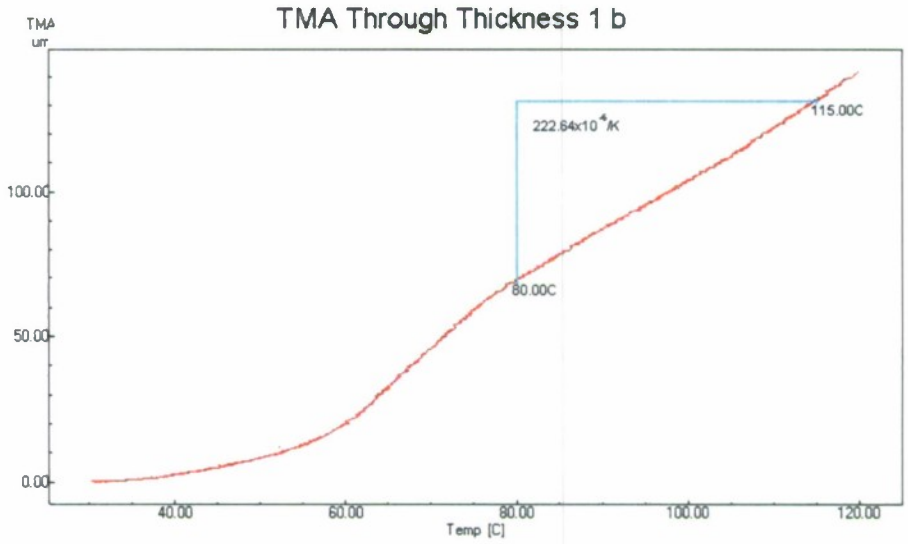

Figure B.1 - Specimen 1b strain-temperature plot and CTE

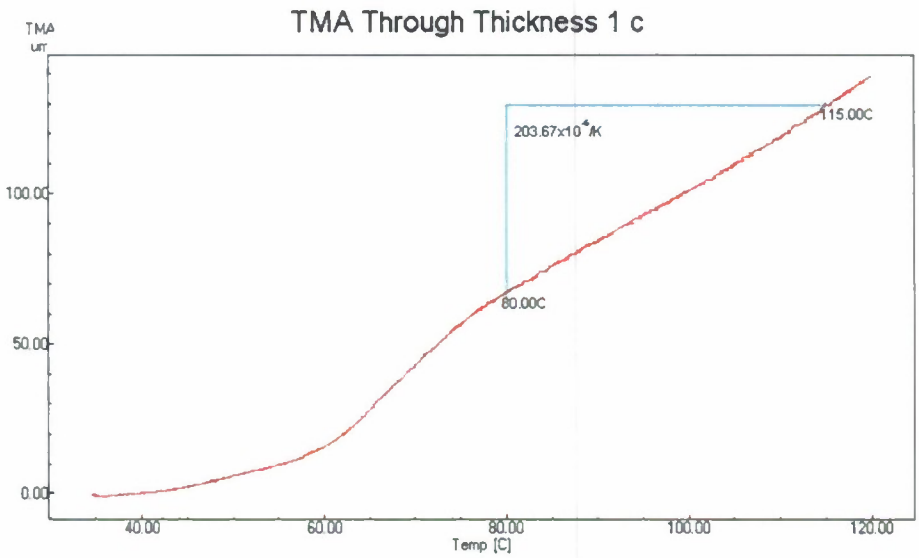

Figure B.2 - Specimen 1c strain-temperature plot and CTE

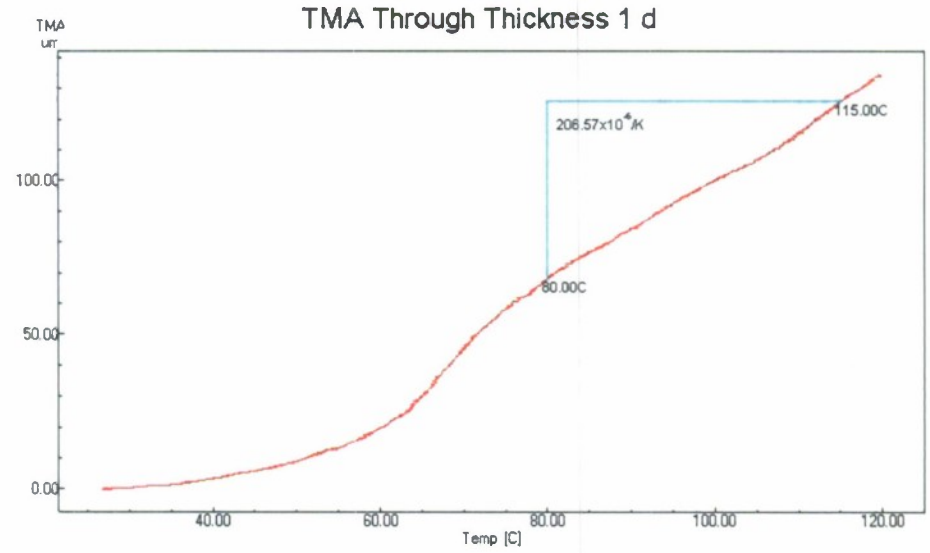

Figure B.3 - Specimen 1d strain-temperature plot and CTE

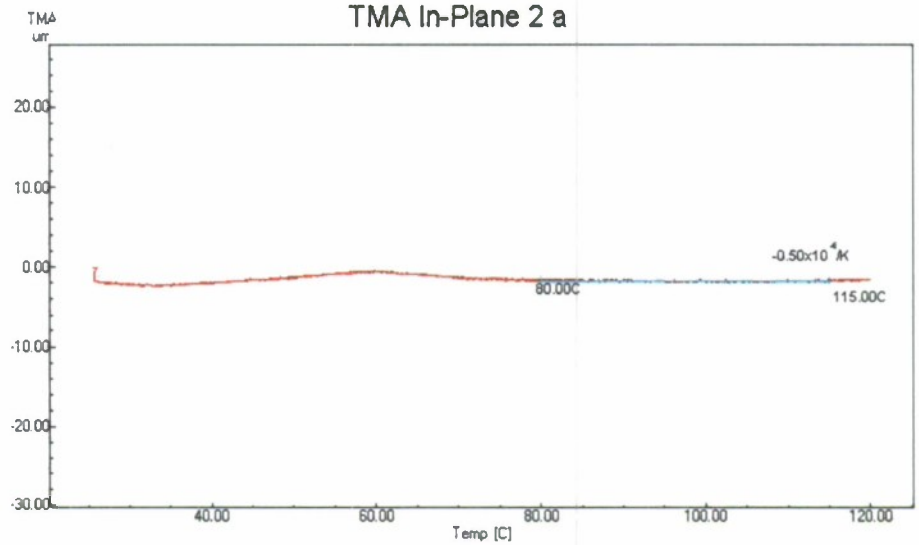

Figure B.4 - Specimen 2a strain-stress plot and CTE

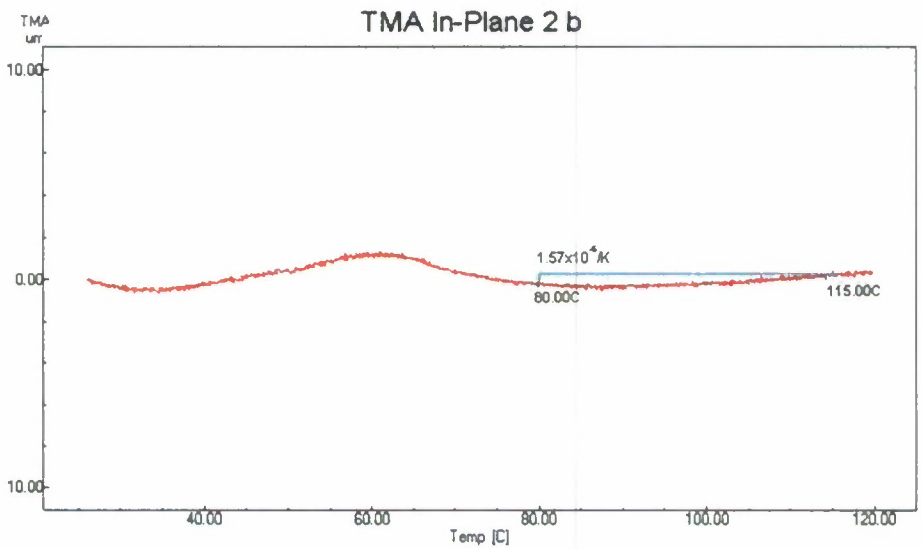

Figure B.5 - Specimen 2b strain-stress plot and CTE

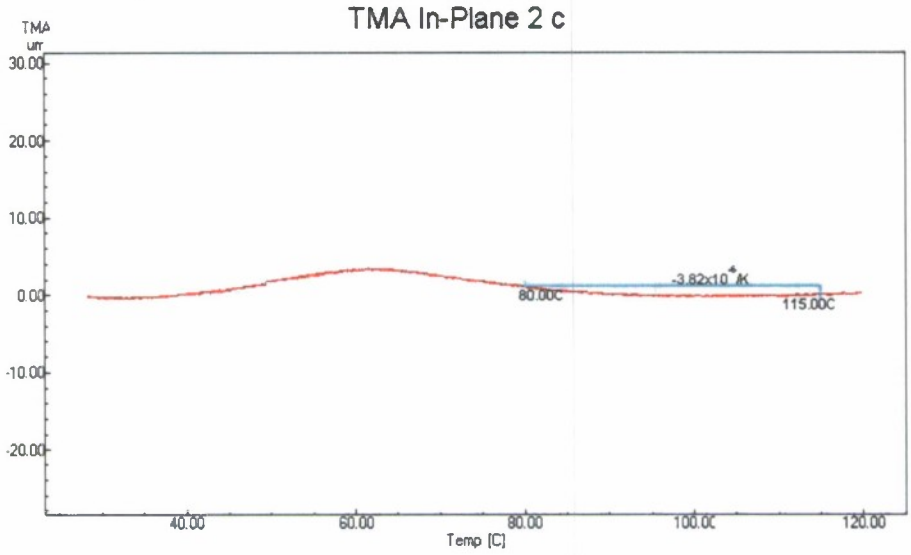

Figure B.6 - Specimen 2c strain-stress plot and CTE

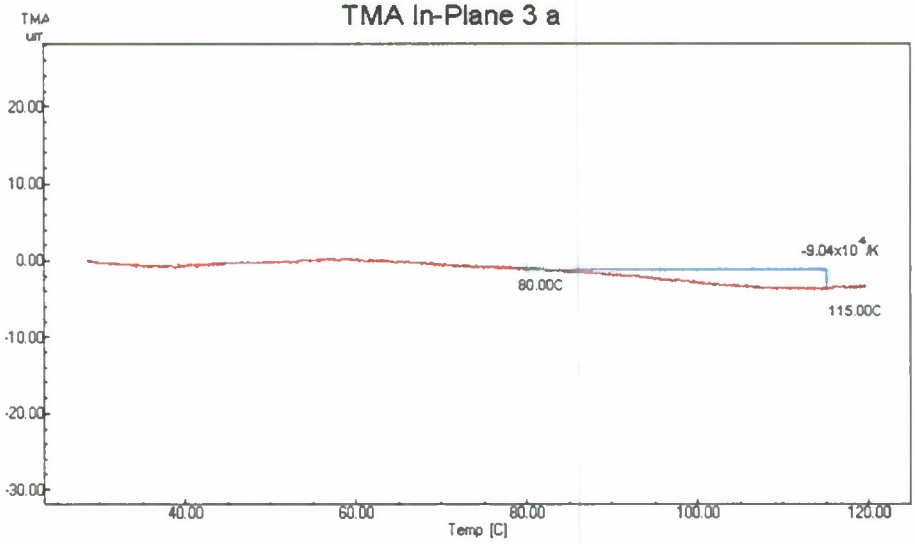

Figure B.7 - Specimen 3a strain-stress plot and CTE

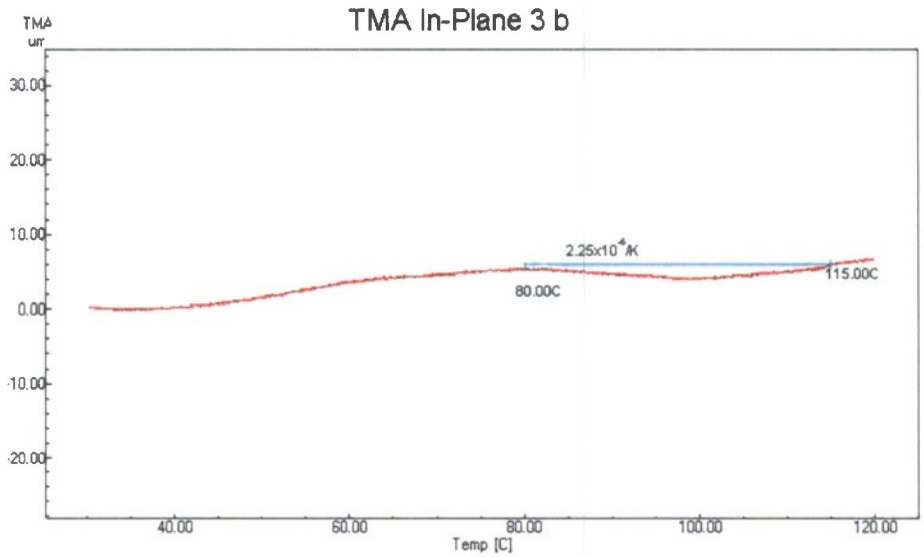

Figure B.8 - Specimen 3b strain-stress plot and CTE

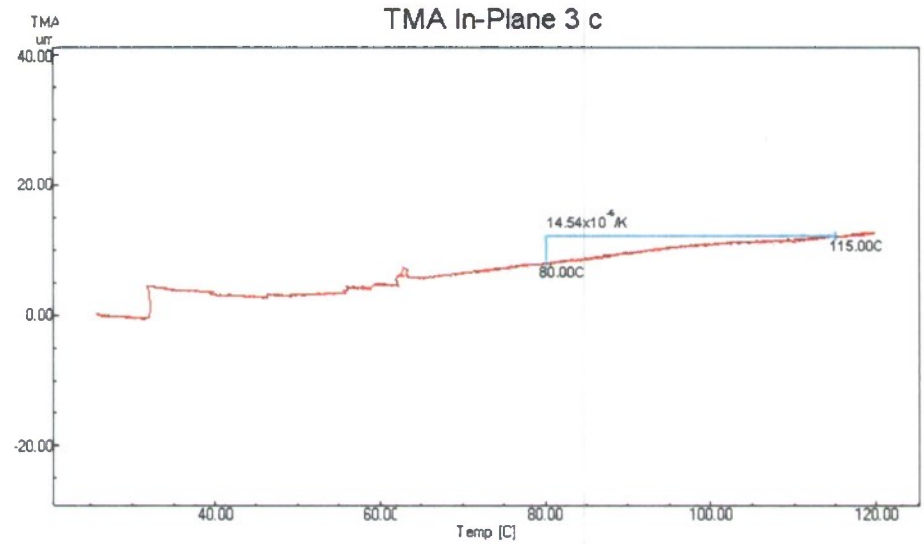

Figure B.9 - Specimen 3c strain-stress plot and CTE

Appendix C. Hybrid Connection Temperature Correction Factor Computation

Figure C.1 displays a screen shot of the Mathcad sheet used to compute the temperature correction factor, Kpt or TFact in the GASmooth application, for the composite bolted to aluminum specimens. Similarly, Figures C.2 to C.4 show the calculation applied to the composite bolted to steel, composite bolted to composite and aluminum bolted to aluminum specimens. The CTE value for the composite material is the figure obtained from the DMA tests. Those for the aluminum and steel are obtained from the literature. To simplify the composite bolted to steel computation, the CTE and Modulus of Elasticity of aluminum have been replaced for those of steel in Figure C.2. Likewise, the composite bolted to composite computation sheet, as shown in Figure C.3, sees the CTE and Modulus of Elasticity of aluminum replaced for those of composite. Finally, for the aluminum bolted to aluminum specimen, the CTE and Modulus of the composite have been replaced to those of aluminum in Figure C.4.

The material properties, as presented in Table 2.10, are:

$\alpha_{Al} := 13 \cdot 10^{-6}$ 1/F $\alpha_b := 6.5 \cdot 10^{-6}$ 1/F $\alpha_c := 25.42\,10^{-6}$ 1/F Value obtained thfough DMA experiments.

$E_{Al} := 10 \cdot 10^{6}$ psi $E_b := 29 \cdot 10^{6}$ psi $E_c := 2.0 \cdot 10^{6}$ psi Value obtained from "Influence of Stress Relaxation in Hybrid Composite/ Metal bolted Connections" report, page 78, Tensile Modulus.

The thicknesses of the aluminum and composite plates are, respectively:

$t_{Al} := \frac{1}{2}$ in $t_c := \frac{1}{2}$ in

The bolt size and the Influence Zone diameter are, respectively:

$D_b := \frac{1}{2}$ in $D_I := 2 \cdot D_b$

The contact area for the aluminum and for the composite plates are, respectively:

$$A_{Al} := \pi \cdot \frac{\left(D_I^{\,2} - D_b^{\,2}\right)}{4} \qquad A_c := \pi \cdot \frac{\left(D_I^{\,2} - D_b^{\,2}\right)}{4}$$

The cross sectional area of the bolt is:

$$A_b := \pi \cdot \frac{D_b^{\,2}}{4}$$

The stiffness for the aluminum and composite materials and that for the bolt material (steel) are found, respectively, as:

$$K_{Al} := \frac{A_{Al} \cdot E_{Al}}{t_{Al}} \qquad K_c := \frac{A_c \cdot E_c}{t_c} \qquad K_b := \frac{A_b \cdot E_b}{t_{Al} + t_c}$$

The thermal elongation due to a temperature change or unconfined growth of the bolt, the aluminum plate and that of the composite plate, per degree F are , respectively:

$\delta_{tb} := \alpha_b \cdot (t_{Al} + t_c)$ $\delta_{tb} = 6.5 \times 10^{-6}$ in/F

$\delta_{tAl} := \alpha_{Al} \cdot (t_{Al})$ $\delta_{tAl} = 6.5 \times 10^{-6}$ in/F

$\delta_{tc} := \alpha_c \cdot (t_c)$ $\delta_{tc} = 1.271 \times 10^{-5}$ in/F

The net length change of the bolt and that of the aluminum and the composite plates is found using the equations:

$$\Delta_b = \delta_{tb} + \frac{P_t}{K_b} \qquad (1)$$

$$\Delta_{Alc} = \delta_{tAl} + \delta_{tc} - \frac{P_t}{K_{Al} + K_c} \qquad (2)$$

To maintain joint integrity, the following condition must be met:

$\Delta_b = \Delta_{Alc}$ (3)

Substituting equations (1) and (2) into equation (3) and solving for Pt gives:

$$P_t := \left(\delta_{tAl} + \delta_{tc} - \delta_{tb}\right) \cdot \frac{K_b \cdot \left(K_{Al} + K_c\right)}{K_{Al} + K_c + K_b} \qquad P_t = 51.592 \text{ lbs/F}$$

Figure C.1 - TFact for the Composite bolted to Aluminum Specimens

The material properties, as presented in Table 2.10, are:

$\alpha_{Al} := 6.5 \cdot 10^{-6}$ 1/F (See *) $\alpha_b := 6.5 \cdot 10^{-6}$ 1/F $\alpha_c := 25.42 \cdot 10^{-6}$ 1/F

In this case, the Al plate has been replaced by a steel plate (A36). Nomenclature is maintained for simplicity.

$E_{Al} := 29 \cdot 10^{6}$ psi (See *) $E_b := 29 \cdot 10^{6}$ psi $E_c := 2.0 \cdot 10^{6}$ psi

Value obtained from "Influence of Stress Relaxation in Hybrid Composite/ Metal bolted Connections" report, page 78, Tensile Modulus.

The thicknesses of the aluminum and composite plates are, respectively:

$t_{Al} := \frac{1}{2}$ in $t_c := \frac{1}{2}$ in

(*) This is the CTE of Steel, because the Al plate is now a steel plate. Nomenclature unchanged for simplicity. Imagine Al is really St.

The bolt size and the Influence Zone diameter are, respectively:

$D_b := \frac{1}{2}$ in $D_I := 2 \cdot D_b$

The contact area for the aluminum and for the composite plates are, respectively:

$$A_{Al} := \pi \cdot \frac{\left(D_I^2 - D_b^2\right)}{4} \qquad A_c := \pi \cdot \frac{\left(D_I^2 - D_b^2\right)}{4}$$

The cross sectional area of the bolt is:

$$A_b := \pi \cdot \frac{D_b^2}{4}$$

The stiffness for the aluminum and composite materials and that for the bolt material (steel) are found, respectively, as:

$$K_{Al} := \frac{A_{Al} \cdot E_{Al}}{t_{Al}} \qquad K_c := \frac{A_c \cdot E_c}{t_c} \qquad K_b := \frac{A_b \cdot E_b}{t_{Al} + t_c}$$

The thermal elongation due to a temperature change or unconfined growth of the bolt, the aluminum plate and that of the composite plate, per degree F are , respectively:

$\delta_{tb} := \alpha_b \cdot (t_{Al} + t_c)$ $\delta_{tb} = 6.5 \times 10^{-6}$ in/F

$\delta_{tAl} := \alpha_{Al} \cdot (t_{Al})$ $\delta_{tAl} = 3.25 \times 10^{-6}$ in/F

$\delta_{tc} := \alpha_c \cdot (t_c)$ $\delta_{tc} = 1.271 \times 10^{-5}$ in/F

The net length change of the bolt and that of the aluminum and the composite plates is found using the equations:

$$\Delta_b = \delta_{tb} + \frac{P_t}{K_b} \qquad (1)$$

$$\Delta_{Alc} = \delta_{tAl} + \delta_{tc} - \frac{P_t}{K_{Al} + K_c} \qquad (2)$$

To maintain joint integrity, the following condition must be met:

$$\Delta_b = \Delta_{Alc} \qquad (3)$$

Substituting equations (1) and (2) into equation (3) and solving for Pt gives:

$$P_t := \left(\delta_{tAl} + \delta_{tc} - \delta_{tb}\right) \cdot \frac{K_b \cdot (K_{Al} + K_c)}{K_{Al} + K_c + K_b} \qquad P_t = 46.601 \text{ lbs/F}$$

Figure C.2 - TFact for the Composite bolted to Steel Specimen

The material properties, as presented in Table 2.10, are:

$\alpha_{Al} := 25.42 \cdot 10^{-6}$ 1/F (See *) $\quad \alpha_b := 6.5 \cdot 10^{-6}$ 1/F $\quad \alpha_c := 25.42 \cdot 10^{-6}$ 1/F

$E_{Al} := 2.0 \cdot 10^{6}$ psi (See *) $\quad E_b := 29 \cdot 10^{6}$ psi $\quad E_c := 2.0 \cdot 10^{6}$ psi

In this case, the Al plate has been replaced by a composite plate. Nomenclature is maintained for simplicity.

Value obtained from "Influence of Stress Relaxation in Hybrid Composite/ Metal bolted Connections" report, page 78, Tensile Modulus.

(*) This is the CTE of the composite, because the Al plate is now a composite plate. Nomenclature unchanged for simplicity. Imagine Al is really composite.

The thicknesses of the aluminum and composite plates are, respectively:

$t_{Al} := \frac{1}{2}$ in $\quad t_c := \frac{1}{2}$ in

The bolt size and the Influence Zone diameter are, respectively:

$D_b := \frac{1}{2}$ in $\quad D_I := 2 \cdot D_b$

The contact area for the aluminum and for the composite plates are, respectively:

$$A_{Al} := \pi \cdot \frac{\left(D_I^2 - D_b^2\right)}{4} \qquad A_c := \pi \cdot \frac{\left(D_I^2 - D_b^2\right)}{4}$$

The cross sectional area of the bolt is:

$$A_b := \pi \cdot \frac{D_b^2}{4}$$

The stiffness for the aluminum and composite materials and that for the bolt material (steel) are found, respectively, as:

$$K_{Al} := \frac{A_{Al} \cdot E_{Al}}{t_{Al}} \qquad K_c := \frac{A_c \cdot E_c}{t_c} \qquad K_b := \frac{A_b \cdot E_b}{t_{Al} + t_c}$$

The thermal elongation due to a temperature change or unconfined growth of the bolt, the aluminum plate and that of the composite plate, per degree F are , respectively:

$\delta_{tb} := \alpha_b \cdot (t_{Al} + t_c)$ $\quad \delta_{tb} = 6.5 \times 10^{-6}$ in/F

$\delta_{tAl} := \alpha_{Al} \cdot (t_{Al})$ $\quad \delta_{tAl} = 1.271 \times 10^{-5}$ in/F

$\delta_{tc} := \alpha_c \cdot (t_c)$ $\quad \delta_{tc} = 1.271 \times 10^{-5}$ in/F

The net length change of the bolt and that of the aluminum and the composite plates is found using the equations:

$$\Delta_b = \delta_{tb} + \frac{P_t}{K_b} \qquad (1)$$

$$\Delta_{Alc} = \delta_{tAl} + \delta_{tc} - \frac{P_t}{K_{Al} + K_c} \qquad (2)$$

To maintain joint integrity, the following condition must be met:

$$\Delta_b = \Delta_{Alc} \qquad (3)$$

Substituting equations (1) and (2) into equation (3) and solving for Pt gives:

$$P_t := \left(\delta_{tAl} + \delta_{tc} - \delta_{tb}\right) \cdot \frac{K_b \cdot (K_{Al} + K_c)}{K_{Al} + K_c + K_b} \qquad P_t = 48.785 \text{ lbs/F}$$

Figure C.3 - TFact for the Composite bolted to Composite Specimen

The material properties, as presented in Table 2.10, are:

$\alpha_{Al} := 13 \cdot 10^{-6}$ 1/F (See *) $\alpha_b := 6.5 \cdot 10^{-6}$ 1/F $\alpha_c := 13 \cdot 10^{-6}$ 1/F (See *)

$E_{Al} := 10 \cdot 10^{6}$ psi $E_b := 29 \cdot 10^{6}$ psi $E_c := 10 \cdot 10^{6}$ psi

In this case, the composite plate has been replaced by an aluminum plate. Nomenclature is maintained for simplicity.

Value obtained from "Influence of Stress Relaxation in Hybrid Composite/ Metal bolted Connections" report, page 78, Tensile Modulus.

The thicknesses of the aluminum and composite plates are, respectively:

$t_{Al} := \frac{1}{2}$ in $t_c := \frac{1}{2}$ in

The bolt size and the Influence Zone diameter are, respectively:

$D_b := \frac{1}{2}$ in $D_I := 2 \cdot D_b$

(*) This is the CTE of Al, because the composite plate is now an Al plate. Nomenclature unchanged for simplicity. Imagine c is really Al.

The contact area for the aluminum and for the composite plates are, respectively:

$$A_{Al} := \pi \cdot \frac{\left(D_I^2 - D_b^2\right)}{4} \qquad A_c := \pi \cdot \frac{\left(D_I^2 - D_b^2\right)}{4}$$

Note: This analysis is all based on the assumption that the Influence Diameter, DI, is twice the diamater of the bolt, Db. This assumption came from pressure prints on C/Al specimens [Pelletier].

The cross sectional area of the bolt is:

$$A_b := \pi \cdot \frac{D_b^2}{4}$$

The stiffness for the aluminum and composite materials and that for the bolt material (steel) are found, respectively, as:

$$K_{Al} := \frac{A_{Al} \cdot E_{Al}}{t_{Al}} \qquad K_c := \frac{A_c \cdot E_c}{t_c} \qquad K_b := \frac{A_b \cdot E_b}{t_{Al} + t_c}$$

The thermal elongation due to a temperature change or unconfined growth of the bolt, the aluminum plate and that of the composite plate, per degree F are , respectively:

$\delta_{tb} := \alpha_b \cdot (t_{Al} + t_c)$ $\delta_{tb} = 6.5 \times 10^{-6}$ in/F

$\delta_{tAl} := \alpha_{Al} \cdot (t_{Al})$ $\delta_{tAl} = 6.5 \times 10^{-6}$ in/F

$\delta_{tc} := \alpha_c \cdot (t_c)$ $\delta_{tc} = 6.5 \times 10^{-6}$ in/F

The net length change of the bolt and that of the aluminum and the composite plates is found using the equations:

$$\Delta_b = \delta_{tb} + \frac{P_t}{K_b} \qquad (1)$$

$$\Delta_{Alc} = \delta_{tAl} + \delta_{tc} - \frac{P_t}{K_{Al} + K_c} \qquad (2)$$

To maintain joint integrity, the following condition must be met:

$$\Delta_b = \Delta_{Alc} \qquad (3)$$

Substituting equations (1) and (2) into equation (3) and solving for Pt gives:

$$P_t := \left(\delta_{tAl} + \delta_{tc} - \delta_{tb}\right) \cdot \frac{K_b \cdot \left(K_{Al} + K_c\right)}{K_{Al} + K_c + K_b} \qquad P_t = 29.808 \text{ lbs/F}$$

Figure C.4 - TFact for the Aluminum bolted to Aluminum Specimen

Appendix D. Subsequent Four Temperature Cycles

Figures D.1 to D.8 display the subsequent four temperature cycles run using a computer controlled autoclave chamber. These figures are grouped in pairs. For example, Figure D.1 shows the first 20 out of 165-hour response of all articles to the second temperature cycle, whereas Figure D.2 shows a 2-hour detail of this response. The relative humidity has not been included in these plots as its influence can not be well appreciated in such a short time span. Refer to Figure 4.18 for a better picture of the effects of relative humidity in the response of the cycled specimens.

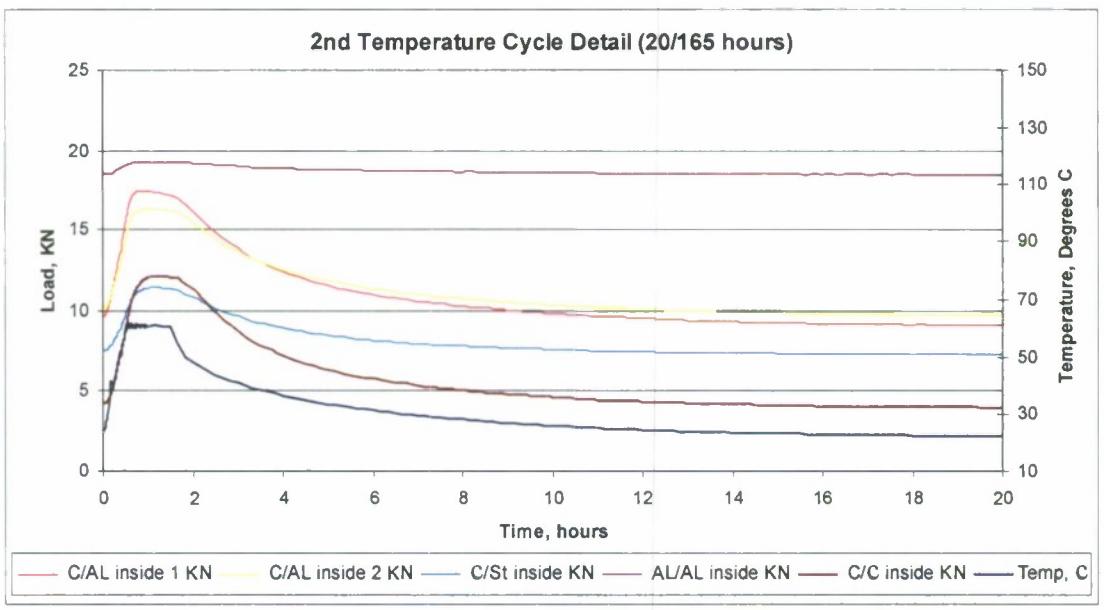

Figure D.1 – Second Temperature Cycle, 20 – hour Detail

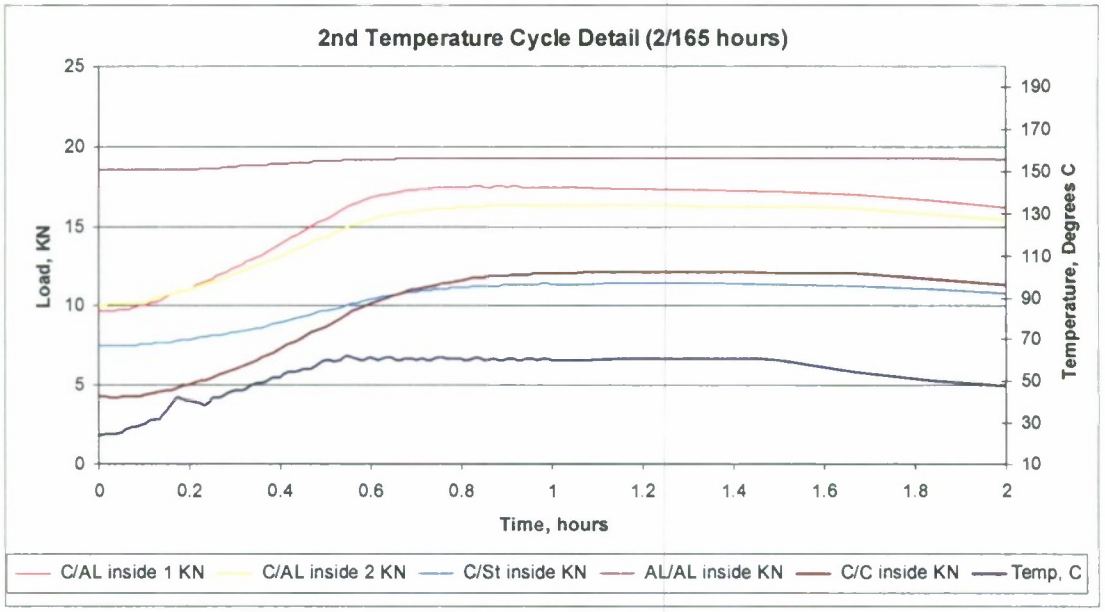

Figure D.2 - Second Temperature Cycle, 2 – hour Detail

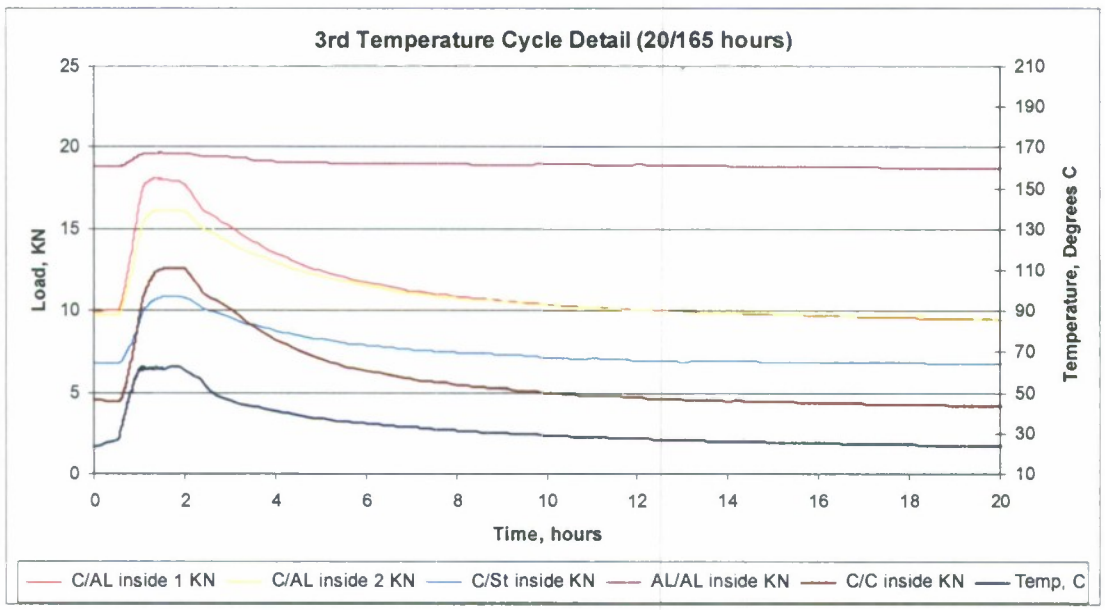

Figure D.3 - Third Temperature Cycle, 20 – hour Detail

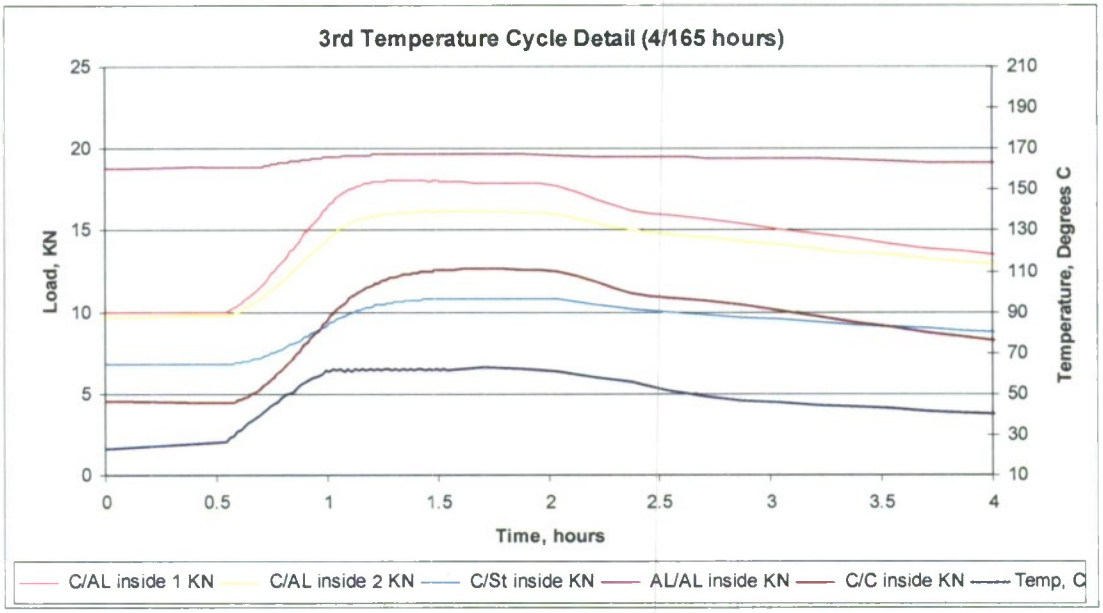

Figure D.4 - Third Temperature Cycle, 4 – hour Detail

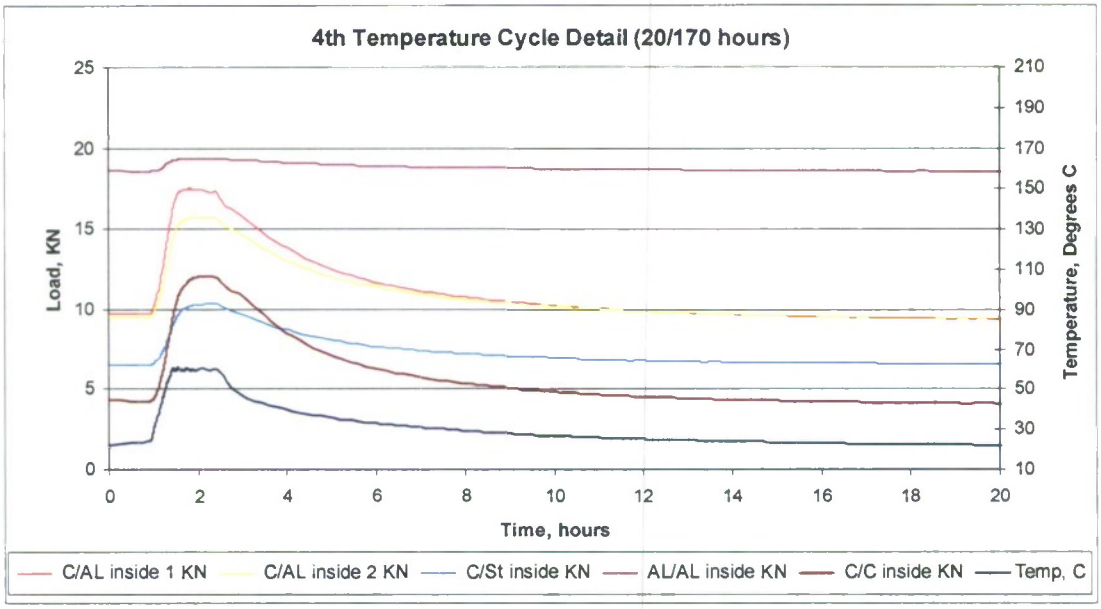

Figure D.5 - Fourth Temperature Cycle, 20 – hour Detail

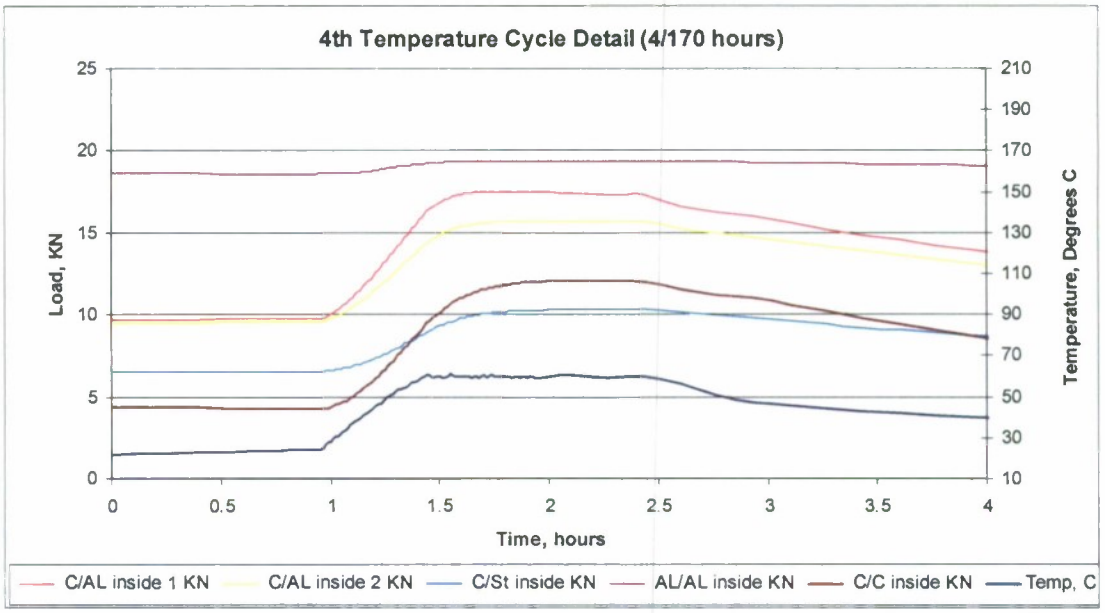

Figure D.6 - Fourth Temperature Cycle, 4 – hour Detail

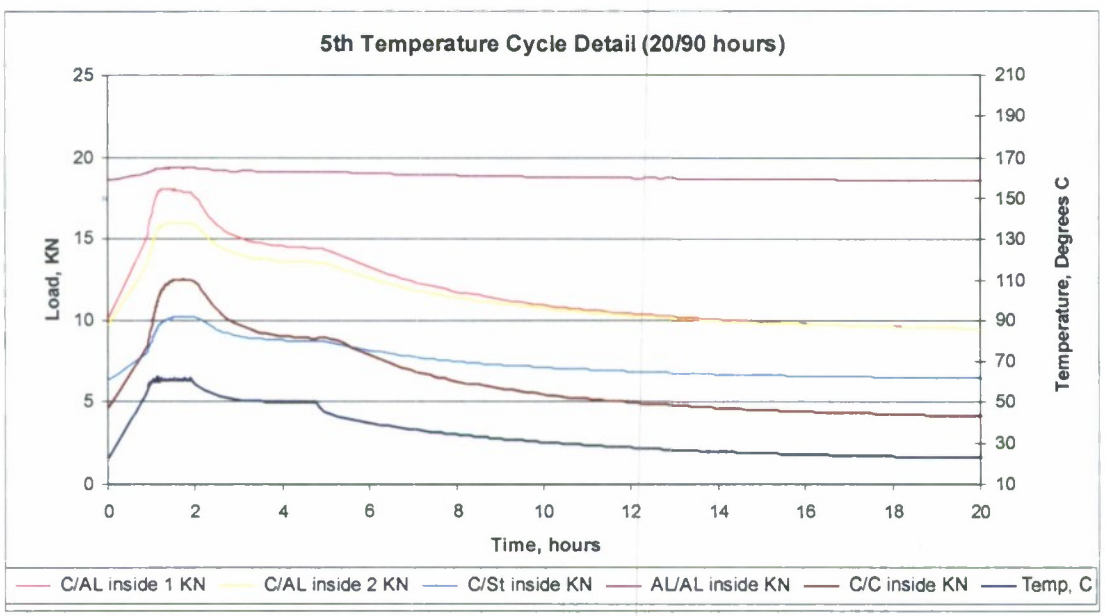

Figure D.7 - Fifth Temperature Cycle, 20 – hour Detail

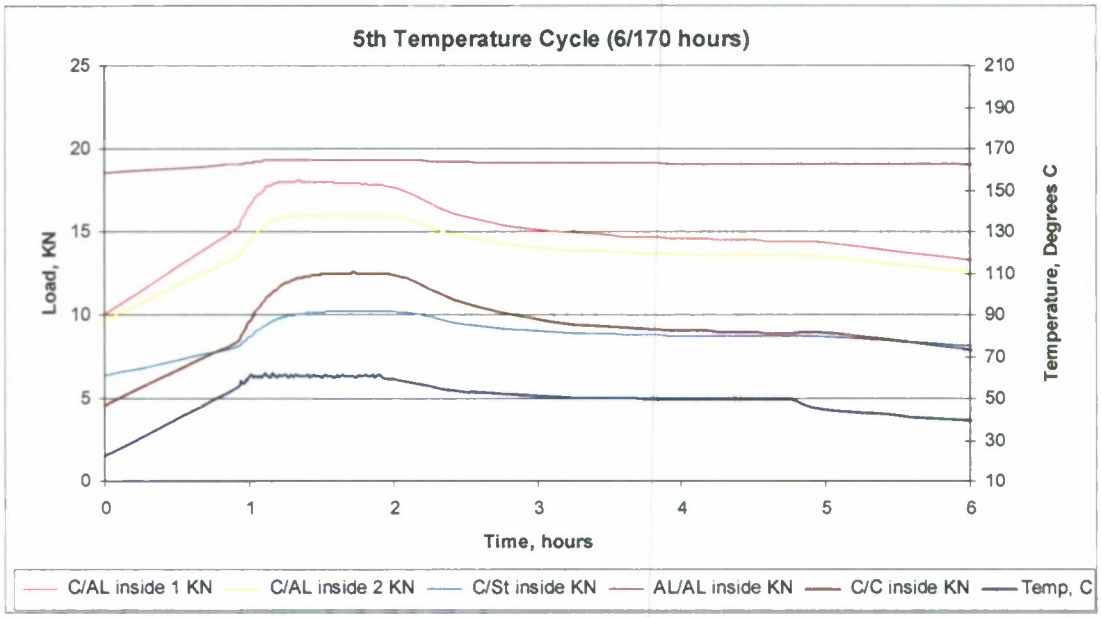

Figure D.8 - Fifth Temperature Cycle, 6 – hour Detail

REPORT DOCUMENTATION PAGE

Form Approved
OMB No. 0704-0188

PLEASE DO NOT RETURN YOUR FORM TO THE ABOVE ADDRESS.

1. REPORT DATE *(DD-MM-YYYY)*	2. REPORT TYPE	3. DATES COVERED *(From - To)*
31-July-2009	Project Report	1-Jun-2005 to 30-June-2009

4. TITLE AND SUBTITLE

EFFECT OF TEMPERATURE AND VISCOELASTIC CREEP ON THE CLAMP-UP LOAD IN HYBRID COMPOSITE/METAL BOLTED JOINTS

5a. CONTRACT NUMBER

5b. GRANT NUMBER

N00014-05-1-0735

5c. PROGRAM ELEMENT NUMBER

6. AUTHOR(S)

Fernandez, Mauricio
Caccese, Vincent
Vel, Senthil S.

5d. PROJECT NUMBER

5e. TASK NUMBER

5f. WORK UNIT NUMBER

7. PERFORMING ORGANIZATION NAME(S) AND ADDRESS(ES)

University of Maine
Office of Research and Sponsored Programs
5717 Corbett Hall
Orono, ME 04469-5717

8. PERFORMING ORGANIZATION REPORT NUMBER

C-2004-015-RPT-03

9. SPONSORING/MONITORING AGENCY NAME(S) AND ADDRESS(ES)

Office of Naval Research
Ballston Center Tower One
800 North Quincy St.
Arlington, VA 22217-5660

10. SPONSOR/MONITOR'S ACRONYM(S)

ONR

11. SPONSORING/MONITORING AGENCY REPORT NUMBER

12. DISTRIBUTION AVAILABILITY STATEMENT

Approved for Public Release, Distribution is Unlimited

13. SUPPLEMENTARY NOTES

14. ABSTRACT

15. SUBJECT TERMS

Hybrid Structures; Stress Relaxation; Bolted Connections; Creep; Composites.

16. SECURITY CLASSIFICATION OF:			17. LIMITATION OF ABSTRACT	18. NUMBER OF PAGES	19a. NAME OF RESPONSIBLE PERSON
a. REPORT	b. ABSTRACT	c. THIS PAGE			Vincent Caccese
U	U	U	UU	145	19b. TELEPONE NUMBER *(Include area code)* (207) 581-2131

Standard Form 298 (Rev. 8-98)
Prescribed by ANSI-Std Z39-18